Modeling of evaporation and its influence on temperature

Juliana Arbelaez Gaviria

Supervisor: doc.Ing. M. Kuráž, PhD

Czech University of Life Sciences Prague

Faculty of Environmental Sciences

Department of Water Resources and Environmental Modeling

June 2020

CZECH UNIVERSITY OF LIFE SCIENCES PRAGUE

Faculty of Environmental Sciences

DIPLOMA THESIS ASSIGNMENT

Juliana Arbelaez Gaviria

Landscape Engineering
Environmental Modelling

Thesis title

Modeling of evaporation and its influence on surface temperature

---

Objectives of thesis

Implementing the mathematical model of evaporation considering surface energy balance into in-house code DRUtES.

Methodology

1. literature retrieval
2. mathematical formulation of the evaporation model
3. software implementation
4. evaluation on benchmark problems

The proposed extent of the thesis

60

Keywords

Richards equation, surface energy balance, energy flux

Recommended information sources

H. Saito, J. Simunek, B. P. Mohanty: Numerical analyses of coupled water, vapour and heat transport, Vadoze Zone Journal, 2006

M. Kuraz, J. R. Bloecher: Hydrodynamics in porous medium, CULS lecture notes, http://drutes.org/documents/notes.pdf

M. Sakai, S. B. Jones, M. Tuller: Numerical evaluation of subsurface soil water evaporation derived from sensible heat balance, Water Resources Research, 2011

Expected date of thesis defence

2019/20 SS – FES

The Diploma Thesis Supervisor

doc. Ing. Michal Kuráž, Ph.D.

Supervising department

Department of Water Resources and Environmental Modeling

Advisor of thesis

Ing. J. R. Bloecher

Electronic approval: 13. 11. 2019

doc. Ing. Martin Hanel, Ph.D.

Head of department

Electronic approval: 25. 11. 2019

prof. RNDr. Vladimír Bejček, CSc.

Dean

Prague on 19. 02. 2020

Author's declaration

I hereby declare that this submitted thesis ***Modeling of evaporation and its influence on temperature*** is my own work and only sources listed in the Bibliography were used.

Prague, 30^{th} June 2020.

Juliana Arbelaez Gaviria

Acknowledgments

I want to express my sincere appreciation to my supervisor, doc. Ing. M. Kuráž, Ph.D., for his guidance. To my advisor, Ing. Johanna Blöcher, for her motivation, and unwavering support, I am genuinely grateful. Thank you for your trust and help, your passion for numerical modeling and kindness inspired to discover soil physics.

Thank you, also, to the Department of Water Resources and Environmental Modeling, and colleagues who have willingly helped me out. I want to thank all my female colleagues. Thanks to them, I found a safe space where to be.

Special thanks to my family and friends in Colombia and the Czech Republic for the love, understanding, and encouragement to always pursue my dreams. To Martin, for being my foothold in the tough times, I am beyond grateful.

"Nothing in life is to be feared, it is only to be understood. Now is the time to understand more, so that we may fear less."

- Marie Curie

Abstract

Evaporation (E) and evapotranspiration (ET) are dynamic and non-linear processes that incorporate various internal transport mechanisms, which are essential in the unsaturated zone in arid regions under low soil moisture conditions. The evaluation of ET from soils and water bodies is necessary for planning and operating water resource projects such as water supply (surface and underground), multipurpose water projects as irrigation, power, waste transportation, and storage, flood control, and many others. FAO Penman-Monteith (PM) equation is the most widespread method to estimate the evaporation rate in saturated soils (Allen et al., 1998). This approach can be implemented as a boundary condition for the Richards' equation and related to the evaporation rate with the soil's water content. However, the PM equation is not valid when the soil moisture is low, and the vapor flux is an essential component of the total water flux. In this case, the governing equations are formed out of the coupled Richards' equation with the heat transport, where the boundary conditions originate from the surface energy balance and the evaporation rate (Saito et al., 2006; Sakai; Jones, et al., 2011).

In this contribution, the numerical implementation of the Penman-Monteith method as the boundary condition of the classical Richards equation is presented. Additionally, the application of the coupled model of heat and water flow was included in the free software Dual Richards Unsaturated Equation Solver. Two scenarios were designed to test the performance of both models under a controlled meteorological environment and the impact of the evaporation rate on the pressure head and water content, including the energy surface balance.

Keywords: Richards' equation, surface energy balance, vapor flow, energy flux.

Abstract

Evaporace (E) a evapotranspirace (ET) jsou dynamické a nelineární procesy, zahrnující nejrůznější interní mechanismy pro transport, které jsou esenciální v nenasycené zóně v aridních oblastech s nízkou vlhkostí půdy. Evaluace ET z půd a vodních ploch je nezbytná pro plánování a provoz projektů vodních zdrojů, jako je zásobování vodou (povrchové a podzemní), víceúčelové vodní projekty určené pro zavlažování, výrobu energie, přepravu a zneškodňování odpadů, protipovodňová opatření a mnoho dalších. FAO Penman-Monteithova (PM) rovnice je nejpoužívanější metodou pro odhad míry evaporace saturovaných půd (Allen et al., 1998). Tento přístup může být implementován jako okrajová podmínka pro Richardsovu rovnici a souviset s mírou evaporace vodního obsahu půdy. PM rovnice však není platná, pokud je vlhkost půdy nízká a proudění páry je klíčovou komponentou celkového proudění vody. V tomto případě jsou řídící rovnice odvozeny od kombinace Richardsovy rovnice s rovnicí pro transport tepla, kde okrajové podmínky vznikají z rovnováhy povrchové energie a míry evaporace (Saito et al., 2006; Sakai; Jones, et al., 2011).

V této publikaci je prezentována numerická implementace Penman-Monteithovy metody jako okrajová podmínka klasické Richardsovy rovnice. Kromě toho, aplikace spojeného modelu proudění tepla a vody byla použita jako vstup pro bezplatný software Dual Richards Unsaturated Equation Solver. Byly navrženy dva scénáře pro testování výkonu obou modelů v kontrolovaném meteorologickém prostředí a testování dopadu míry evaporace na tlakovou výšku a složení vody, včetně rovnováhy povrchové energie.

Klíčová slova: Richardsova rovnice, rovnováha povrchové energie, proudění páry, proudění energie

Contents

List of Figures

List of Tables

List of Symbols

E	Evaporation v, vi, 1, 2, 3, 7, 10, 11, 12
ET	Evaporanspiration v, vi, 1, 2, 3, 8, 11, 12
PM	Penman-Monteith v, vi, 11
R_n	Net radiation flux ix, 12, 13, 14, 27, 29, 30, 42
L	Latent heat of vaporization ix, 12, 13, 35, 36, 39
E_v	Evaporation rate ix, 12, 13, 40, 41
H_s	Sensible heat flux ix, 12, 13
G	Soil heat flux ix, 12, 13, 14, 27, 30, 31, 41
ET_p	Potential evapotranspiration 8, 11
ET_o	Reference evapotranspiration 8, 15, 26, 27
LE_v	Latent heat flux 13
$e_s - e_a$	Vapor pressure deficit of the air 14
ρ_a	Mean air density at constant pressure 14
c_p	Specific heat of the air 14
Δ	Slope of the saturation vapor pressure graph 14, 27, 29
γ	Psychometric constan 14, 27, 29
r_a	Aerodynamic resistance 14, 41
r_s	Bulk surface resistance 14
PDE	Partial differential equation 19, 23, 43, 44, 47
$\vec{q}$	Water volume flux 19, 22
$\mathbf{K}_s$	Saturated hydraulic conductivity 19, 20, 25, 63
H	Total hydraulic head 19, 20, 57
h	Pressure head 19, 23, 24, 25, 32, 34, 36, 37, 38, 39, 72

z	Geodetic head 19, 32
θ_s	Saturated water content 20, 36, 63
$\mathbf{K}(\theta)$	Unsaturated hydraulic conductivity 20, 24
θ_r	Residual water content 20, 63
θ	Water content 20, 21, 23, 24, 25, 32, 34, 72
R_e	Reynold's number 21
d_e	Equivalent grain size 21
υ	Kinematic viscosity 21
$\mathbf{k}$	Permeability tensor 21
g	Gravitational acceleration 21, 38, 39
S	Sink term 23
t	Time 23
$C(h)$	Retention water capacity 23, 24, 34, 65
α	Inverse of air entry value 24, 63
n	Pore-size distribution parameter 24, 63
m	Pore-size distribution parameter 24, 63
Ω	Computational domain 25, 40, 47, 48, 53
Γ	Boundary of computational domain 25, 40, 49
n_3	Vertical component of the normal boundary vector 26
$\mathbf{n}$	Normal boundary vector 26
$q_{\Gamma_{surf}}(t)$	Actual evaporation rate 26, 27
$r(t)$	Rainfall intensity 27
T_a	Mean daily air temperature 27, 29, 41
u_2	Wind speed measured at 2 m height 27, 29
P_{atm}	Atmospheric presure 29
$e_o(T_a)$	Mean saturation vapor pressure 29
e_a	Actual vapor pressure 29, 42
e_s	Saturation vapor pressure 29
z_a	Elevation of the location 29, 30
RH_{air}	Relative humidity of air 29, 41
u_{za}	Wind speed 29
R_a	Extraterrestrial solar radiation 29, 30

R_s	Solar radiation 29, 30, 42
R_{ns}	Shortwave solar radiation 29, 30, 42
R_{so}	Clear-sky solar radiation 29, 30
α	Albedo 29, 30
R_{nl}	Net longwave radiation 30, 42
G_{sc}	Solar constant 30
φ	Latitude 30
d_r	Inverse distance Earth-Sun 30
δ	Solar declination 30
ω_s	Sunset hour angle 30
σ	Stefan-Boltzmann constant 30, 42
C_s	Volumetric soil heat capacity 31, 36
θ_l	Volumetric liquid water content 32, 34, 35, 39
θ_v	Volumetric water vapor content 32, 34, 35
$\vec{q}_w$	Total water flux 32
$\vec{q}_l$	Liquid water flux 32, 40
$\vec{q}_v$	Water vapor flux 32, 33, 40
$\vec{q}_{lh}$	Isothermal liquid water flux 32
$\vec{q}_{lT}$	Thermal liquid water flux 32
T	Soil temperature 32, 34, 36, 37, 38, 39, 41, 42, 72
$\mathbf{K}_{lh}$	Unsaturated isothermal hydraulic conductivity for liquid water 32, 38
$\mathbf{K}_{lT}$	Unsaturated thermal hydraulic conductivity for liquid water 32, 38
$\vec{q}_{vh}$	Isothermal water vapor flux 33
$\vec{q}_{vT}$	Thermal lwater vapor flux 33
$\mathbf{K}_{vh}$	Unsaturated isothermal hydraulic conductivity for water vapor 33, 38
$\mathbf{K}_{vT}$	Unsaturated thermal hydraulic conductivity for water vapor 33, 38
$\mathbf{K}_{Th}$	Total unsaturated isothermal hydraulic conductivity 33

$\mathbf{K}_{TT}$	Total unsaturated thermal hydraulic conductivity 33
θ_{air}	volumetric air content 34
ρ_l	Density of liquid water 34, 39, 41
ρ_v	Density of water vapor 34
ρ_{sv}	Saturated water vapor density 34, 39, 41
RH_s	Soil relative humidity 34, 39, 41
S_T	Storage of heat in the soil 35
$\vec{q_T}$	Total heat flux density 35
C_l	Volumetric heat capacity of liquid water 35
C_v	Volumetric heat capacity of water vapor 35
C_T	Total volumetric heat capacity 36
G_{wT}	Gain factor 38, 39
ϱ	Surface tension of soil water 38, 39
ϱ_0	Surface tension at 25 degree celsius 38, 39
D	Vapor diffusivity in soil 38, 39
R	Universal gas constant 38, 39
M	Molecular weight of water 38, 39
τ	Tortuosity factor 39
D_a	Vapor diffusivity in air 39
η	Enhancement factor 39
f_c	Mass fraction of clay 39
κ	Thermal conductivity of the soil 39
b_1	Empirical regression parameter 39
b_2	Empirical regression parameter 39
b_3	Empirical regression parameter 39
C_a	Volumetric heat capacity of air 41
ε_s	Emissivity of the soil 42
ε_s	Emissivity of of the atmosphere 42
FEM	Finite Element Method 43, 44, 45, 51
$\mathcal{S}$	Trial solution functions space 46, 47
$\mathcal{V}$	Weighting functions space 46, 47
$\mathcal{S}^h$	Galerking trial solution functions space 47

$\mathcal{V}^h$	Galerkin weighting functions space 47, 48
u^h	Galerking trial solution function 47, 48
w^h	Galerkin weighting function 47, 48
N_A	Basis functions 47, 48
Ω_e	Finit element subdomain 48
$\mathbf{c_e}$	Local vector of degrees of freedom of the weigthing function 48
$\mathbf{K_e}$	Local Stiffness matrix 48
$\mathbf{d_e}$	Local vector of degrees of freedom of the trial function 48
$\mathbf{F_e}$	Local force vector 48
n_{sd}	Number of sapce dimensions 48
Γ_D	Boundary of computational domain with Dirichlet boundary condition 49
Γ_N	Boundary of computational domain with Neumann boundary condition 49

Chapter 1

Introduction

Evaporation (E) is one of the components of the hydrological cycle, and accounts for 90% of the moisture in the Earth's atmosphere; the other 10 % is due to plant transpiration know as evapotranspiration (ET) (Jensen; Allen, 2016). It is an essential part of the water budget of any region for water resources planning and management, such as irrigation management (Jensen; Allen, 2016). Particularly, E and ET have played an important role in arid and semiarid irrigated areas across the globe. Its importance has increased due to the growing population and the need to reallocated water sources. Consequently, the determination of E and ET rates is essential for efficient management of reservoirs, especially in water-scarce regions where they rely on water stored in open reservoirs (Helfer et al., 2012). While in humid areas, its importance lies in the expansion of supplemental irrigation and inadequate water storage (Jensen; Allen, 2016).

Evaluation of E from soils and water bodies is necessary for planning and operating water resource projects. Multipurpose water projects as irrigation, power, waste transportation and storage, flood control, water supply, municipal and industrial water use, and wastewater reuse systems, as mentioned by Jensen; Allen, 2016 should take into account evaporation since it is an energy-intensive industrial process that influences costs of food and other products (Or et al., 2013).

Numerous different formulations are available to calculate E and ET (Kay et al., 2008), there are physical and empirical models. Their complexity varies widely based on the number of atmospheric variables involved in the model, from those dependent on just

one variable, commonly temperature (e.g., Thornthwaite, 1948), to those dependent on more than one atmospheric variable, such as wind speed, relative humidity, radiation and temperature (e.g., Penman; Keen, 1948). The primary purpose is to relate E and climate variations based on experimental data collected or mathematical modeling, moreover, to extrapolate E data from regions where are available to other places where few or no data, except meteorological records, are available (Jensen; Allen, 2016). When using empirical or mathematically derived formulations, the scale is also important.

Further estimates of E and ET should be more accurate as of the value of water increases and its competition (Jensen; Allen, 2016). Although standardization of methodology and availability of data for estimating E and ET has improved since the 1950s, the uncertainty from ETevaluation is nowadays of high importance for agriculture and climate change adaptability.

Evaporation and Climate Change

Expected changes in climate variables, particularly the increase in surface air temperature, evaporation is also expected to increase. Hence, it may results in alteration of the hydrological cycle (Helfer et al., 2012). Predictions done by global climate models, not only refers to the increase of air temperature, but also in net radiation, two driven atmospheric parameters of E (Alvarez et al., 2008). Extreme weather events, such as floods or droughts, are more likely to occur, and their effects should be considered in any future evaluation of climate change impact (Potopová et al., 2015). As stated by Alvarez et al., 2008, the dry seasons are expected to last longer with a reduction of rainfall intensity, causing limitations in water storage.

In Australia, it is expected that the potential evapotranspiration will increase by 2% by 2030. The low emission scenario shows increases in evapotranspiration of around 3-6% by 2070, while high emission scenario shows increases in evapotranspiration of around 6-10% (Helfer et al., 2012). Regarding the case of open water bodies, the forecast based on five different global climate models and the Penman model for open water evaporation found an increase of 2.2% for 2030, 3.9% for 2050 and 6.8% for 2070 in a high emission scenario, and 1.7%, 3.9%, and 4.8% respectively, in a low emission scenario (Johnson et al., 2010). In Brazil, Althoff et al., 2020 estimated 7.3% and 18.4% increases in evaporation,

in moderate and pessimistic scenarios, respectively.

In the context of climate change, the evaluation of its effects on evaporation, considering changes between the baseline and future climates leads to a source of uncertainty for hydrological climate change impacts, from the underlying assumption that not only temperature can have a significant effect on overall changes in E, but also other atmospheric variables (Kay et al., 2008). Thus, for climate change assessment, the physical-based formulation of E and ET, such as Penman-Monteith (Allen et al., 1998), are used because they included more atmospheric variables than other formulations, and their effects are better understood. However, when modeling the hydrological impacts of climate change, estimates of E and ET are calculated from other climate variables, and many existing formulations can be applied. What is clear is that with the intrinsic uncertainty of climate change, it is necessary that the models to estimate evaporation be more accurate and intuitively allow the identification of the impacts of each of its parameters and characterizations thereof. The above was demonstrated by the study of Han et al., 2012 in China, which showed that, for a large river basin, the Penman-Monteith equation is more sensitive to relative humidity changes than air temperature.

In the case of the Czech Republic, droughts are known to be the most severe natural disasters after floods, where the evaluation of evaporation is essential for drought studies from different perspectives, particularly in a country where agriculture is essential (Potopová et al., 2015). The increases in droughts' frequency and duration can affect several water dynamics, particularly in the south-eastern part of the country, where it is more sensitive to climate change (Pivec et al., 2006).

Evaporation and Agriculture

In terms of productivity, evaporation represents an economical loss for agriculture and its general perception from public opinion about its sustainability during climate crisis times, where an approximate 70% increase in food production is required to meet the world food demand in 2050, according to Food and Agriculture Organization of the United Nations (FAO, (FAO, 2009)). An increase in agriculture is also an increase in water consumption, and the only way for agriculture to be sustainable is irrigation, and water storage must be efficient in a world with many social, economic, and environmental disparities (Althoff

et al., 2020). Irrigated agriculture has commonly consumed more than two-thirds of the available water supply, according to FAO (Barker et al., 1999).

Improve water management by developing water-saving technologies requires a comprehensive understanding and evaluation of the evaporation process associated with opened reservoirs for storage purposes, where reservoir management strategies must evolve as the expected changes in climate variables are taking place (Althoff et al., 2020). The losses of water due to evaporation threat efficiency and the cost of food production, the enlargement of these losses due to climate change, cannot be neglected, and they need to be quantified. As reported by Gökbulak et al., 2006, more water is lost by evaporation than used for domestic and industrial purposes.

In conclusion, the challenges associated with the evaporation process are becoming more acute as the effects of climate change become visible, and water sources have been limited. The estimation of evaporation and its quantification remains of scientific and industrially relevant, progress must be made to find the most suitable models for the prediction and evaluation of short and long term impacts on different scales.

1.1 Motivation and goals

The primary motivation of this thesis is the understanding of physics of the evaporation process in soils and further mathematical modeling and implementation of two different approaches to address the evaporation problem, which can simulate surface evaporation rate and sub-surface water vapor flow, in the open-source Dual Richards' Unsaturated Equation Solver (*DRUtES*, 2020) and comparing the performance of both methodologies. This work's general objective was to implement the mathematical model of evaporation considering surface energy balance into in-house code DRUtES.

For this main objective, a literature review was carried out to understand soil evaporation physics and the proposed models and methodologies to evaluate it. The FAO Penman-Monteith methodology was chosen to quantify the potential evaporation (Allen et al., 1998), and the coupled water, vapor, and heat transport in soils to account the sub-surface evaporation (Saito et al., 2006; Sakai; Jones, et al., 2011). The mathematical formulation of both models was done and used to proceed to the computational implementation in

DRUtES. Lastly, a case study was proposed to evaluate the implementation under controlled meteorological conditions where it was possible to determine if the selected models were performing as expected.

As a result of this thesis, DRUtEs was expanded to face applications where evaporation is a dominant process and cannot be neglected. This result is then a significant attempt to address the industrial challenges supported by numerical modeling in the hydraulics field. It was also intended to be user-friendly, and able to be applied for carrying out multiples studies to evaluate evaporation. After the mathematical formulation, the implementation phase started with the surface evaporation model and continued with the sub-surface model due to its complexity. It is essential to highlight that implementation entails adding detail to the model, where an iterative and incremental approach can be recommended to construct a result gradually. Although the numerical formulation was not required for the computational implementation, the author provided a numerical context involved in the selected models.

1.2 Thesis structure

This chapter briefly presents in context the evaporation process as an essential part of water management for a wide range of applications; moreover, it states the importance of understanding and modeling it under the climate change crisis and its consequences in agriculture and food security. Lastly, the motivation and goals of this thesis are described in the context of numerical modeling in hydraulics.

Chapter 2 defines some basic concepts to understand the evaporation process and its definitions, then proceeds to describe the surface evaporation, and what is happening in the surface-soil interface, including the surface energy balance. This chapter ends describing the sub-surface evaporation and the explanation of the three stages of this process.

Chapter 3 presents the mathematical formulation of evaporation. Firstly, Richards's equation is stated for variable saturated porous medium, including initial condition and the evaporation as a Neumann boundary condition using the Penman-Monteith equation. The parameterization of the hydraulic functions is also presented. Similarly, the mathematical formulation for liquid water, water vapor, and heat transport in a porous medium is also

stated with their respectively, initial and boundary conditions. Also, the thermodynamics relations used to describe the thermal and non-thermal hydraulic properties are presented.

Chapter 4 describes the Finite Element Method (FEM) and the weak formulation for the system of partial differential equations presented in Chapter 3, some other numeric aspects are included.

Chapter 5 contains the computational implementation of both models presented in Chapter 3, here is also described the source files that were created as part of this thesis, including the required input files to run the models.

Chapter 6 presents the benchmark case where the implementation is evaluated and the comparison of these two models. Chapter 7 concludes this work and present some future research recommendations.

The Appendix section is presented other important results of this work, and collaboration made as well. Lastly, the appendixes include the evaluation of the constitutive relations for the liquid water, water vapor, and heat model done in Matlab as an analysis exercise before proceeding with the implementation in DRUtES. Also, the collaborations, poster presentations, and extra work done as a result of this thesis are presented.

Chapter 2

Evaporation phenomenon in soil physics

2.1 Introduction

This chapter contains a conceptual background to understand the evaporation process, and some definitions are presented as well. It examines the evaporation as a phase transition process controls by the thermodynamics conditions of the system. It continues describing the evaporation accurately when the wetting surface is the soil, referred to as surface evaporation in this work, and when the wet front is inside the porous medium during the drying of the soil as a consequence of an increase of the net evaporation rate. This chapter also summarizes the controlling factors of this process, such as the energy surface balance. The first derivation of the FAO Penman-Monteith equation is also stated and its assumptions to create a standardized method to estimate evaporation in a reference surface, which is possible to apply in different crops across the globe.

2.2 Evaporation

Evaporation (E) is defined as a physical process by which the liquid water is transferred to the gaseous state, so-called vapor. It is possible to identify two major factors involved in phase changes of water, energy, and water content. Evaporation occurs when the rate of evaporation exceeds the rate of condensation. A saturated state exists when these two

process rates are equal, at which point the air capacity to carry water vapor molecules is full (Shuttleworth, 2012).

Evaporation is one of the components of the hydrological cycle on a large scale. It is identified as an essential process in the planet that flows into the global hydrological cycle about the 60% of the precipitation by soil evaporation (20%) or through plant transpiration (Or et al., 2013). Transpiration is defined as the water within the cells plants evaporates to the air through plant surfaces. Evapotranspiration (ET) is the vaporization by evaporation and transpiration. Potential evapotranspiration (ET_p) is the rate of evaporation when all soil-surface interfaces are wet, and no restrictions in the process occur, since this is an ideal state, it also consider as upper value to describe the maximum rate of ET (Jensen; Allen, 2016).

Reference evapotranspiration (ET_o) was developed at the end of the 20th century, as an effort to standardize a methodology for calculating ET independently as possible from land cover and vegetation. Nowadays, this approach has enabled comparing climate effects on evapotranspiration rates across the globe to understand how this process has been influenced by climate variability in different regions and environments. It is based on standard surface parameters, such as albedo, uniform vegetation cover with a fixed surface resistance, and standardized coefficients for aerodynamic part (Allen et al., 1998).

A comprehensive understanding of the evaporation process requires to know the physical properties of liquid water, water vapor, and air. During the phase changes process, it is needed to know the humidity gradients, which refers to water vapor content and energy. When speaking of water vapor, vapor pressure is commonly used for describing the water vapor content since it is a measure of the amount of water in vapor form present in a sample of air (Shuttleworth, 2012).

The air has a total pressure known as atmospheric pressure, which is the sum of the partial pressure of all the compounds in the air, including water vapor, so the vapor pressure is the partial pressure exerted by molecules of water in the gaseous phase. Since water vapor particles are freely flowing from the wetting front to the air and return to the liquid water surface in the water-air interface, at a certain point, these two flows are the same, and the equilibrium state is met where the vapor pressure exerted by water vapor is known as saturation vapor pressure (Jensen; Allen, 2016). The water surface's net evaporation

rate is the difference between the rate at which molecules of water are taken from the water surface to the adjacent air layer minus the rate at which the molecules of water already present in the air are going back into the water (Shuttleworth, 2012). The above is graphically depicted in Figure 2.1, where the arrows towards liquid water represent a condensation process, and the arrows towards water vapor represents the evaporation process.

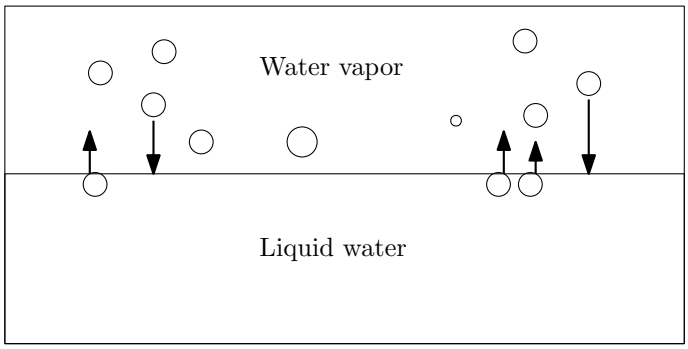

Figure 2.1: Vaporization process and the evaporation rate. Own elaboration based on (Shuttleworth, 2012).

If the rate at which the water molecules are going from liquid water towards water vapor, in a temperature-dependent process, exceeds the rate at which the water molecules are captured back from the air to the water surface, in a concentration-dependent process, the evaporation takes places, and water leaves the surface and transfers to the air (Shuttleworth, 2012).

To move against a force requires work, and therefore, energy must be given to separate water molecules to give changes in phase. The amount of energy needed is directly related to the number of molecules present and, thus, to the mass of water that changes phase. The amount of energy needed for a liquid-to-vapor water transition is called the latent heat of vaporization. Due to the change in separation for a transition from liquid water to water vapor is much larger, the latent heat of vaporization for liquid water is higher than the latent heat of fusion (Shuttleworth, 2012) . The amount of energy needed also depends on the temperature at which the phase changes occur.

In short, the evaporation phenomenon should be understood through the amount of water that is changing phase and, consequently, the energy available for this process.

2.3 Surface evaporation

The current methodology for estimating E is based on the balance of energy on the surface and mass transfer. This approach was rapidly developed in the second half of the 20th century, as a consequence of the demands of the water industry and the competition for available resources (Jensen; Allen, 2016). Most early studies were based on mean air temperature as an index of evaporating demand or as an indicator of solar radiation, where diurnal fluctuations of the air temperature at the soil–atmosphere interface inducing water vapor evaporation at different times of the day were the first approximation to correlate E and meteorological conditions. Few new methods involved air humidity, and none involving wind speed were proposed yet. During the period 1896 - 1939, the scientific community started a detailed study of this phenomenon through data collection and empirical relations to fully understand what affected the quantity of water used by crops and crop yields in irrigation projects (Jensen; Allen, 2016).

In 1916, solar radiation was recognized and taken into account as the primary cause of cyclic change of environmental factors affecting the estimation of E and the importance of the energy in the balance of water (Briggs et al., 1916). Briggs et al., 1916 initiated their studies on applicable requirements of plants in 1910, where they also evaluated the hourly loss of water from evaporation pans in comparison with hourly transpiration and developed predicting equations using vertical component of solar radiation, temperature, and vapor saturation deficit, that laid the foundation for the energy-based E estimating methods. Later on, Hedke, 1924 proposed a method based on the assumption that energy consumed in ET was determined by the energy available; however, the radiant energy was not considered in his hypothesis. From 1920 to 1940, researchers focused on estimating evaporation and seasonal effects on E. Later, Rohwer, 1931 conducted a comprehensive study of evaporation in pans of different sizes, which had led the research of Penman (Penman; Keen, 1948) who later extended and compared his own empirically derived aerodynamic equation with the one obtained by (Rohwer, 1931), the foundations for the current methodology. E was measured in California using sampling methods in 1942 by (Blaney et al., 1942). They developed a method of estimation using mean air temperature, percent of annual daytime hours, and average humidity.

Nevertheless, the two most popular theories were published worldwide in 1948. Thornth-

waite, 1948 correlated the mean air temperature with E as determined by water balance, and Penman developed the combination equation based on the surface energy balance and the empirical aerodynamic relation (Penman; Keen, 1948) . His work was based on an ideal combination of weather parameters in the form of an energy balance equation where the components of evaporation, sensible heat flux, and soil heat flux sum to available net radiation. Moreover, he also formulated evaporation in terms of an empirical aerodynamic resistance (Penman, 1963). Later, he combined both approaches to generate the Penman combination equation, which required only measurements of air temperature, humidity, wind speed, and solar radiation.

Meanwhile, in Europe, engineers also developed empirical equations for estimating E. Makkink, 1957 published an equation based on solar radiation and air temperature in the Netherlands, and Turc, 1961 developed a formula in France for ET_p also based in solar radiation and air temperature. The energy balance method of Penman was used by Tanner et al., 1960 to estimate the potential evapotranspiration in 1960. However, by the time when Jensen; Haise, 1963 developed their simple equation based on solar radiation and mean air temperatures for estimating ET_p for well-watered crops at the full cover, the Penman equation was thought to be too complicated to use, given the status of computational tools, the weather data commonly collected during this period, and expertise of engineers across all the fields where evaporation matters. After Olivier, 1962 developed a method based on the radiation-latitude factor derived from cloudless day solar radiation in 1962, John Monteith reformulated Penman combination equation using a more theoretical equation for aerodynamic transport component (Monteith, 1981). This new equation was named after both scientists, as Penman-Monteith (PM) equation, including the new parameters of aerodynamic resistance and surface resistance, which provided flexibility to the PM equation for application to a wide range of surfaces and vegetation types.

Three factors had been identified as primary factors affecting ET when the evaporating surface is the soil surface, which is the weather, vegetation, and air-surface interface (e.g., soil and water bodies) (Allen et al., 1998). In this work scope, it is only considered the impacts of weather and soil variables; moreover, vegetation is only taken into account using the simplifications already implicit in the methods implemented . Solar radiation

is then the most influential factor from climate variability, and it is considered as the ultimate source of energy required to vaporize water. Air humidity, wind speed, and air temperature are also relevant. The water vapor gradient between soil surfaces and air depends on surface vapor pressure and vapor pressure of the air, or air relative humidity. In addition to weather, the soil's water content, and soil hydraulic and thermal conductivities are also intervening in the evaporation process (Jensen; Allen, 2016).

Studies and historical data of evaporation (E) and evapotranspiration (ET) show that, when the soil water is not constraining, the primary variable controlling ET is the energy provided as solar radiation. However, it is needed to quantify the energy budget at the active surface where the ET process is taking place, to estimate the energy available to vaporize the water (Jensen; Allen, 2016). In this sense, the energy balance relates the net radiation R_n [MJ m^{-2} d^{-1}], the sensible heat H_s [MJ m^{-2} d^{-1}], the latent heat of vaporization L [MJ m^{-3}], the evaporation rate E_v [m d^{-1}], and the soil heat G [MJ m^{-2} d^{-1}] fluxes. The vertical energy balance at the active surface is described by Equation (2.1) and illustrated in Figure 2.2 (Sakai; Jones, et al., 2011)

$$R_n - H_s - LE_v + G = 0 \tag{2.1}$$

The exchange of energy that occurs mainly in the form of surface fluxes. The radiant energy from the sun, latent heat (when water vapor evaporates from or condenses onto the land), sensible heat (that warms or cools the air in contact with the surface), and soil heat that diffuses into or out the ground (Shuttleworth, 2012). A surface flux of any of these is the amount of that entity flowing through and normal to the surface in unit time, per unit surface area. In the case of energy flux exchange with terrestrial surfaces, this is the rate of flow of energy per unit area of a land surface. Moreover, the maximum rates of surface energy transfer are constrained by the incoming energy from the sun (Jensen; Allen, 2016; Shuttleworth, 2012).

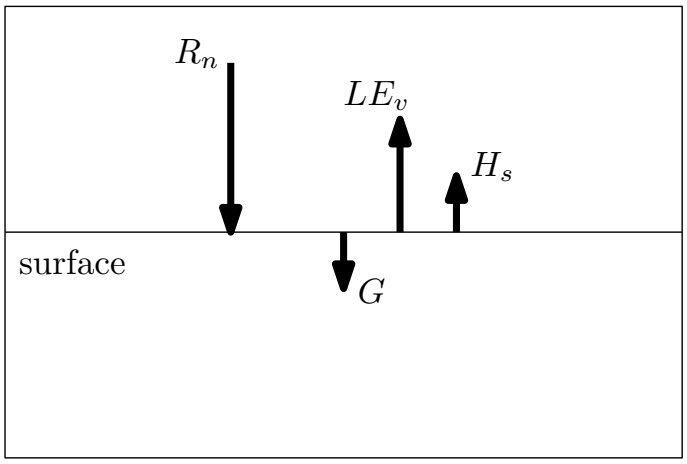

Figure 2.2: Simplified surface energy balance with its components: Net radiation R_n, latent heat of latent heat of vaporization L, evaporation rate E_v, sensible heat H_s and soil heat G.

- Net radiation R_n: the driving input to the surface energy balance is the net flux of radiant energy. The net radiation is itself a balance between four components: incoming and outgoing radiation in the shortwave called solar radiation and the incoming and outgoing radiation in the wavelength determined by temperatures typical of the Earth surface and the lower atmosphere long-wave radiation. Daytime net radiation is dominated by the solar radiation balance, while nighttime net radiation is determined by the long-wave radiation balance (Shuttleworth, 2012).

- Latent heat flux LE_v: the latent heat flux is the flow of energy as latent heat away from the surface if there is evaporation, or toward the surface if there is condensation. During the day, evaporation is often the dominant energy flux into the atmosphere from water surfaces or moist soil or crops, but sometimes there is a downward latent heat flux at night with condensation at the surface as dew or frost (Shuttleworth, 2012).

- Sensible heat flux H_s: warming of the overlying air by an outgoing sensible heat flux occurs if the temperature of the surface is higher than that of the overlying air. Conversely, there is a cooling of overlying air and an incoming sensible heat flux when the surface temperature is less than the air temperature. Because incoming solar radiation during the day raises the surface's temperature, the daytime sensible heat flux is often outward. Commonly at night, when the surface cools, there is a net outward flux of long-wave radiation, the sensible heat flux is inward to help support

this (Shuttleworth, 2012).

- Soil heat flux G: when the soil surface is warming by solar radiation or indirectly by the warming air during the day, heat is transferred downward by thermal conduction into the soil. At night, heat is then conducted back to the surface when the top of the soil cools. This flow is called soil heat flux (Shuttleworth, 2012).

The sign convention most often used for the surface energy balance is biased toward the value of fluxes being positive in daytime conditions. Consequently, all radiation fluxes are defined positive when directed toward the surface, and all the other vertical energy fluxes are defined positive when directed away from the surface.

Lately, the main effort was made on standardization of calculation for PM equation worldwide for different surfaces, in order to establish a benchmark reference ET equation.

2.3.1 Penman-Monteith equation

Penman; Keen, 1948 derived an equation to compute the evaporation from standard meteorological records of sunshine, temperature, humidity, and wind speed. The Equation (2.2) is also named as a combination method since it combines the energy balance and the mass transfer employing aerodynamic resistance and the surface resistance. The surface resistance or bulk surface resistance r_s accounts the resistance of the vapor flow through leaf areas and soil surface, while the aerodynamic resistance refers to resistance from vegetation and involves the friction from air flowing over the crop surface (Allen et al., 1998)

$$LET = \frac{\Delta(R_n - G) + \rho_a c_p \frac{(e_s - e_a)}{r_a}}{\Delta + \gamma\left(1 + \frac{r_s}{r_a}\right)} \tag{2.2}$$

where ET is the evapotranspiration rate [$\mathrm{m\,s^{-1}}$], L is the latent heat [$\mathrm{MJ\,kg^{-1}}$], R_n is the net radiation [$\mathrm{MJ\,m^{-2}\,s^{-1}}$], G is the soil heat flux [$\mathrm{MJ\,m^{-2}\,s^{-1}}$], $e_s - e_a$ the vapor pressure deficit of the air [kPa], ρ_a is the mean air density at constant pressure [$\mathrm{kg\,m^{-3}}$], c_p is the specific heat of the air [$\mathrm{MJ\,kg^{-1}\,K^{-1}}$], Δ is the slope of the saturation vapor pressure graph (see Figure 3.1) [$\mathrm{kPa\,K^{-1}}$], γ is the psychometric constant [$\mathrm{kPa\,K^{-1}}$], and r_a and r_s are the aerodynamic and the bulk surface resistance respectively [$\mathrm{s\,m^{-1}}$]. The parameters of this equation are explained in Chapter 3.

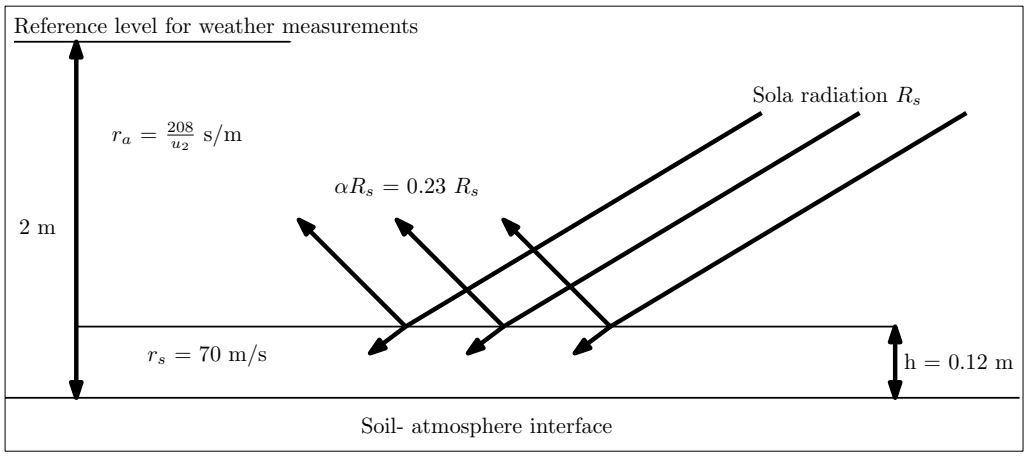

Figure 2.3: Characteristics of the hypothetical reference surface from Penman-Monteith Equation. Own elaboration based on Allen et al., 1998.

The challenge in Equation 2.2 is to calculate the parameters to find a standardized methodology that simplifies the estimation of evaporation, specifically in the agriculture and food industry. To accomplish this, FAO introduces the concept of a reference surface to avoid the need to define unique parameters for each crop and stage of growth. The reference surface was later defined by (Allen et al., 1998) as "a hypothetical reference crop with an assumed crop height of 0.12 m, a fixed surface resistance of 70 s m^{-1}, a constant specific heat of the air 1.013×10^{-3} [kJ kg^{-1} K^{-1}], constant latent heat 2.45 [MJ kg^{-1}], and albedo 0.23 ".

The proposed reference surface refers to an extensive green grass of uniform height, actively growing, shading the ground and enough water (Allen et al., 1998). In Figure 2.3 is depicted the assumptions of the reference surface. As a result of the reference surface, the FAO Penman-Monteith equation was established to calculate the reference evapotranspiration of this reference surface ET_o (Allen et al., 1998).

2.4 Sub-surface evaporation

The FAO Penman-Monteith provides an estimate of the potential rate of evaporation based on meteorological conditions. These types of methods are suitable for open water reservoirs or saturated soil surfaces. When the soil becomes unsaturated, the evaporation rate decreased relative to the potential rate of evaporation due the inability of the soil to maintain the potential rate of evaporation (Wilson et al., 1994).

Evaporation in soils is a dynamic process characterized by low fluxes typically a few mil-

limeters per day. However, the evaporation and consequently drying of the porous medium exhibits dynamic changes in rates that lead to consider the dominance of various internal transport mechanisms driven by the motion of the drying fronts and the redistribution of the reaming liquid water (Or et al., 2013). It can be divided into three crucial stages (Jensen; Allen, 2016).

The first stage is the phase transition to vapor at the wet soil surface, which is constrained by the atmospheric demand and energy input and it may last only for few days in mid-summer; however, the duration of the first stage is sharply limited by the evaporation rate, the higher the rate of evaporation, the shorter the duration of this period. The soil depth, the soil hydraulic properties, and land use (e.g., crops) are also factors affecting the duration of the first stage (Jensen; Allen, 2016; Or et al., 2013). The first stage is characterized by an initially high and relatively constant evaporation rate.

The transition from the first to the second stage begins when there are dry places on the soil surface, and the capillary action cannot longer supply the water demand of the potential evaporation rate. Since the surface has begun to dry, the source of water to evaporate is mainly below the soil-atmosphere interface, and the evaporation process extends from the drying surface to the subsurface soil. Therefore this stage is controlled by upward water movement toward the soil surface, and during the third stage, the evaporation process is taking place below the surface and inside the porous medium, where the water vapor is moving through dry soil to the soil-atmosphere interface and then to the atmosphere (Or et al., 2013). As a result of sub-surface evaporation, water vapor moves towards the surface by molecular diffusion and mass flow due to vapor pressure fluctuations and vapor gradients. During the second stage, a lower and gradually dropping of evaporation rate reflecting a transition to diffusion-limited vapor transport is observed (Jensen; Allen, 2016; Or et al., 2013; Wilson et al., 1994).

Figure 2.4 shows the typical shape of the of the stages during the evaporation in soils, where the stage I is the maximum rate of drying when the soil surface is at or near saturation. Stage II is when the drying begins when the hydraulic conductivity of the soil no longer supplies enough water to the surface to keep the maximum rate. The drying continuous until the vapor deficit between the soil and air ceases to exist. It reaches the residual water content of the soil (Wilson et al., 1994).

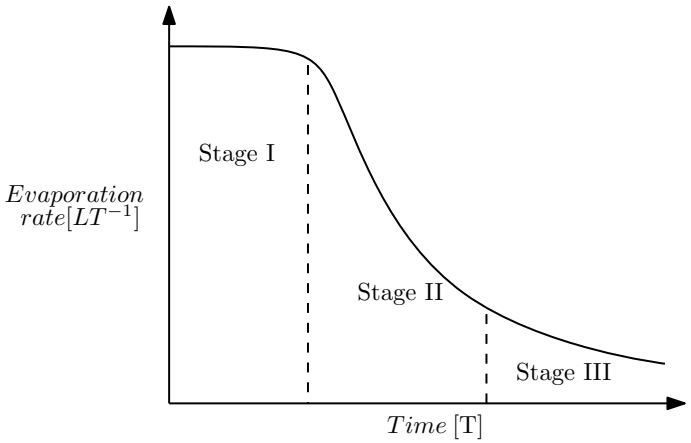

Figure 2.4: Typical curve describing the three stages of evaporation. Own elaboration based on (Wilson et al., 1994).

So far, it has been clear that atmospheric conditions, meteorological data, and water flow must be taken into account in the mathematical model to evaluate evaporation in soils. However, water vapor seems to be then, another factor to consider, which must be modeled since it is the primary variable in the second and third stages of the evaporation process. The vapor concentration gradient drives sub-surface evaporation between nearly saturated vapor at water-table and air vapor concentration. Lastly, fluxes from porous material are limited by rates of energy supply for the phase change of liquid to vapor, by constraints on soil water content to the vaporization interface, and by the rate by which vapor moves from the soil into the atmosphere through the partially dry porous medium and above terrestrial surfaces (Jensen; Allen, 2016) .

As the dominant presence of water vapor movement also characterized the comprehensive studies of evaporation, especially in semiarid and arid regions where it can represent the major part of the overall water flow, it is crucial to take it into account the liquid water flow when evaluating hydrological fluxes and its consequences. Finally, it is worth mentioning; water vapor flow significantly affects the movement of heat. It transports a substantial amount of energy as the latent heat of vaporization which is at the same time an essential flux in the surface energy balance; thus, the simultaneous evaluation of liquid water, water vapor, and heat movement in soils are essential to understand this phenomenon (Noborio et al., 1996; Sakai; Toride, et al., 2009) fully.

Chapter 3

Mathematical model

3.1 Introduction

This chapter presents the derivation of the mathematical model that allows the evaluation of surface evaporation and sub-surface evaporation. The classic Richards' equation (Richards, 1931) is presented for the flow in porous media under conditions of variable saturation, with a Neumann boundary condition lining at the interface of the soil and the adjacent atmosphere where the Penman-Monteith equation (Allen et al., 1998) was used to calculate the potential evapotranspiration rate. Variably saturated flow conditions occur above aquifers, in the vadose zone. Due to the heterogeneities of porous media, the proper characterization of the hydraulic properties of unsaturated soils is crucial for the modeling and understanding of any industrial application where the soil is a fundamental part; thus, the constitutive functions are presented as well.

A second model is presented to evaluate the sub-surface evaporation with a coupled flow of liquid water, vapor water, and heat, where the total water flux is scattered into four components, consisting of liquid water and water vapor fluxes driven by either water content or temperature gradients (Sakai; Jones, et al., 2011; Saito et al., 2006). In this context, an extended Richards equation is presented, including the thermal effects coupled with the heat flow equation. Thermal and non-thermal hydraulic conductivities are also stated, with a Neumann boundary condition for water flow equation and Robin boundary condition for the heat flow equation based on the surface energy balance.

3.2 Water flow model

This section presents the formulation of the surface evaporation model. The Penman-Monteith equation is coupled to the governing equation for the flow of water in a porous medium: Richards equation. The evaporation rate is applied as Neumann boundary condition for the partial differential equation (PDE), and decrease the water content in the soil consequently. The mathematical model is based on hydrodynamics in a porous medium where the PDE is stated, including the initial condition, boundary conditions, and constitutive functions.

3.2.1 Governing Equations

Darcy's law describes water flow and transport in a porous medium. This law was published in 1956 by Henry Darcy (Darcy, 1856), where the complex flow in the porous material was simplified built on the macro continuum approach. According to his observations and experiments, the volume flux $\vec{q}$ is proportional to the energy gradient, which is considered as the total hydraulic head gradient. The equation is expressed as

$$\vec{q} = -\mathbf{K}_s \boldsymbol{\nabla} H \tag{3.1}$$

where $\vec{q}$ is the flux [L T^{-1}], $\mathbf{K}_s$ is the saturated hydraulic conductivity [L T^{-1}], and H [L] is total hydraulic head defined as follows

$$H = h + z \tag{3.2}$$

where h is the pressure head [L], z is the geodetic head [L] which can be expressed as

$$z = \begin{pmatrix} 0 \\ 0 \\ z \end{pmatrix} \tag{3.3}$$

if the coordinate system is considered positive upward, the gradient of the geodetic head is defined as

$$\boldsymbol{\nabla} z = \begin{pmatrix} 0 \\ 0 \\ 1 \end{pmatrix} \tag{3.4}$$

Darcy, 1856 proposed his law under saturated conditions of the porous medium, where all the pores are filled with water, and the pressure head is positive, for instance, aquifers. Mathematically, this can be expressed as

$$\theta = \theta_s \quad \text{and} \quad \mathbf{K}(\theta) = \mathbf{K}_s, \quad h \geq 0 \tag{3.5}$$

where θ_s [$\mathrm{L}^3\,\mathrm{L}^{-3}$] and $\mathbf{K}_s$ [$\mathrm{L}\,\mathrm{T}^{-1}$] are the water content and hydraulic conductivity under a saturated state, $\mathbf{K}(\theta)$ [$\mathrm{L}\,\mathrm{T}^{-1}$] is the unsaturated hydraulic conductivity that depends on the water content. Darcy's assumption accurately describes the flow in aquifers; however, it does not represent the flow of water in the vadose zone. Hence, the unsaturated state refers to when the porous material is not filled by water, and it can be quantified by water content or moisture, for instance, the root zone in soils. The pressure head takes negatives values as a result of capillary force, and it depends on the saturation of porous media. Similarly, the unsaturated state can be mathematically defined as

$$\theta \in (\theta_r, \theta_s) \quad \text{and} \quad \mathbf{K}(\theta) < \mathbf{K}_s, \quad h < 0 \tag{3.6}$$

where θ_r is the residual water content [$\mathrm{L}^3\,\mathrm{L}^{-3}$]. Later, Edgar Buckingham (Buckingham et al., 1907) derived a similar law for the unsaturated state, where the constant of proportionality, knows as hydraulic conductivity, depends on the water content θ introducing $\mathbf{K}(\theta)$ as the unsaturated hydraulic conductivity. Subsequently, Darcy- Buckingham law was established and named after the contribution of both, can be written in terms of total hydraulic head H as follows.

$$\vec{q} = -\mathbf{K}(\theta)\boldsymbol{\nabla} H \tag{3.7}$$

where θ is the water content [-], and $\mathbf{K}(\theta)$ is the unsaturated hydraulic conductivity

function [L T^{-1}]. By including Equation (3.2) in Equation (3.7), the Darcy-Buckingham law can be written in terms of pressure head and geodetic head as

$$\vec{q} = -\mathbf{K}(\theta)(\boldsymbol{\nabla} h + \boldsymbol{\nabla} z) \tag{3.8}$$

Flow regime conditions constrain both Darcy's and Darcy-Buckingham's laws, and they only apply to laminar flow regimes. Thus, the Darcy and Darcy- Buckingham laws' validity can be addressed by Reynold's number R_e [-]. For porous media, the limit for laminar flow is often assumed as 10, where $R_e < 10$ describes the range for laminar flow. Reynold's number is defined for the saturated state as

$$Re = \frac{\|\vec{q}\| d_e}{\upsilon} \tag{3.9}$$

where d_e is the equivalent grain size [L], υ is the kinematic viscosity [L^2 T^{-1}].For the unsaturated state, the d_e is a function of the water content θ. In general, the hydraulic conductivity is described as tensor where $\mathbf{x} = (x, y, z)$

$$\mathbf{K}(\mathbf{x}, \theta) = \begin{pmatrix} K_{xx} & K_{xy} & K_{xz} \\ K_{yx} & K_{yy} & K_{yz} \\ K_{zx} & K_{zy} & K_{zz} \end{pmatrix} \tag{3.10}$$

The hydraulic conductivity depends on properties of the porous media and liquid, and the gravity field. It is defined as

$$\mathbf{K} = \frac{\mathbf{k} g}{\upsilon} \tag{3.11}$$

where $\mathbf{k}$ is the permeability tensor [L^2], and g is the gravitational acceleration [L T^{-2}]. By combining Equation (3.10) and Equation (3.8) it is obtained

$$\vec{q} = -\begin{pmatrix} K_{xx} & K_{xy} & K_{xz} \\ K_{yx} & K_{yy} & K_{yz} \\ K_{zx} & K_{zy} & K_{zz} \end{pmatrix} \begin{pmatrix} \frac{\partial h}{\partial x} \\ \frac{\partial h}{\partial y} \\ \frac{\partial h}{\partial z} \end{pmatrix} - \begin{pmatrix} K_{xx} & K_{xy} & K_{xz} \\ K_{yx} & K_{yy} & K_{yz} \\ K_{zx} & K_{zy} & K_{zz} \end{pmatrix} \begin{pmatrix} 0 \\ 0 \\ 1 \end{pmatrix} \tag{3.12}$$

and the volumetric flux can be written in components of vector $\vec{q}$ as follows

$$\begin{aligned} q_x &= -K_{xx}\frac{\partial h}{\partial x} - K_{xy}\frac{\partial h}{\partial y} - K_{xz}\left(\frac{\partial h}{\partial z} + 1\right) \\ q_y &= -K_{yx}\frac{\partial h}{\partial x} - K_{yy}\frac{\partial h}{\partial y} - K_{yz}\left(\frac{\partial h}{\partial z} + 1\right) \\ q_z &= -K_{zx}\frac{\partial h}{\partial x} - K_{zy}\frac{\partial h}{\partial y} - K_{zz}\left(\frac{\partial h}{\partial z} + 1\right) \end{aligned} \tag{3.13}$$

The hydraulic conductivity tensor can be simplified when the axes of anisotropy of the domain are aligned with the global coordinate system.

$$\mathbf{K}(\mathbf{x}) = \begin{pmatrix} K_{xx} & 0 & 0 \\ 0 & K_{yy} & 0 \\ 0 & 0 & K_{zz} \end{pmatrix} \tag{3.14}$$

By combining Equation (3.14) and Equation (3.7) it is obtained

$$\vec{q} = -\begin{pmatrix} K_{xx} & 0 & 0 \\ 0 & K_{yy} & 0 \\ 0 & 0 & K_{zz} \end{pmatrix} \begin{pmatrix} \frac{\partial h}{\partial x} \\ \frac{\partial h}{\partial y} \\ \frac{\partial h}{\partial z} \end{pmatrix} - \begin{pmatrix} K_{xx} & 0 & 0 \\ 0 & K_{yy} & 0 \\ 0 & 0 & K_{zz} \end{pmatrix} \begin{pmatrix} 0 \\ 0 \\ 1 \end{pmatrix} \tag{3.15}$$

and the volumetric flux can be written in components as follows

$$\begin{aligned} q_x &= -K_{xx}\frac{\partial h}{\partial x} \\ q_y &= -K_{yy}\frac{\partial h}{\partial y} \\ q_z &= -K_{zz}\left(\frac{\partial h}{\partial z} + 1\right) \end{aligned} \tag{3.16}$$

Assuming an isotropic unsaturated hydraulic conductivity, Equation (3.14), the Darcy-Buckingham law can be expressed as

$$\vec{q} = -\mathbf{K}(\mathbf{x}, \theta)\boldsymbol{\nabla} h - K_{zz}(\theta) \tag{3.17}$$

The law of mass conservation for a non-deformable porous medium and incompressible fluids is defined by the following PDE

$$\boldsymbol{\nabla} \cdot \vec{q} - S = -\frac{\partial \theta}{\partial t} \tag{3.18}$$

where S is the sink term [T^{-1}] and t is the time [T]. Replacing the flux $\vec{q}$ by the Darcy-Buckingham's law (Equation (3.8)), the mixed-form of Richards' is obtained. This law was proposed in 1931 by Lorenzo A. Richards as the following second-order partial differential equation (Richards, 1931)

$$\boldsymbol{\nabla} \cdot (\mathbf{K}(\theta)\boldsymbol{\nabla} h) + \frac{\partial K_{zz}(\theta)}{\partial z} - S = \frac{\partial \theta}{\partial t} \tag{3.19}$$

The Equation (3.19) is known as the mixed-form of Richards' equation because there are two primary variables, h, and θ. As it is explained later in this chapter (see 3.2.2), the relationship between the water content and the pressure head, and the water content and the unsaturated hydraulic conductivity is given by suitable constitutive functions.

For an homogeneous porous medium, the term $\frac{\partial K_{zz}(\theta)}{\partial z}$ can be stated as $\frac{\mathrm{d}K_{zz}}{\mathrm{d}h}\frac{\partial h}{\partial z}$. For this thesis, Richards' equation is expressed in the so-called h-based form, to get only as primary solved variable the pressure head in Equation (3.19) is needed to introduce the retention water capacity $C(h)$ [L^{-1}] which is considered as

$$C(h) = \frac{\mathrm{d}\theta}{\mathrm{d}h} \quad \text{for} \quad \theta \in (\theta_r, \theta_s) \quad \text{and} \quad h \in (-\infty, +\infty) \tag{3.20}$$

However, for a positive pressure head $h \geq 0$, the retention water capacity is defines as $C(h) = 0$. Thus, the capacity term can be replaced by

$$\frac{\partial \theta}{\partial t} = \frac{\mathrm{d}\theta}{\mathrm{d}h}\frac{\partial h}{\partial t} = C(h)\frac{\partial h}{\partial t} \tag{3.21}$$

Finally, the h-based form of Richards' equation states as

$$\boldsymbol{\nabla} \cdot (\mathbf{K}(\theta)\boldsymbol{\nabla} h) + \frac{\partial K_{zz}(\theta)}{\partial z} - S = C(h)\frac{\partial h}{\partial t} \tag{3.22}$$

The Richards' equation has a pattern of a convection-diffusion-reaction equation, where $\boldsymbol{\nabla} \cdot (\mathbf{K}(\theta)\boldsymbol{\nabla} h)$ is the diffusion term, $\frac{\partial K_{zz}(\theta)}{\partial z}$ represents the convection term, and $C(h)\frac{\partial h}{\partial t}$, as mentioned before, is the capacity term. The sink term S can be consider as reaction term of zero order.

3.2.2 Constitutive functions

In order to solve Equation (3.22), constitutive equations should be supplied as the parameters in Equation (3.22), $C(h)$, $\mathbf{K}(\theta)$, and $\theta(h)$ depend on pressure head.

The first function presented here is the water retention curve and states the relation between water content and pressure head. The van Genuchten's equation presented in 1980 (Van Genuchten, 1980) is one of the most widely used and states as

$$\theta(h) = \begin{cases} \theta_r + \frac{\theta_s - \theta_r}{(1+(-\alpha h)^n)^m}, & \forall h \in (-\infty, 0) \\ \theta_s, & \forall h \in \langle 0, \infty) \end{cases} \tag{3.23}$$

where α [L^{-1}] is inverse of air entry value, n and m are pore-size distribution parameters [-] (they are usual treated as $m = 1 - 1/n$). The water retention capacity is parameterized as

$$C(h) = \begin{cases} \frac{\alpha m n (-\alpha h)^{n-1}(\theta_s - \theta_r)}{(1+(-\alpha h)^n)^{1+m}}, & \forall h \in (-\infty, 0) \\ 0, & \forall h \in \langle 0, \infty) \end{cases} \tag{3.24}$$

For describing unsaturated hydraulic conductivity, the van Genuchten's equation for the soil water retention curve, coupled with Mualem's pore-size distribution model (Mualem, 1976) was used to define the unsaturated hydraulic conductivity function as follows.

$$\mathbf{K}(h) = \begin{cases} \mathbf{K}_s \frac{(1-(-\alpha h)^{nm}(1+(-\alpha h)^n)^{-m})^2}{(1+(-\alpha h)^n)^{\frac{m}{2}}}, & \forall h \in (-\infty, 0) \\ \mathbf{K}_s, & \forall h \in \langle 0, \infty) \end{cases} \tag{3.25}$$

where $\mathbf{K}_s$ is saturated hydraulic conductivity [L T^{-1}].

3.2.3 Initial and boundary conditions

In order to solve the proposed partial differential equation presented in Equation (3.22), initial and boundary conditions must be given. They exert a set of additional constraints to the problem on specified boundaries or the initial time of the solution.

Initial Condition

The initial condition provides the state of the system at the starting point of the computation. For Richards' equation, the initial state accounts either information about the pressure head or the water content, since the function which relates h and θ is known. The initial condition is often provided as a known distribution of the pressure head as follows.

$$h(\mathbf{x}, t_0) = h_0(\mathbf{x}) \quad \forall \mathbf{x} \in \Omega \tag{3.26}$$

or similarity

$$\theta(\mathbf{x}, t_0) = \theta_0(\mathbf{x}) \quad \forall \mathbf{x} \in \Omega \tag{3.27}$$

where Ω is the computational domain bounded by $\Gamma = \partial\Omega$.

Boundary Condition

The boundary conditions is a concept that applies to both ordinary and partial differential equations, which is the case of Richards' equation. The boundary can be Dirichlet, Neumann, Robin, Mixed, and Cauchy. However, later in this thesis, the Robin type is explored.

In general, Dirichlet condition is defined when the boundary prescribes a value of the independent variable, in the particular case of the Equation (3.22), it refers to a known pressure head or water content.

$$h(\mathbf{x}, t) = h_\Gamma \equiv \theta(\mathbf{x}, t) = \theta_\Gamma \quad \forall (\mathbf{x}, t) \in \Gamma \times [0, T) \tag{3.28}$$

On the other hand, the Neumann condition is defined as the boundary that prescribes the derivative of the independent variable; in other words, it refers to a known boundary diffusion flux.

$$\mathbf{K}(h)\left(\frac{\partial h(\mathbf{x},t)}{\partial \mathbf{n}} + n_3(\mathbf{x})\right) = q_\Gamma \quad \forall(\mathbf{x},t) \in \Gamma \times [0,T) \tag{3.29}$$

Where n_3 is the vertical component of the normal boundary vector $\mathbf{n}$, practically, the Neumann condition can be used to simulate various physical states of the system often exhibit in nature. For instance, free drainage is a homogeneous Neumann condition, which refers to when the pressure head gradient is zero; thus, only the geodetic gradient is taken into account.

$$\frac{\partial h(\mathbf{x},t)}{\partial \mathbf{n}} + n_3(\mathbf{x}) = 0 \quad \forall(\mathbf{x},t) \in \Gamma \times [0,T) \tag{3.30}$$

When the vertical coordinate system is aligned with the vertical component of the normal vector of the boundary, the free drainage condition leads to the following.

$$\frac{\partial H}{\partial z} = \frac{\partial h + z}{\partial z} = \frac{\partial h}{\partial z} + \frac{\partial z}{\partial z} = 0 + 1 = 1 \tag{3.31}$$

Hence, the boundary flux is equal to unsaturated hydraulic conductivity. Such a situation often occurs when the water table lies far below the domain of interest.

Evaluation of Evaporation Boundary

Another important application of the Neumann boundary condition is to simulate precipitation or evaporation when it applies to the physical domain's surface boundary. Hence, the boundary flux $q_{\Gamma_{surf}}(t)$ is defined as the actual evaporation, which is time-dependent, and its evaluation takes into account the variability of atmospheric conditions.

$$\mathbf{K}(h)\left(\frac{\partial h(\mathbf{x},t)}{\partial \vec{n}} + n_3(\mathbf{x})\right) = q_{\Gamma_{surf}}(t) \quad \forall(\mathbf{x},t) \in \Gamma_{surf} \times [0,T) \tag{3.32}$$

The actual evapotranspiration rate $q_{\Gamma_{surf}}(t)$ [L T^{-1}] is equal the reference evapotranspiration $ET_o(t)$ [L T^{-1}] if the rainfall intensity $r(t)$ [L T^{-1}] is greater than the reference

evapotranspiration $ET_o(t)$, and if the rainfall intensity $r(t)$ is small than the reference evapotranspiration $ET_o(t)$, then the actual evapotranspiration $q_{\Gamma_{surf}}(t)$ is calculated by the reference evapotranspiration using the water content as follows (Kuraz; Holub, 2015)

$$q_{\Gamma_{surf}}(t) = \begin{cases} r(t) - ET_o(t) & \text{if} \quad r(t) - ET_o(t) \geq 0 \\ r(t) - ET_o(t)\theta_l(h)^{2/3} & \text{if} \quad r(t) - ET_o(t) < 0 \end{cases} \tag{3.33}$$

At this point, the problem that arises is how to calculate the reference evaporation. The Penman-Monteith was implemented for evaluating the actual evaporation boundary flux.

$$ET_o = \frac{0.408\Delta(R_n - G) + \gamma \frac{900}{T+273} u_2 (e_s - e_a)}{\Delta + \gamma\,(1 + 0.34u_2)} \tag{3.34}$$

where ET_o is the reference evapotranspiration [mm d^{-1}], R_n is the net radiation at the crop surface [MJ m^{-2} d^{-1}], G is soil heat flux density[MJ m^{-2} d^{-1}], T_a is mean daily air temperature at 2 m height [°C], u_2 is the wind speed measured at 2 m height [m s^{-1}], e_s is saturation vapor pressure [kPa], e_a is the actual vapor pressure [kPa], Δ is the slope vapor pressure curve [kPa $^\circ\mathrm{C}^{-1}$], and γ is psychometric constant [kPa $^\circ\mathrm{C}^{-1}$].

In general, the methods for calculating evapotranspiration from meteorological data require various meteorological and physical parameters. Apart from the site location, the Equation (3.34) uses standard meteorological records of relative humidity, solar radiation, wind speed, and air temperature . To ensure the PM equation's applicability, the weather measurements should be made at 2 m above a large surface of green grass, shading the ground and not short of water (Allen et al., 1998).

In Equation (3.34), it is possible to recognize three types of variables that affected the reference evapotranspiration. First group intents to describe the atmospheric conditions, which help to quantify the effect of principal weather variables on the estimation of evaporation. Atmospheric pressure is fundamental to determine the amount of water vapor since it is directly related to the partial pressure performed by the water vapor in the air (Allen et al., 1998). Furthermore, evaporation at high altitudes is driven by low atmospheric pressure, and the atmospheric pressure estimation depends on the altitude of the

site location (Shuttleworth, 2012). Despite atmospheric pressure, latent heat of vaporization varies only slightly over normal temperatures, and one value of 2.45 MJ kg^{-1} is used in the FAO Penman-Monteith equation. The psychometric constant relates to the atmospheric pressure and the latent heat using the specific heat at constant pressure to increased the temperature of a unit mass of air by one degree (Allen et al., 1998). It is kept constant for each location, and it is defined by using atmospheric pressure. The last parameter in this group is the vapor pressure since the water vapor is a gas, its pressure contributes to the atmospheric pressure in air, and it is known as the partial pressure of water vapor, which relates the amount of water in the air and consequently it is a direct measure of the air-water content. One important value of the vapor pressure is so-called saturation vapor pressure that is the condition when it is said the air to be saturated, and it cannot store more water vapor molecules. Saturation vapor pressure depends on temperature; the higher the air temperature, the bigger the storage capacity; thus, the higher the saturation vapor pressure.

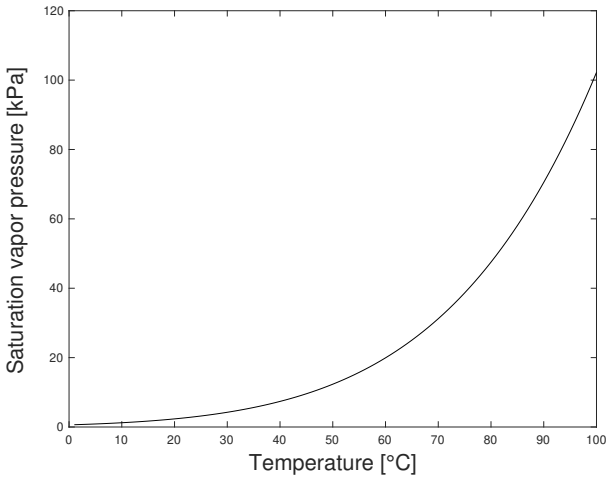

Figure 3.1: Saturation vapor pressure as function of temperature.

As shown in Figure 3.1, the slope changes exponentially, where at low temperatures, the slope varies slightly as the temperature increases, while at high temperatures, a small change in temperature leads significant changes in slope. Hence, the slope is a crucial parameter in the calculation of evaporation using the FAO Penman-Monteith equation. The actual vapor pressure is the vapor pressure exerted by the current amount of vapor particle in the air, and when the air is not saturated, the actual vapor pressure is lower than the saturation vapor pressure. The difference between actual and saturation vapor

pressure is known as vapor pressure deficit, and it is an indicator of the actual evaporative capacity of the air (Allen et al., 1998). The atmospheric parameters are mathematically described in table 3.1.

Table 3.1: Atmospheric parameters for Penman-Monteith Method (Allen et al., 1998).

Parameter	**Symbol**	**Units**	**Equation/Constant** [a]
Atmospheric pressure	P_{atm}	kPa	$101.3\left(\frac{293-0.0065z_a}{293}\right)^{5.26}$
Psychrometric constant	γ	kPa ℃$^{-1}$	$6.65\times10^{-4}P_{atm}$
Mean saturation vapor pressure	$e_o(T_a)$	kPa	$0.6108\exp\left[\frac{17.27T_a}{T_a+237.3}\right]$
Slope of saturation vapor curve	Δ	kPa ℃$^{-1}$	$4098\left[0.6108\exp\left(\frac{17.27T_a}{T_a+237.3}\right)\right]/(T_a+237.3)^2$
Actual vapor pressure	e_a	kPa	$(e^o(T_{amin})+e^o(T_{amax}))RH_{air}/2$
Saturation vapor pressure	e_s	kPa	$(e^o(T_{amin})+e^o(T_{amax})/2$
Wind Speed	u_2	m s^{-1}	$4.87u_{za}/\log(67.82z_a-5.42)$

[a] z_a is the elevation of the location, T_a is temperature of air in ℃, RH_{air} is the relative humidity of air, and u_{za} is the wind speed from meteorological records.

The net radiation data, R_n required in Equation (3.34), are not commonly available but can be estimated from the shortwave radiation, or average daily actual duration of bright sunshine. The intensity of radiation depends on various factors, as the angle between the direction of the sun's rays and the normal to the surface of the atmosphere (Allen et al., 1998; Jensen; Allen, 2016). It changes during the day, latitudes, and seasons. The solar radiation that falls upon the top of the earth's atmosphere on a horizontal surface is called the extraterrestrial solar radiation, R_a (Allen et al., 1998; Jensen; Allen, 2016). Once the radiation passes through the atmosphere, some of the radiation is scattered, reflected, or absorbed by atmospheric gases, clouds, and dust. The amount of radiation reaching a horizontal plane is known as solar radiation (R_s), and it widely measured across the globe. Solar radiation is also known as shortwave radiation R_{ns}. R_{so} is known as clear-sky solar radiation, which is the solar radiation that would reach the same surface as the solar radiation in the same period but under cloudless conditions. The fraction of solar radiation reflected by the earth's surface is known as albedo (α), which varies widely for the incidence angle of the sun's rays and surfaces. In the case of the FAO Penman-Monteith equation, the albedo is assumed to be a value of 0.23, which corresponds to a green grass

reference crop (Allen et al., 1998; Jensen; Allen, 2016). The net solar radiation, R_n, is the fraction of the solar radiation that is not reflected. The radiation that is absorbed by the earth is transformed to heat energy; as the sun, the earth also loses energy and emits energy with wavelengths longer than waves from the sun. Therefore the terrestrial radiation is known as the longwave radiation.

Consequently, the earth's surface emits and receives longwave radiation, where the difference between the incoming and outgoing longwave radiation is called net longwave radiation R_{nl}. Lastly, the net radiation,R_n, is the difference between incoming and outgoing radiation of short and longwave. Usually, the net radiation is positive during the daytime and negative during nighttime (Jensen; Allen, 2016).

Table 3.2: Net radiation parameters for Penman-Monteith Method (Allen et al., 1998).

Parameter	**Symbol**	**Units**	**Equation/Constant**[a]
Net radiation	R_n	MJ m^{-2} d^{-1}	$R_{ns} - R_{nl}$
Extraterrestrial radiation	R_a	MJ m^{-2} d^{-1}	$(1440/\pi)G_{sc}d_r\,[\omega_s \sin\varphi \sin\delta + \cos\varphi\cos\delta\sin\omega_s]$
Solar constant	G_{sc}	MJ m^{-2} min^{-1}	0.0820
Geographic latitude	φ	rad	$\frac{\pi}{180}[decimal\ degrees]$
Inverse distance Earth-Sun	d_r	rad	$1 + 0.033\cos\left(\frac{2\pi}{365}J\right)$
Solar declination	δ	rad	$0.409\sin\left(\frac{2\pi}{365}J - 1.39\right)$
Sunset hour angle	ω_s	rad	$\arccos[-\tan(\varphi)\tan(\delta)]$
Clear-sky radiation	R_{so}	MJ m^{-2} d^{-1}	$(0.75 + 2\times10^{-5}z)R_a$
Net shortwave radiation	R_{ns}	MJ m^{-2} d^{-1}	$(1-\alpha)R_s$
Long-wave radiation	R_{nl}	MJ m^{-2} d^{-1}	$\sigma\left[\frac{T_{max}^4+T_{min}^4}{2}\right](0.34 - 0.14\sqrt{e_a})\left(1.35\frac{R_s}{R_{so}} - 0.35\right)$
Stefan-Boltzmann constant	σ	MJ K^{-4} m^{-2} d^{-1}	4.903×10^{-9}

[a] J is the number of the day in the year between 1 (1st January) and 365 or 366 (31st December), α is the albedo [-], z_a is the elevation of the location,T is absolute temperature of air, and R_s is radiation from meteorological records.

To estimate the evaporation, it is crucial to quantify all the terms in the surface energy balance Equation (2.1), the soil heat flux G is the energy consumed in heating the soil. It is positive when the soil is warming and negative when the soil is cooling. Since the heat flux is small compared to net solar radiation and maybe often ignored, the exchange of energy through the soil should be taking into account (Allen et al., 1998). In this particular model, the uncertainty increases in the estimation of the heat flux, where for

$\Delta t < 1$ day, it may be ignored $G = 0$, in general, the heat flux is defined as the difference of the air temperature in a predefined time step Δt as follows.

$$G = C_s \frac{T_i - T_{i-1}}{\Delta t} \Delta z \tag{3.35}$$

Where G is the heat flux [MJ m^{-2} d^{-1}], C_s is the soil heat capacity [MJ m^{-3} °C^{-1}], T_i and T_{i-1} are the air temperature at the time i and time $i-1$ respectively, Δt is the length of time interval [d], and Δz [m] is the effective soil depth, which is determined by the length of the time interval, for few days, Δz can be around 0.20 m, but it can be 2 m for months. For monthly periods and assuming a constant soil heat capacity of 2.1 MJ m^{-3} °C^{-1} (Allen et al., 1998), soil heat flux can be approximate as follows

$$G_m = 0.07(T_{i+1} - T_{i-1}) \tag{3.36}$$

or, if T_{i+1} is unknown,

$$G_m = 0.14(T_i - T_{i-1}) \tag{3.37}$$

where T_i is the meant air temperature for month [°C], T_{i-1} is the meant air temperature for previous month [°C], and T_{i+1} is the meant air temperature for next month [°C]. For hourly estimations, the heat flux can be estimated during daylight as $G = 0.1R_n$, or during the nighttime as $G = 0.5R_n$ (Allen et al., 1998).

3.3 Liquid water, water vapor and heat flow model

In Section 3.2 was presented the model only for the flow of liquid water in porous media accounting the surface evaporation as a Neumann boundary condition of the governing partial differential equation. Unlike the water flow model, the following model addresses surface evaporation and the sub-surface evaporation rate by modeling the water vapor movement in the porous media. Moreover, the heat is also mathematically modeled by coupling with the two phases of water flow. Knowing the temperature distribution in the porous medium is fundamental to quantify the energy available at the surface to lead

and fuel an evaporation process. Initial and boundary conditions must be provided for both PDE in terms of pressure head and temperature, which define the evaporation in the soil-atmosphere interface by using meteorological records, and hydraulic and thermal conductivities of soil.

3.3.1 Governing equations

Liquid water and water vapor flow

The governing equation for the flow of liquid water and water vapor in a variably saturated non-deformable porous medium is given by the law of mass conservation presented in Equation (3.18). However, for modeling liquid water and water vapor transport, the total water content and the total water flux is divided into two terms by the contribution of the water presence in two different phases. Hence, the total volumetric water content θ is defined as the sum of θ_l, the volumetric liquid water content [-] and θ_v ,the volumetric water vapor content [-], as follows

$$\theta = \theta_l + \theta_v \tag{3.38}$$

Similarly, the total water flux $\vec{q}_w$ [$\mathrm{L\,T^{-1}}$] can be described as the sum of the liquid water flux and the water vapor flux as

$$\vec{q}_w = \vec{q}_l + \vec{q}_v \tag{3.39}$$

where $\vec{q}_l$ and $\vec{q}_v$ are the flux densities of liquid water and water vapor [$\mathrm{L\,T^{-1}}$], respectively. The flux density of liquid water $\vec{q}_l$ is described using a modified the Darcy-Buckingham law proposed by Philip et al., 1957:

$$\vec{q}_l = \vec{q}_{lh} + \vec{q}_{lT} = -\mathbf{K}_{lh}(\boldsymbol{\nabla} h + \boldsymbol{\nabla} z) - \mathbf{K}_{lT}\boldsymbol{\nabla} T \tag{3.40}$$

where $\vec{q}_{lh}$ and $\vec{q}_{lT}$ are the isothermal and thermal liquid water flux densities [$\mathrm{L\,T^{-1}}$], respectively, h is the pressure head [L], z is the geodetic head [L], T is the temperature [Θ], and $\mathbf{K}_{lh}$ [$\mathrm{L\,T^{-1}}$] and $\mathbf{K}_{lT}$ [$\mathrm{L\,\Theta^{-1}\,T^{-1}}$] are the unsaturated isothermal and thermal hy-

draulic conductivities for water liquid phase due to pressure and temperature respectively. The flux density of water vapor $\vec{q}_v$ can also be separated into isothermal $\vec{q}_{vh}$ [L T^{-1}], and thermal $\vec{q}_{vT}$ [L T^{-1}], vapor flux densities as follows Philip et al., 1957

$$\vec{q}_v = \vec{q}_{vh} + \vec{q}_{vT} = -K_{vh}\boldsymbol{\nabla} h - K_{vT}\boldsymbol{\nabla} T \tag{3.41}$$

where $\mathbf{K}_{vh}$ [L T^{-1}] and $\mathbf{K}_{vT}$ [L Θ^{-1} T^{-1}] are the unsaturated isothermal and thermal-hydraulic conductivities for water vapor phase. By replacing Equation (3.39) into Equation (3.18), it is obtained the equation for the flow of liquid water and water vapor in a variably saturated non-deformable porous medium as

$$\frac{\partial \theta}{\partial t} = -\boldsymbol{\nabla} \cdot (\vec{q_l} + \vec{q_v}) - S \tag{3.42}$$

The liquid water and water vapor flux densities can be replaced using Equation (3.40) and Equation (3.41) into Equation (3.42) as follows

$$\frac{\partial \theta}{\partial t} = \boldsymbol{\nabla} \cdot [\mathbf{K}_{lh}(\boldsymbol{\nabla} h + \boldsymbol{\nabla} z) + \mathbf{K}_{lT}\boldsymbol{\nabla} T] + \boldsymbol{\nabla} \cdot [K_{vh}\boldsymbol{\nabla} h + K_{vT}\boldsymbol{\nabla} T] - S \tag{3.43}$$

Moreover, it is possible to apply the divergence operator among the Equation (3.43) to cluster the equation as given in Equation (3.44).

$$\frac{\partial \theta}{\partial t} = \boldsymbol{\nabla}\cdot(\mathbf{K}_{lh}\boldsymbol{\nabla} h)+\boldsymbol{\nabla}\cdot(\mathbf{K}_{lh}\boldsymbol{\nabla} z)+\boldsymbol{\nabla}\cdot(\mathbf{K}_{lT}\boldsymbol{\nabla} T)+\boldsymbol{\nabla}\cdot(K_{vh}\boldsymbol{\nabla}\cdot h)+\boldsymbol{\nabla}\cdot(K_{vT}\boldsymbol{\nabla} T)-S \tag{3.44}$$

By grouping the isothermal and thermal hydraulic conductivities, it is obtained the total hydraulic conductivities where $\mathbf{K}_{Th}$ [L T^{-1}] is the isothermal total hydraulic conductivity and $\mathbf{K}_{TT}$ [L Θ^{-1} T^{-1}] is the thermal total hydraulic conductivity, as:

$$\mathbf{K}_{Th} = \mathbf{K}_{lh} + K_{vh}\mathbf{I} \tag{3.45}$$

$$\mathbf{K}_{TT} = \mathbf{K}_{lT} + K_{vT}\mathbf{I} \tag{3.46}$$

Combing Equation (3.44), Equation (3.45), and Equation (3.46) it is obtained the governing liquid water and water vapor flow equation in a variably saturated porous medium in the mixed-form where the solution is θ, h and T.

$$\frac{\partial \theta}{\partial t} = \boldsymbol{\nabla} \cdot (\mathbf{K}_{Th} \boldsymbol{\nabla} h) + \boldsymbol{\nabla} \cdot (\mathbf{K}_{lh} \boldsymbol{\nabla} z) + \boldsymbol{\nabla} \cdot (\mathbf{K}_{TT} \boldsymbol{\nabla} T) - S \tag{3.47}$$

The left- side of Equation (3.47) can be expressed as the sum of the liquid water content and the water vapor content according to 3.38 as follows.

$$\frac{\partial \theta}{\partial t} = \frac{\partial \theta_v}{\partial t} + \frac{\partial \theta_l}{\partial t} \tag{3.48}$$

As stated in Section 3.2 in Equation (3.21), $\frac{\partial \theta_l}{\partial t}$ is equivalent to the capacity term in Richards' equation. In order to simplify the primary solved variables, it is known θ_l is function of the pressure head $\theta_l(h)$ and therefore a water retention capacity term $C(h)$ [L^{-1}] is introduced as well.

The volumetric water vapor content can be expressed as an equivalent water content in terms of volumetric air content θ_{air} [-], density of liquid water ρ_l [$\mathrm{M\,L}^{-3}$], and density of water vapor ρ_v as (Philip et al., 1957)

$$\theta_v = \theta_{air} \frac{\rho_v}{\rho_l} = (\theta_s - \theta_l) \frac{\rho_{sv} RH_s}{\rho_l} \tag{3.49}$$

When the liquid and vapor phases of water in soil are in equilibrium, the vapor density of the soil can be described as the product of the saturated vapor density ρ_{sv} [$\mathrm{M\,L}^{-3}$] and the soil relative humidity RH_s [-] (Saito et al., 2006).Thus, $\frac{\partial \theta_v}{\partial t}$ is solved numerically and θ_v is not consider as primary solved variables in Equation (3.50). A modified h-based form of Richards equation is presented, where the primary solved variables are both the pressure head and temperature.

$$C_h \frac{\partial h}{\partial t} = \boldsymbol{\nabla} \cdot (\mathbf{K}_{Th} \boldsymbol{\nabla} h) + \boldsymbol{\nabla} \cdot (\mathbf{K}_{TT} \boldsymbol{\nabla} T) + \boldsymbol{\nabla} \cdot (\mathbf{K}_{lh} \boldsymbol{\nabla} z) - \frac{\partial \theta_v}{\partial t} - S \tag{3.50}$$

In terms of the convection-diffusion- reaction equation, $C_h \frac{\partial h}{\partial t}$ represents the capacity term, $\boldsymbol{\nabla} \cdot (\mathbf{K}_{Th} \boldsymbol{\nabla} h) + \boldsymbol{\nabla} \cdot (\mathbf{K}_{TT} \boldsymbol{\nabla} T)$ represents the diffusion term by pressure and temperature gradient, $\boldsymbol{\nabla} \cdot (\mathbf{K}_{lh} \boldsymbol{\nabla} z)$ represents the convective term. Since θ_v is not a primary solved variable and it can be calculated using the liquid water content θ_l, thus $\frac{\partial \theta_v}{\partial t}$ is can considered as a zero order reaction term or also sink term.

Heat flow

The governing equation for the heat flow in a variably saturated non-deformable porous medium is given by the law of energy conservation presented in equation 3.51:

$$\frac{\partial S_T}{\partial t} = -\boldsymbol{\nabla} \cdot (\vec{q_T}) + Q \tag{3.51}$$

where S_T is the storage of heat in the soil [$\mathrm{M\,L^{-1}\,T^{-2}}$], $\vec{q_T}$ is the total heat flux density [$\mathrm{M\,T^{-3}}$] and Q accounts for sources and sinks of energy [$\mathrm{M\,L^{-1}T^{-3}}$]. The total heat flux, $\vec{q_T}$, is defined as the sum of conduction of the sensible heat, the sensible heat by convection of liquid water and water vapor, and the latent heat of vapor flow as shown in Equation (3.52) (Saito et al., 2006).

$$\vec{q_T} = -\kappa \boldsymbol{\nabla} T + C_l T \vec{q_l} + C_v T \vec{q_v} + L \vec{q_v} \tag{3.52}$$

Where κ [$\mathrm{M\,L\,T^{-3}\,\Theta^{-1}}$] is the thermal conductivity of soil which is dependent on the water content, C_l and C_v [$\mathrm{M\,T^{-2}\,L^{-1}\,\Theta^{-1}}$] are the volumetric heat capacity of liquid water and water vapor, respectively, and L [$\mathrm{M\,L^{-1}\,T^{-2}}$] is the volumetric latent heat of vaporization of liquid water. In Equation (3.51) and (3.52), the local thermal equilibrium between the solid porous medium, liquid water, and water vapor is assumed. The storage of heat in the soil is defined as the sum of the sensible heat in the rock, water phases, liquid water and water vapor, and latent heat as follows (Saito et al., 2006)

$$S_T = C_s T \theta_s + C_l T \theta_l + C_v T \theta_v + L \theta_v \tag{3.53}$$

where θ_s [-] is the volumetric fraction of solid phase which is equal to the porosity, C_s [$\mathrm{M\,T^{-2}\,L^{-1}\,\Theta^{-1}}$] is the volumetric heat capacity of the solid phase, and L is the volumetric latent heat of vaporization of liquid water [$\mathrm{M\,L^{-1}\,T^{-2}}$]. It is known that the sum of volumetric fraction of the three phases, solid, liquid water, and water vapor is equal to one

$$\theta_l + \theta_s + \theta_v = 1 \tag{3.54}$$

Moreover, in Equation (3.55) is defined as the total volumetric heat capacity C_T as the sum of each phase volumetric heat capacity [$\mathrm{M\,T^{-2}\,L^{-1}\,\Theta^{-1}}$].

$$C_T = C_s + C_l + C_l \tag{3.55}$$

Hence, the storage of heat in Equation (3.53) can be simplified by the using Equation (3.54) and Equation (3.55) as follows

$$S_T = C_T T + L\theta_v \tag{3.56}$$

Combing Equation (3.52) and Equation (3.56) in Equation (3.51), results in the governing equation for heat flow variably saturated porous medium.

$$C_T \frac{\partial T}{\partial t} + L\frac{\partial \theta_v}{\partial t} = \boldsymbol{\nabla} \cdot (\kappa \boldsymbol{\nabla} T) - \boldsymbol{\nabla} \cdot (C_l \vec{q_l} T) - \boldsymbol{\nabla} \cdot (C_v \vec{q_v} T) - L\boldsymbol{\nabla} \cdot (\vec{q_v}) + Q \tag{3.57}$$

As defined previously in Equation (3.41), the water vapor flux can be used in Equation (3.57), it is obtained the governing heat equation in terms of the main variables h and T

$$\begin{aligned} C_T \frac{\partial T}{\partial t} + L\frac{\partial \theta_v}{\partial t} = {} & \boldsymbol{\nabla} \cdot (\kappa \boldsymbol{\nabla} T) - \boldsymbol{\nabla} \cdot [(C_l \vec{q_l} + C_v \vec{q_v}) T] \\ & + L\boldsymbol{\nabla} \cdot [(K_{vh} \boldsymbol{\nabla} h + K_{vT} \boldsymbol{\nabla} T)] + Q \end{aligned} \tag{3.58}$$

Similarly as Equation (3.50), $L\frac{\partial \theta_v}{\partial t}$ is assumed as sink term in Equation (3.59). By

rearranging the terms, it is possible to group and organize the diffusion coefficients due to temperature and pressure head gradients as follows

$$C_T\frac{\partial T}{\partial t}+L\frac{\partial \theta_v}{\partial t}=\boldsymbol{\nabla}\cdot[(\kappa+LK_{vT})\boldsymbol{\nabla}T]-\boldsymbol{\nabla}\cdot[(C_l\vec{q_l}+C_v\vec{q_v})T] \\ +\boldsymbol{\nabla}\cdot[LK_{vh}\boldsymbol{\nabla}h]+Q \tag{3.59}$$

Using as a common factor the temperature gradient and the pressure head gradient, the terms are grouped to obtain two diffusion coefficients and simplify Equation (3.59)

$$\mathbf{B}_{TT}=\kappa\mathbf{I}+LK_{vT}\mathbf{I} \tag{3.60}$$

$$\mathbf{B}_{Th}=LK_{vh}\mathbf{I} \tag{3.61}$$

The diffusion coefficients are introduced in Equation (3.59). Finally, the heat transport equation is presented in Equation (3.62), where the primary solved variables are both the pressure head and temperature.

$$C_T\frac{\partial T}{\partial t}=\boldsymbol{\nabla}\cdot(\mathbf{B}_{TT}\boldsymbol{\nabla}T)+\boldsymbol{\nabla}\cdot(\mathbf{B}_{Th}\boldsymbol{\nabla}h)-\boldsymbol{\nabla}\cdot[(C_l\vec{q_l}+C_v\vec{q_v})T]-L\frac{\partial\theta_v}{\partial t}+Q \tag{3.62}$$

In terms of the convection-diffusion- reaction equation, $C_T\frac{\partial T}{\partial t}$ represents the capacity term, $\boldsymbol{\nabla}\cdot(\mathbf{B}_{TT}\boldsymbol{\nabla}T)+\boldsymbol{\nabla}\cdot(\mathbf{B}_{Th}\nabla h)$ represents the diffusion term by pressure and temperature gradient, $-\boldsymbol{\nabla}\cdot[(C_l\vec{q_l}+C_v\vec{q_v})T]$ represents the convective term, and as mentioned before $L\frac{\partial\theta_v}{\partial t}$ is considered as sink term.

In general, a non- linear system with two unknowns, h and T, and two equations. In Equation (3.63) is presented the mathematical model for the flow of liquid water, water vapor and heat in a variably saturated non-deformable porous medium:

$$\begin{cases} C_h\dfrac{\partial h}{\partial t}=\boldsymbol{\nabla}\cdot(\mathbf{K}_{Th}\boldsymbol{\nabla}h)+\boldsymbol{\nabla}\cdot(\mathbf{K}_{TT}\boldsymbol{\nabla}T)+\boldsymbol{\nabla}\cdot(\mathbf{K}_{lh}\boldsymbol{\nabla}z)-\dfrac{\partial\theta_v}{\partial t}-S \\ C_T\dfrac{\partial T}{\partial t}=\boldsymbol{\nabla}\cdot(\mathbf{B}_{TT}\boldsymbol{\nabla}T)+\boldsymbol{\nabla}\cdot(\mathbf{B}_{Th}\boldsymbol{\nabla}h)-\boldsymbol{\nabla}\cdot[(C_l\vec{q_l}+C_v\vec{q_v})T])-L\dfrac{\partial\theta_v}{\partial t}+Q \end{cases} \tag{3.63}$$

3.3.2 Constitutive functions

As the unknown variables in Equation (3.63) are h pressure head and T temperature, constitutive relations must be given in order to solve the system of equations, and these relations should depend on these two primary solved variables. In addition to the equations already presented, it must be supplied mathematical definition for isothermal liquid hydraulic conductivity $\mathbf{K}_{lh}(h)$, thermal liquid hydraulic conductivity $\mathbf{K}_{lT}(h,T)$, isothermal vapor hydraulic conductivity $\mathbf{K}_{vh}(h,T)$, and thermal vapor hydraulic conductivity $\mathbf{K}_{vT}(h,T)$.

The isothermal liquid hydraulic conductivity $\mathbf{K}_{lh}(h)$ is defined in Equation (3.11) as Richards' equation. The thermal liquid hydraulic conductivity function, which depends on the temperature and the pressure head, is given by (Noborio et al., 1996)

$$\mathbf{K}_{lT}(h,T) = \mathbf{K}_{lh}\left(hG_{wT}\frac{1}{\varrho_0}\frac{\mathrm{d}\varrho(T)}{\mathrm{d}T}\right) \tag{3.64}$$

where G_{wT} is the gain factor that quantifies the temperature dependence of the water retention curve [-], ϱ is the surface tension of soil water [$\mathrm{M\,T^{-2}}$], and ϱ_0 is the surface tension at 25 °C. The isothermal vapor hydraulic conductivity $\mathbf{K}_{vh}$ is described as (Noborio et al., 1996)

$$K_{vh}(h,T) = \frac{D}{\rho_l}\rho_{vs}\frac{Mg}{RT}RH_s(h,T) \tag{3.65}$$

where D is the vapor diffusivity in soil [$\mathrm{L^2\,T^{-1}}$], R [$\mathrm{M\,L^2\,mol^{-1}\,\Theta^{-1}}$] is the universal gas constant, g is the gravitational acceleration [$\mathrm{L\,T^{-2}}$], and M is the molecular weight of water [$\mathrm{M\,mol^{-1}}$]. The thermal vapor hydraulic conductivity function, which depends on the temperature and the pressure head, is given by (Noborio et al., 1996)

$$K_{vT} = \frac{D}{\rho_l}\eta\frac{d\rho_{sv}}{dT}RH_s(h,T) \tag{3.66}$$

Equations presented for isothermal and thermal-hydraulic conductivities for liquid and vapor phase are based in thermodynamics relations that seek to describe the pressure and temperature conditions of the system to mathematically quantify water flux in soils driven

by both pressure head and temperature (Saito et al., 2006).

In Table 3.3 is summarized the expressions and constant values of various physical properties needed to adequately address the coupled flow of water and heat in a porous medium.

Table 3.3: Thermodynamics constitutive functions for water and heat flow model.

Parameter	**Symbol**	**Units**	**Equation/Constant**[a]
surface tension of soil-water	$\varrho(T)$	$\mathrm{g\,s^{-2}}$	$75.6 - 0.1425T - 2.38 \times 10^{-4}T^2$
the surface tension at 25 ℃	ϱ_0	$\mathrm{g\,s^{-2}}$	71.89
the gain factor	G_{wT}	–	7
vapor diffusivity in soil	D	$\mathrm{m^2\,s^{-1}}$	$\tau\theta_{air}D_a$
tortuosity factor	τ	–	$\frac{\theta_{air}^{7/3}}{\theta_s^2}$
vapor diffusivity in air	D_a	$\mathrm{m^2\,s^{-1}}$	$2.12 \times 10^{-5}\left(\frac{T_{abs}}{273.15}\right)^2$
universal gas constant	R	$\mathrm{J\,mol^{-1}\,K^{-1}}$	8.314
gravitational acceleration	g	$\mathrm{m\,s^{-2}}$	9.81
molecular weight of water	M	$\mathrm{kg\,mol^{-1}}$	0.018015
relative humidity in soil	$RH_s(h, T_{abs})$	–	$\exp\left(\frac{hMg}{RT_{abs}}\right)$
saturated vapor density	$\rho_{sv}(T_{abs})$	$\mathrm{kg\,m^{-3}}$	$\frac{10^{-3}\exp\left(31.3716 - \frac{6014.79}{T_{abs}} - 7.924\,95 \times 10^{-3}T_{abs}\right)}{T_{abs}}$
liquid water density	$\rho_l(T)$	$\mathrm{kg\,m^{-3}}$	$1000 - 7.37 \times 10^{-3}(T-4)^2 + 3.79 \times 10^{-5}(T-4)^3$
latent heat of vaporization	$L(T)$	$\mathrm{J\,kg^{-1}}$	$2.501 \times 10^{-6} - 2369.2T$
enhancement factor	η	–	$9.5 + 3\frac{\theta_l}{\theta_s} - 8.5\exp\left\{-\left[\left(1 + \frac{2.6}{\sqrt{f_c}}\right)\frac{\theta_l}{\theta_s}\right]^4\right\}$
mass fraction of clay	f_c	–	0.02
thermal conductivity	$\kappa(\theta_l)$	$\mathrm{W\,m^{-1}\,℃^{-1}}$	$b_1 + b_2\theta_l + b_3\sqrt{\theta_l}$

[a] T is temperature in ℃, T_{abs} is absolute temperature, h is pressure head, θ_l is the volumetric liquid water content, b_1, b_2,b_3 are empirical regression parameter.

The physical properties of water phases are strongly dependent on the soil temperature distribution, while the pore-space structure and water content influence the soil's vapor diffusivity. As the movement of water vapor couples heat and water flow, the relative humidity is controlled by both pressure head and temperature.

Commercial software commonly uses a factor so-called enhancement factor η to account for the increase in the thermal vapor flux due to high-saturated liquid zones and an increase in temperature gradients in the air phase (Saito et al., 2006). Another reason for the enhanced vapor movement is that the actual local temperature gradient in air-filled

pores may be significantly higher than the average temperature gradient for the bulk soil. Regarding the soil thermal properties as thermal conductivity, they are more affected by water content than by the mineral composition of the solid medium, according to Jury et al., 2004.

3.3.3 Initial and boundary conditions

In comparison with Equation (3.22), the system of equation presented in Equation (3.63) requires to be supplied an initial distribution of both, water and temperature; likewise, a boundary condition must be provided for each equation.

Initial conditions

The initial conditions defined in Equation (3.26) and Equation (3.27) for Richards' equation also apply for Equation (3.50). In this case, the initial state accounts for information about the temperature distribution. Hence, the initial condition is provided as follows.

$$T(\mathbf{x}, t_0) = T_0(\mathbf{x}) \quad \forall \mathbf{x} \in \Omega \tag{3.67}$$

where Ω is the computational domain bounded by $\Gamma = \partial\Omega$.

Boundary conditions

The soil-atmosphere interface is a critical boundary condition that has a significant effect on the subsurface flow of liquid water, water vapor, and heat. At the boundary, the evaporation rate and the heat flux must be equal to the total water flux and the heat flux in the soil to evaluate how changes in atmospheric conditions affect the flow of water and heat in the system.

Therefore, a suitable surface boundary for the liquid water and water vapor flow is a Neumann boundary condition defined as the sum of the liquid water flux, $\vec{q}_l(\mathbf{x}, t)$, and water vapor flux, $\vec{q}_v(\mathbf{x}, t)$ in the surface, is equal to the evaporation rate $E_v(t)$ [$\mathrm{L\,T^{-1}}$] (Saito et al., 2006).

$$\| \vec{q}_v(\mathbf{x}, t) \|_{\mathbf{x}=\mathbf{n}} + \| \vec{q}_l(\mathbf{x}, t) \|_{\mathbf{x}=\mathbf{n}} = E_v(t) \quad \forall \mathbf{x} \in \Gamma_{surf} \times [0, T) \tag{3.68}$$

Since the evaporation rate $E_v(t)$ is influenced by soil and atmosphere conditions, more specifically by atmospheric and soil temperature, surface, and soil moisture, it is necessary an expression that accounts for all the driven variables. The surface evaporation rate is often defined as proposed by (Milly, 1984)

$$E_v(t) = \frac{RH_s(h,T)\rho_{sv}(T) - RH_{air}\rho_{sv}(T_a)}{\rho_l r_a} \tag{3.69}$$

where , RH_s is the soil relative humidity [-] evaluated at the soil temperature T, RH_{air} is the air relative humidity [-] evaluated at the air temperature T_a, ρ_{sv} is the saturated vapor density [kg m^{-3}], ρ_l is the liquid water density [kg m^{-3}], r_a is the aerodynamic resistance to water vapor flow [s m^{-1}], and $E_v(t)$ is the evaporation rate [m s^{-1}].

From the surface energy balance is possible to know the soil heat flux G [W m^{-2}] in the soil- atmosphere interface, which should be equal to the total heat flux prescribed in 3.52 since the law of energy conservation also applies at the boundary as Robin boundary type as follows (Saito et al., 2006)

$$-\kappa\frac{\partial T}{\partial \mathbf{n}} + [C_v \parallel \vec{q}_v \parallel)T]_{\mathbf{x}=\mathbf{n}} = -G - L[\parallel \vec{q}_v \parallel]_{\mathbf{x}=\mathbf{n}} \quad \forall \mathbf{x} \in \Gamma_{surf} \times [0,T) \tag{3.70}$$

Where the soil heat flux G is calculated from the surface energy balance presented in 2.1. Commonly, the equation defined in 3.70 is known as a convective boundary condition in heat transfer problems. In general, Robin's condition is defined when the boundary prescribes a linear combination of the values of a function and the values of its derivative on the boundary of the domain; it can also be defined as a weighted combination of Dirichlet and Neumann boundary conditions.

In order to calculate the soil heat flux, it is needed an equation for sensible heat, since the air and soil temperatures are known in the boundary, it is possible to calculate the sensible heat flux H_s [W m^{-2}] as proposed by (Van Bavel et al., 1976)

$$H_s = C_a\frac{T - T_a}{r_a} \tag{3.71}$$

Where C_a is the volumetric heat capacity of air [J m^{-3}K^{-1}], T_a is the temperature of the

air.

The net radiation R_n [W m^{-2}] is the sum of the net shortwave radiation R_{ns} [W m^{-2}] and the net longwave radiation R_{nl} [W m^{-2}].

$$R_n = R_{ns} + R_{nl} \tag{3.72}$$

Based on the Stefan-Boltzmann law, the longwave radiation can be expressed as

$$R_{nl} = \sigma \varepsilon_s (\varepsilon_a T_a^4 - T_s^4) \tag{3.73}$$

Where ε_s is the emissivity of the soil [-] which depends on the water content and land cover, ε_s is the emissivity of the atmosphere [-] which is related to the air temperature and relative humidity (Saito et al., 2006), σ is the Stefan-Boltzmann constant equal to 5.67×10^{-5} [W m^{-2} K^{-4}], T is the air temperature [K] and T is the soil temperature [K]. The emissivity of soil can be calculated as proposed by Van Bavel et al., 1976 as a function of the water content as follows

$$\varepsilon_s = \min(0.90 + 0.180\theta_l, 1.0) \tag{3.74}$$

The atmospheric emissivity can be expressed as

$$\varepsilon_a = 0.70 + 5.95 \times 10^{-5} e_a \exp\left(\frac{1500}{T_a}\right) \tag{3.75}$$

where e_a is the actual atmospheric vapor pressure [kPa], and it can be defined as follows

$$e_a = 0.611 \exp\left(\frac{17.27(T_a - 273.15)}{T_a - 35.85}\right) RH_{air} \tag{3.76}$$

The shortwave radiation based on albedo and the incoming global shortwave radiation R_s [W m^{-2}], which in this work is consider as input

$$R_{ns} = (1 - \alpha) R_s \tag{3.77}$$

Chapter 4

Numerical solution

4.1 Introduction

In this chapter, an overview of the numerical solution and numerics related to Richards' equation and the coupled systems of PDE for modeling the flow of liquid water, water vapor, and heat in porous media are presented. Finite Difference Method is briefly described as the application in the particular $PDEs$ that govern both models. The weak formulation of both problems is stated as one of the standard results of the application of FEM. Finally, some remarks are included to provide a broader context on how the numerical solution is implemented in DRUtES. It is important to mention the coding and computational implementation of the solution of both models were not part of this work.

4.2 Preliminary remarks

Analytical solutions for boundary-value problems are not always available for solving PDE, except for well-defined problems in simple geometries. For complex geometries, material characteristics, and non-linear problems, numerical methods are often used (Chari et al., 2000b).

Finite difference methods are one of the oldest techniques for solving boundary-value problems, and it is an elementary form of the point-value techniques (Chari et al., 2000a). This idea underlying this method approximates the derivatives in the partial differential equation by a difference approximations. The computational domain is discretized in

a mesh which determines the number of the unknowns in the resulting set of algebraic equations. The first derivative can be approximate by forward, backward, or central scheme according to the points used to calculate the derivative; different schemes lead to different accuracy of the method. The second-order derivatives can be approximate by using the first orders differences, e.g., central scheme.

Another principal mathematical technique for solving boundary-value problems is the variational method. In this method, the PDE is expressed as an energy-related formula called a functional, and the solution of the PDE is then obtained by minimizing the functional (Chari et al., 2000b), in continuum mechanics the solution results in the minimum potential energy. The variational method has advantages over traditional methods for solving PDE, such as finite differences. It applies to a broader range of problems, geometries, and media, such as homogeneous isotropic, non-linear heterogeneous anisotropic.

The energy functional can be expressed by using the inner product as

$$\mathcal{F} = (u, u) - 2(f, u) \tag{4.1}$$

where the inner product is defined as an integral expression

$$(u, v) = \int_{\Omega} uvd\Omega \tag{4.2}$$

Ritz's method minimizes the energy functional appropriate to the PDE. This method assumes the unknown solution as a subject of trial functions and its parameters; the trial functions are chosen from a family of functions to assure the functional is stationary. For instance, the desired solution can be composed of a linear combination of trial functions, which are defined over the entire solution domain, and imply all the boundary conditions. The implementation of this method consists in substituting the trial solutions in the functional and constraint the first variation of the functional to zero for each parameter. This procedure yields to n equations that need to be solved for determining the n parameters (Chari et al., 2000b). Ritz's method is considered to be one of the predecessors of FEM.

The finite element method is a particular case of Ritz's method. It is a versatile procedure that offers flexibility for modeling complex geometry and results in stable and accurate

solutions (Chari et al., 2000c). FEM has become one of the most used strategies for solving initial boundary-value problems. This method lies in the variational techniques, where the variational or weak statement of the problem is needed, and the approximate solution of the weak equation by using the finite element functions (Hughes, 2000).

First, the initial boundary-value problem must be defined by partial differential equations, knows as the strong formulation of the problem. Then, the problem's variational formulation needs to be obtained through the energy-related functional or weighted residual expressions. It is the so-called weak formulation of the problem. The physical domain is subdivided into sub-regions known as finite elements, where the trial solution is chosen based on the nodal values of the elements. A set of algebraic equations is obtained either by minimizing the functional or directly by the Galerkin procedure (Chari et al., 2000c). Finally, the solution of the algebraic system is the parameters of the potential solution.

The weak or variational formulation of the problem is determined by two classes of functions. The first one and already mentioned is the trial solution, which needs to satisfy the Dirichlet boundary condition (e.g., $u = h$ on Γ_D) and the Neumann boundary condition is not required in the definition. It is needed that the derivative of the trial solutions be square-integrable. Assume that u is the trial solution and u' is its derivative, this condition can be mathematically stated as

$$\int_{\Omega} (u')^2 d\Omega < \infty \tag{4.3}$$

Functions that comply with Equation 4.3 are called H^1- functions. Therefore, the set of trial solutions $\mathcal{S}$ is all functions that have squared-integrable derivatives and satisfy the Dirichlet boundary condition on Γ_D (Hughes, 2000); this can be written as

$$\mathcal{S} = \left\{ u \in H^1(\Omega) | u = h \, on \, \Gamma_D \right\} \tag{4.4}$$

The second set of equations is the weighting functions, they are similar to the trial solution, but in this case, the homogeneous counterpart of the Dirichlet boundary is required as follows (Hughes, 2000)

$$\mathcal{V} = \left\{ w \in H^1(\Omega) | w = 0 \, on \, \Gamma_D \right\} \tag{4.5}$$

The finite element methods are built on the idea to approximate $\mathcal{S}$ and $\mathcal{V}$ by a convenient and finite-dimensional set of functions where the weak formulation is solved in this finite-dimensional context (Hughes, 2000).

Moreover, it is crucial to mention the strong and weak formulation of the problem is equivalent through the integration by parts that state the following.

$$\int_\Omega u' w d\Omega = -\int_\Omega u w' + \int_\Gamma u w \cdot \mathbf{n} d\Gamma \tag{4.6}$$

The weak form can be obtained multiplying the equation by the weighting function and integrate by parts.

To illustrate the reader and clarify preliminary concepts, suppose the following one-dimensional boundary-value problem defined in $x \in [0, 1]$ using the strong form as

Given $f : \Omega \to \mathbb{R}$ and constants q and p, find $u : \Omega \to \mathbb{R}$ such that

$$\begin{aligned} u_{xx} + f = 0 \quad on \quad \Omega \\ u(1) = q \\ -u_x(0) = p \end{aligned} \tag{4.7}$$

where f is scalar-valued function, smooth, and defined on [0,1]. The subscripts stand for first (u_x) and second derivative (u_{xx}) respectively of the field u. In order to obtain the weak formulation, the differential equation is multiplied by the weighting function and integrate over the domain as follows

$$\int_0^1 (u_{xx} + f) w dx = 0 \tag{4.8}$$

$$\int_0^1 u_{xx} w dx = -\int_0^1 f w dx \tag{4.9}$$

Using the integration by parts in the left side of the Equation 4.9 as

$$\int_0^1 u_{xx} w dx = u_x w\Big|_0^1 - \int_0^1 w_x u_w dx \tag{4.10}$$

According to the strong formulation of the problem (Equation 4.7), $-u_x(0) = p$ and the definition of the function space $\mathcal{V}$ (Equation 4.5), $w(1) = 0$ due to at $x = 1$ is a Dirichlet boundary condition, it can be stated the weak form of the boundary-value problems as

Given $f : \Omega \to \mathbb{R}$ and constants q and p. Find $u \in \mathcal{S}$ such that for all $w \in \mathcal{V}$

$$\int_0^1 w_x u_x dx = \int_0^1 w f dx + w(0)p \tag{4.11}$$

The Galerkin's approximation method is based on the definition of finite-dimensional sets, denoted by $\mathcal{S}^h$ and $\mathcal{V}^h$, respectively. They are subsets of $\mathcal{S}$ and $\mathcal{V}$ and they are represented over discretization of the domain Ω. Subsequently, u^h and w^h are defined by Equation 4.4 and Equation 4.5 as follows

$$\mathcal{S}^h \subset \mathcal{S}, if \quad u^h \in \mathcal{S}^h \quad then \quad u^h \in \mathcal{S} \tag{4.12}$$

$$\mathcal{V}^h \subset \mathcal{V}, if \quad w^h \in \mathcal{V}^h \quad then \quad w^h \in \mathcal{V} \tag{4.13}$$

Galerkin's method states that the approximated solution's error is orthogonal to finite-dimensional approximation space $\mathcal{V}^h$ (Kuraz, 2011).Thus, the projection of the error on the space $\mathcal{V}^h$ is zero. It is part of the so-called weighted residual methods. This procedure shows that it is possible to approximate a second-order PDE by basis functions without even knowing its second derivatives (Kuraz, 2011).

Galerkin's approximation results in a system of linear algebraic equations due to the structure of w^h. Therefore, the weighting function is a linear combination of the basis functions N_A, also knows as shape or interpolation functions defined as if $w^h \in \mathcal{V}^h$, then there exist constants c_A, $A = 1, 2, ..., n$ such that

$$w^h(\mathbf{x}) = \sum_{A=1}^{n} c_A N_A(\mathbf{x}) \tag{4.14}$$

N_A implies that at the Dirichlet boundary $N_A = 0, A = 1, 2, ..., n$, since $w^h = 0$ as necessary in $\mathcal{V}^h$. Similarly, the trial solution u^h is defined as

$$u^h(\mathbf{x}) = \sum_{A=1}^{n} d_A N_A(\mathbf{x}) \tag{4.15}$$

Where d_A are known as the degree of freedoms. Recalling the weak formulation in Equation 4.11, and substituting the definition of w^h and u^h in Equation 4.11 it is obtained the matrix notation as follows

$$\int_0^1 \left(\sum_{A=1}^{n} c_A N_{Ax} \right) \left(\sum_{B=1}^{n} d_B N_{Bx} \right) dx = \int_0^1 \left(\sum_{A=1}^{n} c_A N_{Ax} \right) f dx + N_A(0)p \tag{4.16}$$

In order to solve the Equation 4.16 is needed a local representation of the trial solution and the weighting function. The local representation is then based on the partition of the domain into finite elements Ω_e which are disjoint subdomains of Ω. therefore, $\Omega = \cup_{e=1}^{n_e} \Omega_e$.

As a result of local representation, Equation 4.16 is defined locally at each element in matrix-vector notation as

$$\mathbf{c}_e^T \mathbf{K}_e \mathbf{d}_e = \mathbf{c}_e^T \mathbf{F}_e \tag{4.17}$$

Where $\mathbf{c_e}$ is the local vector of the degrees of freedom of the weighting function, $\mathbf{K_e}$ is the local stiffness matrix, also knows as the conductivity matrix,$\mathbf{d_e}$ is the local vector of degrees of freedom of the trial solution and the unknown in the system, and $\mathbf{F_e}$ is the local force or source vector. After the local definition of the system, it is required to assembly the global system to solve it finally.

4.3 Galerkin's approximation of the problem

Initial boundary-value problems can be defined in two or three space dimensions as well. Therefore, $\Omega \subset \mathbb{R}^{n_{sd}}$ where $n_{sd} (= 1, 2, 3)$ is the number of space dimensions. Ω is consider

as an open set with a boundary Γ. As mentioned before, the boundary can be either Dirichlet or Neumann type, and it can be decomposed in two sets, Γ_D, consists of all the endpoints that imply a Dirichlet boundary condition, and Γ_N, consist of all the endpoints that imply a Neumann boundary condition. Hence, Γ is a closed set of points contained in the boundary ($\Gamma = \overline{\Gamma_D \cup \Gamma_N}$) and there is no point contained in both types of boundaries Γ_D or Γ_N ($\Gamma_D \cup \Gamma_N = \varnothing$). In terms of the preceding definitions, it is possible to conclude $\bar{\Omega}$ is the union of the set and its boundary $\bar{\Omega} = \Omega \cup \Gamma$.

4.3.1 Strong o classical formulation

In Chapter 3, two mathematical models were presented. The first model consists of one unknown field approximated by the trail function h^h. The second model is the coupled system of partial differential equations that consist of two unknown fields approximated by h^h and T^h. The solution of both models was implemented in DRUtES using Galerkin's Finite Element Method to solve the right side of the Equation 4.18 and 4.19. The time derivative term is defined implicitly by the Backward Euler Method.

Water flow model

A formal statement for the strong formulation for the initial boundary-value problem given by the Richards' equation is the following:
Given $C(h), \mathbf{K}(\theta), S, h_0(\mathbf{x}) : \Omega \to \mathbb{R}$, $q_{\Gamma_N^h}(\mathbf{x}, t) : \Gamma_N \to \mathbb{R}$, and $h_{\Gamma_D}(\mathbf{x}, t) : \Gamma_D \to \mathbb{R}$, find $h : \bar{\Omega} \to \mathbb{R}$ such that

$$\begin{aligned} C(h)\frac{\partial h}{\partial t} = \boldsymbol{\nabla} \cdot (\mathbf{K}(\theta)\boldsymbol{\nabla} h) + \frac{\partial K_{zz}(\theta)}{\partial z} - S \quad (\mathbf{x}, t) \in \ \Omega \times [0, T) \\ h(\mathbf{x}, 0) = h_0(\mathbf{x}) \quad \mathbf{x} \in \Omega \\ \frac{\partial h(\mathbf{x}, t)}{\partial \mathbf{n}} = q_{\Gamma_N^h}(\mathbf{x}, t) \quad (\mathbf{x}, t) \in \Gamma_N \times [0, T) \\ h(\mathbf{x}, t) = h_{\Gamma_D}(\mathbf{x}, t) \quad (\mathbf{x}, t) \in \Gamma_D \times [0, T) \end{aligned} \tag{4.18}$$

Liquid water, water vapor and heat model

Likewise, the strong formulation of the initial boundary -value problem for the coupled liquid water, water vapor and heat transport can be formally expressed as follows:
Given $C(h), \mathbf{K}_{Th}, \mathbf{K}_{TT}, K_{lh}, \mathbf{B}_{TT}, \mathbf{B}_{Th}, S, Q, h_0(\mathbf{x}) : \Omega \to \mathbb{R}$, $q_{\Gamma_N^h}(\mathbf{x}, t), q_{\Gamma_N^T}(\mathbf{x}, t) : \Gamma_N \to \mathbb{R}$,

and $h_{\Gamma_D}(\mathbf{x},t), T_{\Gamma_D}(\mathbf{x},t : \Gamma_D \to \mathbb{R}$, find $h, T : \bar{\Omega} \to \mathbb{R}$ such that

$$\begin{aligned}
C_h \frac{\partial h}{\partial t} &= \boldsymbol{\nabla} \cdot (\mathbf{K}_{Th} \boldsymbol{\nabla} h) + \boldsymbol{\nabla} \cdot (\mathbf{K}_{TT} \boldsymbol{\nabla} T) \\
+\boldsymbol{\nabla} \cdot (\mathbf{K}_{lh} \boldsymbol{\nabla} z) - \frac{\partial \theta_v}{\partial t} - S \quad (\mathbf{x},t) &\in \ \Omega \times [0,T) \\
C_T \frac{\partial T}{\partial t} &= \boldsymbol{\nabla} \cdot (\mathbf{B}_{TT} \boldsymbol{\nabla} T) + \boldsymbol{\nabla} \cdot (\mathbf{B}_{Th} \boldsymbol{\nabla} h) \\
-\boldsymbol{\nabla} \cdot [(C_l \vec{q_l} + C_v \vec{q_v})T] - L \frac{\partial \theta_v}{\partial t} + Q \quad (\mathbf{x},t) &\in \ \Omega \times [0,T) \\
h(\mathbf{x},0) &= h_0(\mathbf{x}) \quad \mathbf{x} \in \Omega \\
T(\mathbf{x},0) &= T_0(\mathbf{x}) \quad \mathbf{x} \in \Omega \\
\vec{q_w}(\mathbf{x},t) \cdot \mathbf{n} &= q_{\Gamma_N^h}(\mathbf{x},t) \quad (\mathbf{x},t) \in \Gamma_N \times [0,T) \\
h(\mathbf{x},t) &= h_{\Gamma_D}(\mathbf{x},t) \quad (\mathbf{x},t) \in \Gamma_D \times [0,T) \\
\vec{q_T}(\mathbf{x},t) \cdot \mathbf{n} &= q_{\Gamma_N^T}(\mathbf{x},t) \quad (\mathbf{x},t) \in \Gamma_N \times [0,T) \\
T(\mathbf{x},t) &= T_{\Gamma_D}(\mathbf{x},t) \quad (\mathbf{x},t) \in \Gamma_D \times [0,T)
\end{aligned} \tag{4.19}$$

4.3.2 Weak or variational formulation

By multiplying the strong formulation by the weighting function and applying the integration by parts as explained in this chapter, the weak formulation can be obtained. The time derivative term is once again solved by the implicit Euler scheme.

Water flow model

A formal statement for the weak or variational formulation for the initial boundary-value problem given by the Richards' equation is the following:

Given $C(h), \mathbf{K}(\theta), S, h_0(\mathbf{x}) : \Omega \to \mathbb{R}$, $q_{\Gamma_N^h}(\mathbf{x},t) : \Gamma_N \to \mathbb{R}$, and $h_{\Gamma_D}(\mathbf{x},t) : \Gamma_D \to \mathbb{R}$, find $h^h \in \mathcal{S}^h$ such that for all $w^h \in \mathcal{V}^h$

$$\begin{aligned}
\int_\Omega C(h) \frac{\partial h^h}{\partial t} w^h d\Omega = -\int_\Omega (\mathbf{K}(\theta) \boldsymbol{\nabla} h^h) \boldsymbol{\nabla} w^h d\Omega + \int_{\Gamma_N} q_{\Gamma_N^h} w^h d\Gamma_N + \\
\int_\Omega \frac{\partial K_{zz}(\theta)}{\partial z} w^h d\Omega - \int_\Omega S w^h d\Omega
\end{aligned} \tag{4.20}$$

Liquid water, water vapor and heat model

Likewise, the weak formulation of the initial boundary -value problem for the coupled liquid water, water vapor and heat transport can be formally expressed as follows:

Given $C(h), \mathbf{K}_{Th}, \mathbf{K}_{TT}, K_{lh}, \mathbf{B}_{TT}, \mathbf{B}_{Th}, S, Q, h_0(\mathbf{x}) : \Omega \to \mathbb{R}$, $q_{\Gamma_N^h}(\mathbf{x},t), q_{\Gamma_N^T}(\mathbf{x},t) : \Gamma_N \to \mathbb{R}$, and $h_{\Gamma_D}(\mathbf{x},t), T_{\Gamma_D}(\mathbf{x}, t : \Gamma_D \to \mathbb{R}$, find $h^h, T^h \in \mathcal{S}^h$ such that for all $w_1^h, w_2^h \in \mathcal{V}^h$

$$\begin{aligned}\int_\Omega C_h \frac{\partial h^h}{\partial t} w_1^h d\Omega = &- \int_\Omega (\mathbf{K}_{Th}\boldsymbol{\nabla} h^h)\boldsymbol{\nabla} w_1^h d\Omega - \int_\Omega (\mathbf{K}_{TT}\boldsymbol{\nabla} T^h)\boldsymbol{\nabla} w_1^h d\Omega \\ &+ \int_{\Gamma_N} q_{\Gamma_N^h} w_1^h d\Gamma_N + \int_{\Gamma_N} q_{\Gamma_N^T} w_1^h d\Gamma_N \\ &+ \int_\Omega \boldsymbol{\nabla}\cdot(\mathbf{K}_{lh}\boldsymbol{\nabla} z) w_1^h d\Omega - \int_\Omega \frac{\partial \theta_v}{\partial t} w_1^h d\Omega - \int_\Omega S w_1^h d\Omega\end{aligned} \tag{4.21}$$

$$\begin{aligned}\int_\Omega C_T \frac{\partial T^h}{\partial t} w_2^h d\Omega = &- \int_\Omega (\mathbf{B}_{TT}\boldsymbol{\nabla} T^h)\boldsymbol{\nabla} w_2^h d\Omega - \int_\Omega (\mathbf{B}_{Th}\boldsymbol{\nabla} h^h)\boldsymbol{\nabla} w_2^h d\Omega \\ &+ \int_{\Gamma_N} q_{\Gamma_N^h} w_2^h d\Gamma_N + \int_{\Gamma_N} q_{\Gamma_N^T} w_2^h d\Gamma_N \\ &- \int_\Omega \boldsymbol{\nabla}\cdot\left[(C_l\vec{q_l} + C_v\vec{q_v})T^h\right] w_2^h d\Omega - \int_\Omega L\frac{\partial \theta_v}{\partial t} w_2^h d\Omega + \int_\Omega Q w_2^h d\Omega\end{aligned} \tag{4.22}$$

4.3.3 Local matrix-vector equations

In DRUtES, one-dimensional and two-dimensional Galerkin FEM are implemented using linear basis functions for both dimensions. In two-dimensional problems, the domain is divided into triangular elements.

Water flow model

The solution of the water flow model consist in one unknown field, the pressure head, thus, the local stiffness matrix has dimension 3x3 and the source vector has dimension 3. By using the definition of trial and weighting functions in Equation 4.14 and Equation 4.15, where for two-dimensional with triangular elements $n = 3$. The local stiffness matrix is defined for $\mathbf{K_e}[i,j](i = 1,2,3; j = 1,2,3)$ as

$$\mathbf{K}_e[i,j] = -\int_{\Omega^e} C(h)\frac{\partial h^h}{\partial t} w^h d\Omega - \int_{\Omega^e} (\mathbf{K}(\theta)\boldsymbol{\nabla} h^h)\boldsymbol{\nabla} w^h d\Omega^e + \int_\Omega \frac{\partial K_{zz}(\theta)}{\partial z} w^h d\Omega \tag{4.23}$$

and the local source vector is defined as

$$\mathbf{F}_e[i] = \int_\Omega S w^h d\Omega \tag{4.24}$$

Liquid water, water vapor and heat model

The water flow solution coupled with the heat flow model consists of two unknown fields coupled together: the pressure head and temperature; thus, the local stiffness matrix has dimension 6x6, and the source vector has dimension 6.

The matrix structure is divided into four block matrices based on the equation and variable associated with the diffusion, convection, and reaction terms. The structure is schematized as follows.

Pressure domain terms in water equation	Temperature domain terms in water equation
Pressure domain terms in heat equation	Temperature domain terms in heat equation

Using the definition of trial and weighting functions in Equation 4.14 and Equation 4.15, the matrix of the pressure domain terms in the water equation is defined for $\mathbf{K_e}[i,j](i = 1,2,3; j = 1,2,3)$ as

$$\begin{aligned}\mathbf{K_e}[i,j] = \int_{\Omega^e} C_h \frac{\partial h^h}{\partial t} w_1^h d\Omega^e - \int_{\Omega^e} (\mathbf{K}_{Th} \boldsymbol{\nabla} h^h) \boldsymbol{\nabla} w_1^h d\Omega^e - \\ + \int_{\Omega^e} \boldsymbol{\nabla} \cdot (\mathbf{K}_{lh} \boldsymbol{\nabla} z) w_1^h d\Omega^e\end{aligned} \tag{4.25}$$

The matrix of the pressure domain terms in the heat equation is defined for $\mathbf{K_e}[i, j+3](i = 1,2,3; j = 1,2,3)$

$$\mathbf{K_e}[i, j+3] = \int_{\Omega^e} (\mathbf{B}_{Th} \boldsymbol{\nabla} h^h) \boldsymbol{\nabla} w_2^h d\Omega^e \tag{4.26}$$

The matrix of the temperature domain terms in the water equation is defined as $\mathbf{K_e}[i+3, j](i = 1,2,3; j = 1,2,3)$

$$\mathbf{K_e}[i+3,j] = \int_{\Omega^e} (\mathbf{K}_{TT}\boldsymbol{\nabla}T^h)\boldsymbol{\nabla}w_1^h d\Omega^e \tag{4.27}$$

The matrix of the temperature domain terms in the heat equation is defined as $\mathbf{K_e}[i+3, j+3](i=1,2,3; j=1,2,3)$

$$\begin{aligned}\mathbf{K_e}[i+3,j+3] = \int_{\Omega^e} C_T \frac{\partial T^h}{\partial t} w_2^h d\Omega^e - \int_{\Omega^e} (\mathbf{B}_{TT}\boldsymbol{\nabla}T^h)\boldsymbol{\nabla}w_2^h d\Omega^e \\ - \int_{\Omega^e} \boldsymbol{\nabla}\cdot\left[(C_l\vec{q_l} + C_v\vec{q_v})T^h\right] w_2^h d\Omega^e\end{aligned} \tag{4.28}$$

The source vector for the water equation is defined as $\mathbf{F_e}[i](i=1,2,3)$

$$\mathbf{F}_e[i] = -\int_\Omega \frac{\partial \theta_v}{\partial t} w_1^h d\Omega - \int_\Omega S w_1^h d\Omega \tag{4.29}$$

And the source vector of the heat water equation is defined as $\mathbf{F_e}[i+3](i=1,2,3)$

$$\mathbf{F}_e[i+3] = -\int_\Omega L\frac{\partial \theta_v}{\partial t} w_2^h d\Omega + \int_\Omega Q w_2^h d\Omega \tag{4.30}$$

where Ω_e is an arbitrary element in the domain discretization Ω.

For the elements that have a node in the boundaries, the source vector is modified by adding a Neumann vector that contains the definition of the flux in the nodes that belong to the Neumann boundary and 0 for the rest of nodes that do not belong to the boundary.

The local matrices are built to store the coefficients of both equations. Due to non-linearity of the hydraulic conductivity and retention water capacity, the solution in the elements is numerically integrated using a three-point Gaussian quadrature formula. Then, the assembly to the global stiffness matrix and the source vector is performed in order to solve the linear system. The resulting linear system is solved in one-dimensional problems by LU decomposition as the direct method, and for a two-dimensional problem by the preconditioned conjugate gradient (PCG), as an iterative method. The non-linear problem is solved by the standard Picard method.

Chapter 5

Computational implementation

5.1 Introduction

This chapter explains the computational process that was carried out to implement the surface and sub-surface evaporation models to the Dual Richards' Unsaturated Equation Solver (DRUtES). For the implementation, two directories named `Evaporation` and `REevap` were created within the directory `models`, following the modular architecture of the selected computer program where all the source files created as result of this work are available. The configuration files are also presented and explained.

5.2 DRUtES

The surface evaporation and sub-surface evaporation models were implemented in the Dual Richards' Unsaturated Equation Solver (DRUtES) (*DRUtES*, 2020) object-oriented library written in Fortran 2003/2008 for solving coupled nonlinear convection-diffusion-reaction equations. DRUtES was first created as part of the doctoral research of Doc. Ing. M. Kuráž as free software that can be redistributed and modified under the terms of the GPL v3 license. As open-source code, DRUtES is continuously evolving due to the developer team's contribution, or independent contributors.

5.3 Surface evaporation

As stated in previous chapters, the surface evaporation model has two main parts, the Richards' equation and the Penman-Monteith equation as a surface boundary condition of the PDE. Richards' equation was already implemented in DRUtES and was not part of this work. Therefore, this implementation's main task was to create the evaporation boundary subroutine, including the time-dependent meteorological records and coupling the boundary condition with the Richards' equation. New source files were created as part of this implementation, but Richards' equation source files were also modified. Within the directory `Evaporation` two source codes file were created: `Re_evap_bc.f90`, and `Re_evap_reader.f90`.

The `Re_evap_bc.f90` module includes the evaporation rate calculation by PM equation, all the parameters needed for, defined in Table 3.1 and Table 3.2. This source file is divided into two subroutines and six functions.

- `evap_datadt_bc`: since the calculation of the evaporation rate strongly depends on the time interval of meteorological records, it is important to identify the data frequency to determine the further treatment of the parameters in the Penman-Monteith equation. The atmospheric data can be provided as hourly, daily, monthly, or yearly data.
- `evap_pm_bc`:this subroutine begins with calling `evap_datadt_bc` to determined the time interval of the meteorological data, and proceed to read maximum temperature, minimum temperature, relative humidity, wind speed, hours of sunlight, and incoming solar radiation. Then, the following functions are used to calculate all the parameters needed for the evaporation rate calculation.
  - `pressure_atm`: calculates the atmospheric pressure based on the elevation.
  - `e_o`: calculates the mean vapor saturation pressure by means of the air temperature.
  - `num_day_fcn`: calculates de number of the day in the year of the current simulation time.
  - `wind_fcn`: calculates the conversation factor for the reference wind speed

measured at 2 m based on the height of measurement.

- `soilheat_fcn`: calculates the soil heat flux based on the difference of temperatures between the current simulation time and the previous simulation time, and the time interval of the data.
- `radiation_fcn`: calculates the net radiation based on the balance of incoming/outgoing longwave and shortwave radiation. Moreover, it takes into account the geographic location of the measured data

Finally, the evaporation rates is evaluated and used in the boundary condition stated in Equation (3.33).

The module `Re_evap_reader.f90` only includes one subroutine `Re_evap_var` where it is read the site location and extra meteorological data information. Since the boundary condition was coupled with the Richards' equation, two existing modules were also modified: `RE_globals.f90` and `RE_pointers.f90`.

`RE_globals.f90` module is allocated for defining all the parameters, and the variable used in the Richards' equations also included the additional variables used in the Penman-Monteith equation. For calculating the net radiation is necessary to know the elevation and latitude where the meteorological records were measured. Additionally, the albedo is also a parameter needed for this implementation. Moreover, to determine the influence of the sun and its rays it is important to consider the annual fluctuations of radiation and its seasonal effect, so the current date is determined by the simulation time and the initial period of the records, then the initial day, month and year should be specified in `evap.conf`.

The potential evapotranspiration boundary condition was included as a case for the boundary conditions options already available in DRUtES. The user can select a range of boundary types for the bottom boundary. For time-dependent boundary types, additional data needs to be supplied. The boundaries are identified by the ID, which for one-dimensional case 101 ID refers to the bottom boundary, and 102 ID refers to the surface boundary, where the meteorological records need to be supplied.

The following boundary types currently implemented for selection of the user are: (0) no boundary condition for this domain, (1) Dirichlet boundary condition where total head

H must be supplied as constant, (- 1) Dirichlet boundary condition, where the pressure is equal to the vertical distance from the defined value, (2) Constant or time-dependent Neumann boundary, (3) Free Drainage condition, (4) Seepage condition, (5) Atmospheric boundary condition where the potential evapotranspiration rate was included. The allocation of the boundary is done by using the case statement, and assigning the subroutine `evap_pm_bc` for the corresponding case.

This model requires three configuration files `global.conf`, `matrix.conf`, `evap.conf`. `global.conf` contains the definition of type of model which for this cases is RE (Richards' equation), the problem dimension, currently implemented in 1D or 2D, the mesh generator, simulation time units (e.g seconds for this implementation), the final simulation time, initial time step and max/min time step. Here, is also needed to define the observation points for printing the simulation results. Finally, in this file more advanced numerical settings can be provided. `matrix.conf` contains all the porous medium parameters needed in the Richards' equation, as the initial condition and specification of the boundary conditions. The last required file is `evap.conf`, here as mentioned before it is needed to specify the latitude, elevation, albedo, initial day, month, and year of the meteorological records.

Additionally, the meteorological records are defined in the file 102.bc, where the following data must be supplied: time[seconds], minimum temperature [°C], maximum temperature [°C], relative humidity [%], wind speed [$\mathrm{m\,s^{-1}}$], hours of sunshine [hours], radiation [$\mathrm{MJ\,m^{-2}\,d^{-1}}$], intensity of rain [$\mathrm{m\,s^{-1}}$], in the same order as described. Overall, this model does not need large additional input information, which can limit its use. On the other hand, the additional data required is widely available, even online. The data for the `evap.conf` the file is always part of any meteorological records, except for albedo. However, albedo is a known value for regions where evaporation evaluation and water management projects were done before since it is an important factor for the evaporation process.

In Figure 5.1 is summarized the relevant files to the implemented surface evaporation model where configuration files structure and subroutines is presented.

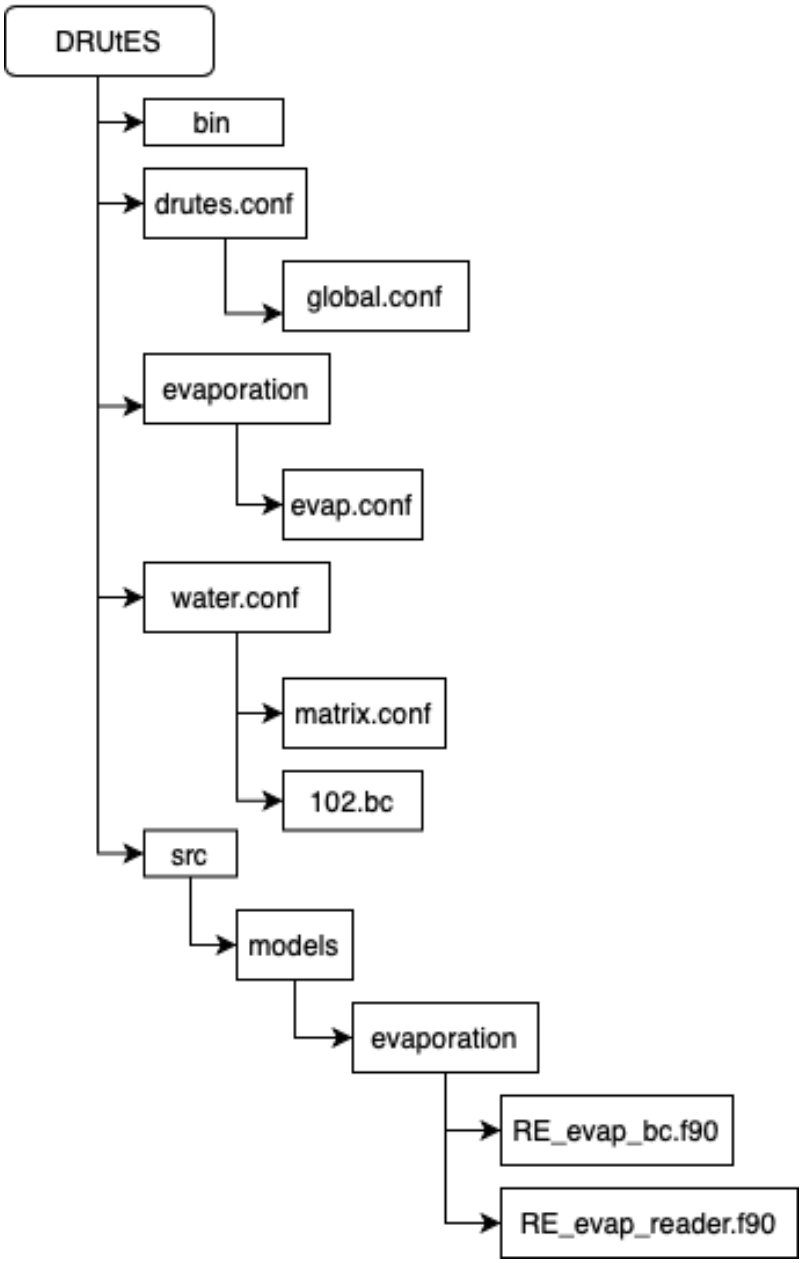

Figure 5.1: Simplified module tree for surface evaporation model.

5.4 Sub-surface evaporation

Due to the object architecture of DRUtES, adding new diffusion-convection-reaction differential equations is possible without having to modify the subroutines intended for the numerical solution of the equations or their linear algebra complements. It is only necessary to identify the coefficients of convection, diffusion, reaction, and capacity, implement and assign them correctly to the corresponding variables.

From Equation (3.63), it is possible to identify the coefficients. Each equation has two

diffusion coefficients due to both pressure and temperature gradient, one convection coefficient, one capacity coefficient, and one reaction coefficient. In Equation (5.1), it is stated the same system of equations with the respective coefficients, where i, j refers to the i-equation and j-coefficient.

$$\begin{cases} E_{1,1}\dfrac{\partial h}{\partial t} = \boldsymbol{\nabla}\cdot(\mathbf{D}_{1,1}\boldsymbol{\nabla}h) + \boldsymbol{\nabla}\cdot(\mathbf{D}_{1,2}\boldsymbol{\nabla}T) + \boldsymbol{\nabla}\cdot(\mathbf{C}_{1,1}\boldsymbol{\nabla}z) - R_{1,1} \\ E_{2,1}\dfrac{\partial T}{\partial t} = \boldsymbol{\nabla}\cdot(\mathbf{D}_{2,1}\boldsymbol{\nabla}h) + \boldsymbol{\nabla}\cdot(\mathbf{D}_{2,2}\boldsymbol{\nabla}T) + +\boldsymbol{\nabla}\cdot(\mathbf{C}_{2,1}\boldsymbol{\nabla}z) - R_{2,1} \end{cases} \tag{5.1}$$

where $E_{i,j}$ are the capacity coefficients, $D_{i,j}$ are the diffusion coefficients, $C_{i,j}$, and $R_{i,j}$ are the reaction terms, define as follows

$$\begin{aligned} E_{1,1} = C_h \quad E_{2,1} = C_T \\ \mathbf{D}_{1,1} = \mathbf{K}_{Th} \quad \mathbf{D}_{1,2} = \mathbf{K}_{TT} \quad \mathbf{D}_{2,1} = \mathbf{B}_{Th} \quad \mathbf{D}_{2,2} = \mathbf{B}_{TT} \\ \mathbf{C}_{1,1} = \mathbf{K}_{lh} \quad C_{2,1} = C_l\vec{q_l} + C_v\vec{q_v} \\ R_{1,1} = -\frac{\partial\theta_v}{\partial t} \quad R_{2,1} = -L\frac{\partial\theta_v}{\partial t} \end{aligned} \tag{5.2}$$

At this point, it is possible to identify that $E_{1,1}$ and $C_{1,1}$ are the same capacity and convection coefficients as the classical Richard's equation, already implemented in DRUtES. In total, six new source files were created during this model implementation as follows:

- `evapglob.f90`: in this file are defined all the parameters used, and input variable used in the sub-surface model.
- `evapextras.f90`: thermodynamics and auxiliary functions were defined in this module according to Chapter 3.
- `evap_RE_fnc.f90`: this module contains the capacity, diffusion, convective, and reaction coefficients of water flow partial differential equation.
- `evap_heat_fnc.f90`: this module contains the capacity, diffusion, convective, and reaction coefficients of heat flow partial differential equation.
- `REevapbc.f90`: the Neumann boundary condition for water equations was implemented in this module
- `heatevapbc.f90`: the Robin boundary condition for heat equation was imple-

mented in this module.

- `evappointers.f90`: is the source file where the construction of the PDEs is happenning. First the allocation of the couple problem is stated, after, the call of the needed subroutine is done to allocate $E_{1,1}$ and $C_{1,2}$ from the classical Richard's equation, and the overwrite by the subroutines in `evap_RE_fnc.f90` and `evap_heat_fnc.f90`. In the allocation, it is also assigned the flux and the boundary conditions to each differential equation.

By allocating the classical Richards' and heat equations already implemented in DRUtES, it is granted access for the definition of initial and boundary conditions (Neumann and Dirichlet type), which still applies to these two new formulations. Although, the model presented in Chapter 3 suggested a Robin Boundary type for the heat equation at the soil surface, the boundary condition was implemented as Neumann boundary type. The Neumann boundary condition can be mathematically stated as

$$\vec{q}_T \cdot \mathbf{n} = -G \quad \forall \mathbf{x} \in \Gamma_{surf} \times [0, T) \tag{5.3}$$

Since the allocation of the initial condition is the same as the classical heat equation, `heat.conf` should also be supplied as a configuration file.

In Figure 5.2 is summarized the relevant files to the implemented sub-surface evaporation model where configuration files structure and subroutines are presented. The `mesh` directory is reserved for the mesh configuration files; for this work, the internal 1-dimensional mesh generator of DRUtES was used. However, it is possible to read different third-party mesh files.

The fully coupled set of equations for liquid water, water vapor, and heat transport may seem at first sight that significantly more parameters are needed than the classical Richards' model decoupled heat model. As presented, the soil non-thermal hydraulic properties are described by the same parameters needed to simulate variably saturated liquid water flow based on the Richards equation. The thermal liquid and vapor fluxes are fully described by the functions presented in Table 3.3.

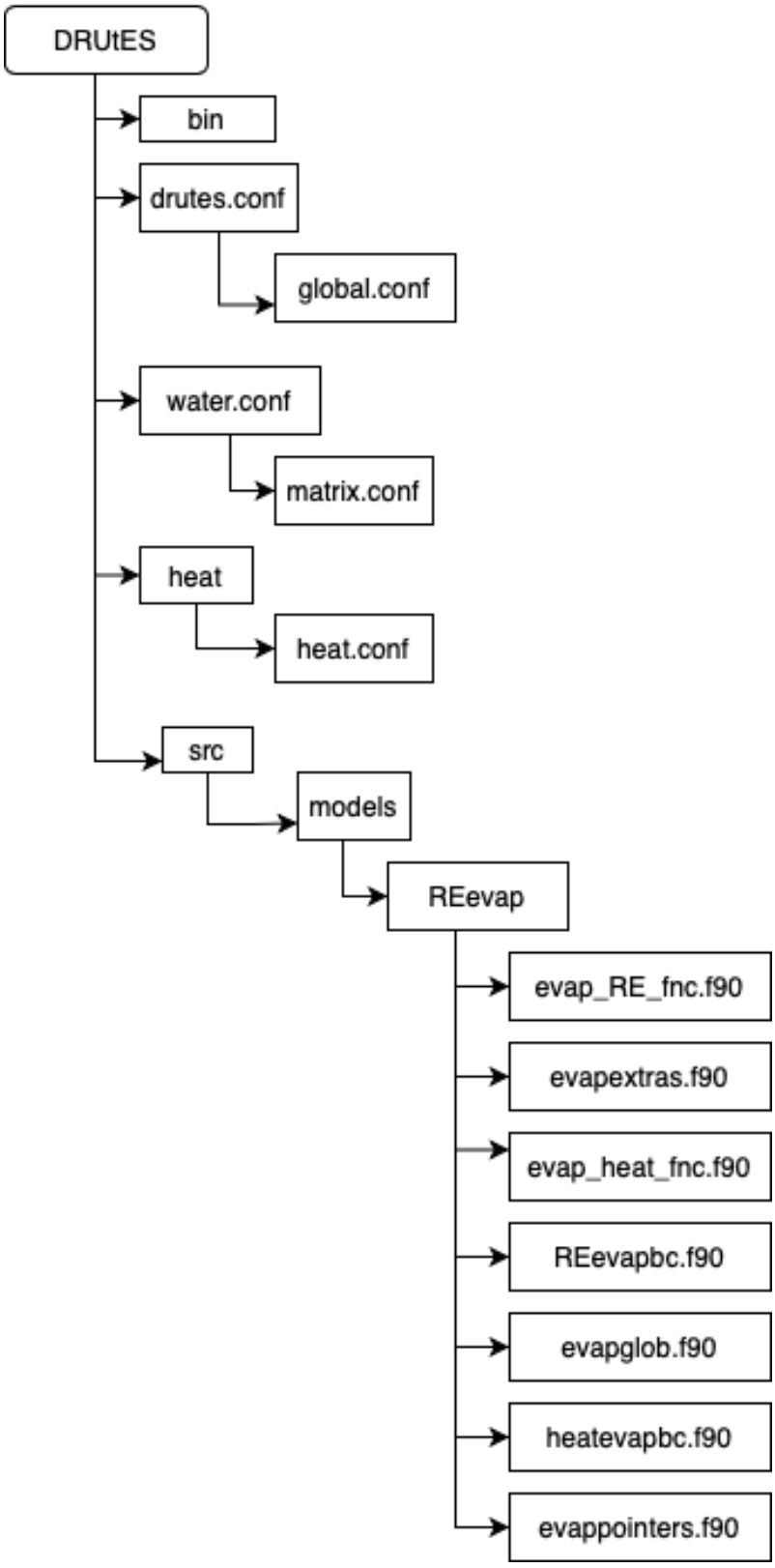

Figure 5.2: Simplified input tree for sub-surface evaporation model.

Chapter 6

Benchmark case of study

6.1 Introduction

This chapter presents the benchmark cases used to test and evaluate the performance of both models, the surface, and the sub-surface evaporation. Two scenarios were proposed under controlled meteorological conditions that allowed to identify the effect of variables to the system and validate with the theory given in Chapter 2.

Incoming shortwave radiation is a substantial factor affecting the evaporation process, and it was selected to be the constraint variable to evaluate the implementation of the models. The first scenario is known as a dark condition where no incoming shortwave radiation was considered, $Rs = 0$; the second scenario is characterized by constant incoming shortwave radiation, Rs= constant. Under these two simulation conditions, the results were depicted and analyzed.

This chapter begins with the description of the shared input for both models simulations and continues describing the particular conditions of the simulations with the surface evaporation model and its results. Furthermore, this chapter finalizes describing the particular conditions of the simulations with the coupled water and heat flow, and its results.

6.2 Input

In this study, one soil texture was chosen from the database of Carsel et al., 1988. Hydraulic conductivity is one of the sources of numerical difficulties when using the Richards

equation. Sand, for instance, has a significant α and n parameters that cause the curve to be steeper and numerically challenging. To avoid numerical instability, the parameters shown in Table 6.1 were slightly modified to guarantee smooth simulations.

Table 6.1: Soil hydraulic parameters based on van Genuchten and Mualem models.

Input	**Symbol**	**Units**	**Value**
inverse of air entry value	α	m^{-1}	5e-2
Saturated hydraulic conductivity	$\mathbf{K}_s$	$\mathrm{m\,s}^{-1}$	5.7e-6
Saturated volumetric water content	θ_s	-	0.36
Residual volumetric water content	θ_r	-	0.07
shape parameter	n	-	1.09
shape parameter	m	-	0.082

Based on the hydraulic parameter, water retention and hydraulic conductivity were generated and depicted in Figure 6.1.

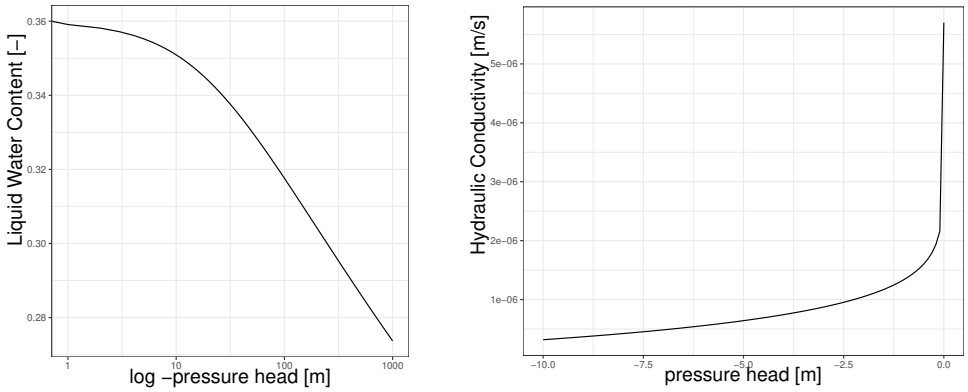

(a) Soil water retention curve (b) Soil hydraulic conductivity

Figure 6.1: Soil hydraulic curves used in the simulation cases.

Besides the hydraulic properties, the numeric parameters were consistent across all the simulations and constraint by the need for small time-steps for solving Richard's equation in both models, including the couple water and heat. The simulated experiments had a total simulation time of 14 days. For the classical Richards' equation, 14 observation times were used the same as a day in the simulation, for the coupled heat and water flow model 17 observation times were used to capture the first stage of evaporation in more detail. The simulation parameters are shown in Table 6.2.

Table 6.2: Simulation parameters used in simulation case on DRUtES.

Input	**Units**	**value**
Simulation time	s	1209600
Minimum time step	s	0.001
Maximum time step	s	10
iteration criterion Picard method	-	1e-04

To ease the analysis and assess the models' respect for the accuracy of capturing the phenomena involved, the experiments were carried out in one dimension (1D). A simple evaluation of the mesh was complete, in order to minimize any numerical oscillations in the results and differences while comparing. For the hydrodynamic model, the mesh density was 0.002, generating 100 nodal points. However, this density was not optimum for the couple hydro and thermodynamics simulations. The sparse matrix for the coupled problem has more non-zero elements that increase the computational time when the direct LU decomposition is used to solve the linear system of equations. Due to the matrix structure, the mesh density was set as 0.01 generating 20 nodal points. The author acknowledges the importance to execute a mesh optimization process during the simulation study, and strongly recommend to evaluate in detail the impact of the mesh density on the coupled water and heat model in the future.

6.3 Surface evaporation

Surface evaporation was evaluated using the model presented in the first part of the Chapter 3. The 20 cm long soil profile was divided into 100 elements, with observation points at depths 0, 5, 10, 15, 18, and 2 cm. DRUtES generated the observation files at these points to compare pressure head, water content, and Darcy flux. The bottom boundary of the domain was set as Neumann no flux boundary type (at $z = 0$), mathematically expressed as follows.

$$\frac{\partial h(\mathbf{x}, t)}{\partial \mathbf{n}} + n_3(\mathbf{x}) = 0 \quad (z = 0, t) \in \Gamma_{bottom} \times [0, T) \tag{6.1}$$

Furthermore, the boundary condition at the soil interface was set as the Neumann atmospheric boundary (at $z = 0.2$). mathematically expressed as

$$\mathbf{K}(h)\left(\frac{\partial h(\mathbf{x},t)}{\partial \mathbf{n}}+n_3(\mathbf{x})\right)=q_{\Gamma_{surf}}(t)\quad (z=0.2,t)\in\Gamma_{surf}\times[0,T) \tag{6.2}$$

It is essential to mention that there is not a Dirichlet boundary condition defined in the system; thus, the uniqueness of the solution is not guaranteed when the water retention capacity term $C(h)$ vanishes. The initial condition can be seen as a Dirichlet temporal-spatial condition as well if the initial conditions can keep the connection with both Neumann boundaries. This situation is critical under near-saturated conditions in the soil for the Richards equation when the retention capacity term becomes small. If the retention capacity is zero, the system is singular, and it nos possible to be solved. Hence, the system is not fully defined as only the first derivatives are provided when a problem is only allocated by Neumann boundary conditions.

During the drying process, the problem arises with the hydraulic conductivity and its parameterization, where van Genutchen- Mualem model has been proved to lead to numerical instabilities. Also, the model underestimates the unsaturated hydraulic conductivity when the water content is closed to the residual water content (Sakai; Jones, et al., 2011). Furthermore, the motivation to set this boundary as Neumann is purely physical. This condition assumes the water table is located far below the domain. It is especially useful to evaluate the drying process where the system has no other flux of water but only the one driven by the evaporation (Saito et al., 2006; Sakai; Jones, et al., 2011). This previous statement was assumed for both models implemented in this work. Figure 6.2 illustrates the domain used to conduct the simulation experiments.

Uniform total hydraulic head of -0.1 m was given as initial condition that implies a linear distribution of pressure head along with the vertical domain $h = 0.1 - z$. It can be expressed mathematically as

$$H(z,0)=-0.1\quad \forall z\in\Omega \tag{6.3}$$

The controlled atmospheric conditions were assured by setting up constant value for maximum and minimum temperature, air relative humidity, and wind speed. For the dark scenario, the value of sunshine hours and incoming solar radiation were set both as zero.

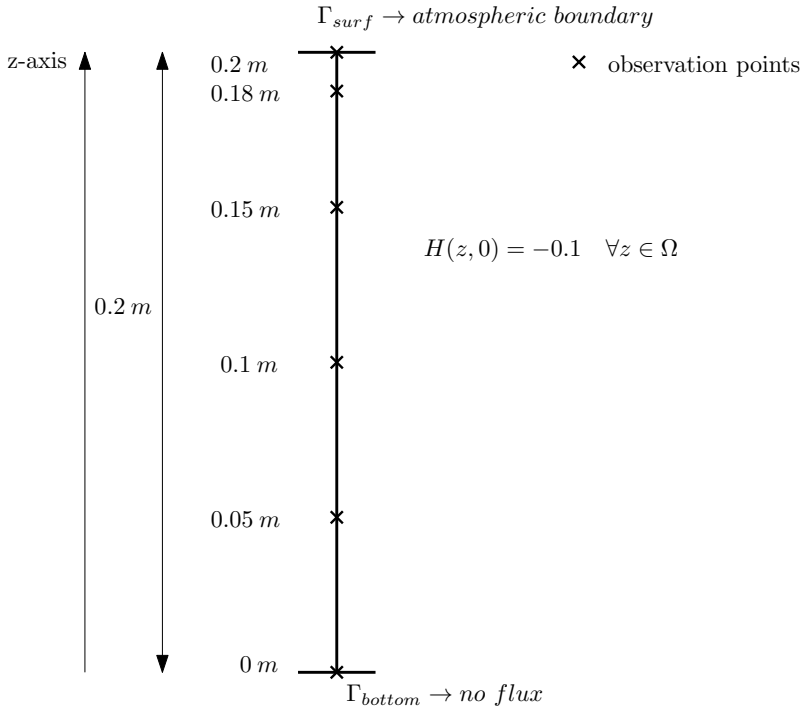

Figure 6.2: 1D domain set-up of Richards equation coupled with Penman-Monteith equations as a boundary condition.

While for the constant radiation, they were constant non zero values as 2 and 8, respectively. The atmospheric conditions are summarized in Table 6.3.

Table 6.3: Input atmospheric parameters for zero shortwave radiation and constant shortwave radiation.

Input	**units**	**Rs=0**	**Rs=const**
Minimum temperature	°C	20	20
Maximum temperature	°C	25	25
Relative humidity	%	50	50
Wind speed	$\mathrm{m\,s^{-1}}$	2	2
Sunshine hours	hrs	0	2
Solar radiation	$\mathrm{MJ\,m^{-2}\,d^{-1}}$	0	8
Albedo	-	0.23	0.23

6.3.1 Results and discussion

As the atmospheric parameters were constant during all the simulation for both scenarios, shortwave radiation equal to zero and constant, the evaporation rate is constant. According to the Penman-Monteith equation (see Equation (3.34)), the energy flux is balanced by the difference between the net radiation and the soil heat flux. As the air temperature is constant, the soil heat flux is zero for both cases, and the net radiation dominated the evaporation process. Hence, an increase in the shortwave radiation caused an increment

in the net radiation and, consequently, in the evaporation rate.

Table 6.4: Results of numerical simulation of evaporation rate and energy fluxes for scenario without shortwave radiation and without shortwave radiation.

Scenario	**Rs = 0**	**Rs = const**
Evaporation rate [mmd^{-1}]	1.6988	4.4138
Soil heat flux [$MJd^{-1}m^{-2}$]	0	0
Net radiation [$MJd^{-1}m^{-2}$]	2.035	5.988

The approximation provided by the Penman-Monteith method corresponds to the maximum value of stage I of the evaporation process. It is often seen as the upper boundary of the evaporation rate and called the potential evaporation rate. This approach ignores the evaporation happening inside the soil and only takes into account that evaporation occurs at the surface of the soil. Therefore, stage II is not considered, and the vapor flux is neglected. The assumptions of the PM equation have been proved to be insufficient for estimating the evaporation rate in several experimental studies and simulations (e.g., (Wilson et al., 1994)). During stage I, the evaporation process is controlled primarily by the atmospheric conditions and, to a lesser extent, by the soil properties, which validate this model during this stage.

Figure 6.3 shows the depth distribution of pressure head and water content along with the soil profile for all the simulated days, without shortwave radiation and with shortwave radiation. For the scenario without shortwave radiation, the profiles have a linear distribution with depth, expected behavior for the stage I.

Usually, during the transition from stage I and II, the non-linearity characterizes the pressure head, and water content profile distribution during stage II. The development of non-linearity in the profiles can be correlated with high evaporation rates, which are observed with shortwave radiation. Since this model does not capture the stage II of the evaporation process, the non-linear trend for the scenario with shortwave radiation, the onset of stage II is not the explanation.

As the evaporation progress, the surface dried out, and the water content is close to the residual water content, as shown in Figure 6.4. Although the evaporation rate keeps constant, the system generates a large pressure gradient at the surface to maintain the boundary condition, approximately -15000 m (see Figure 6.3). At this moment, small

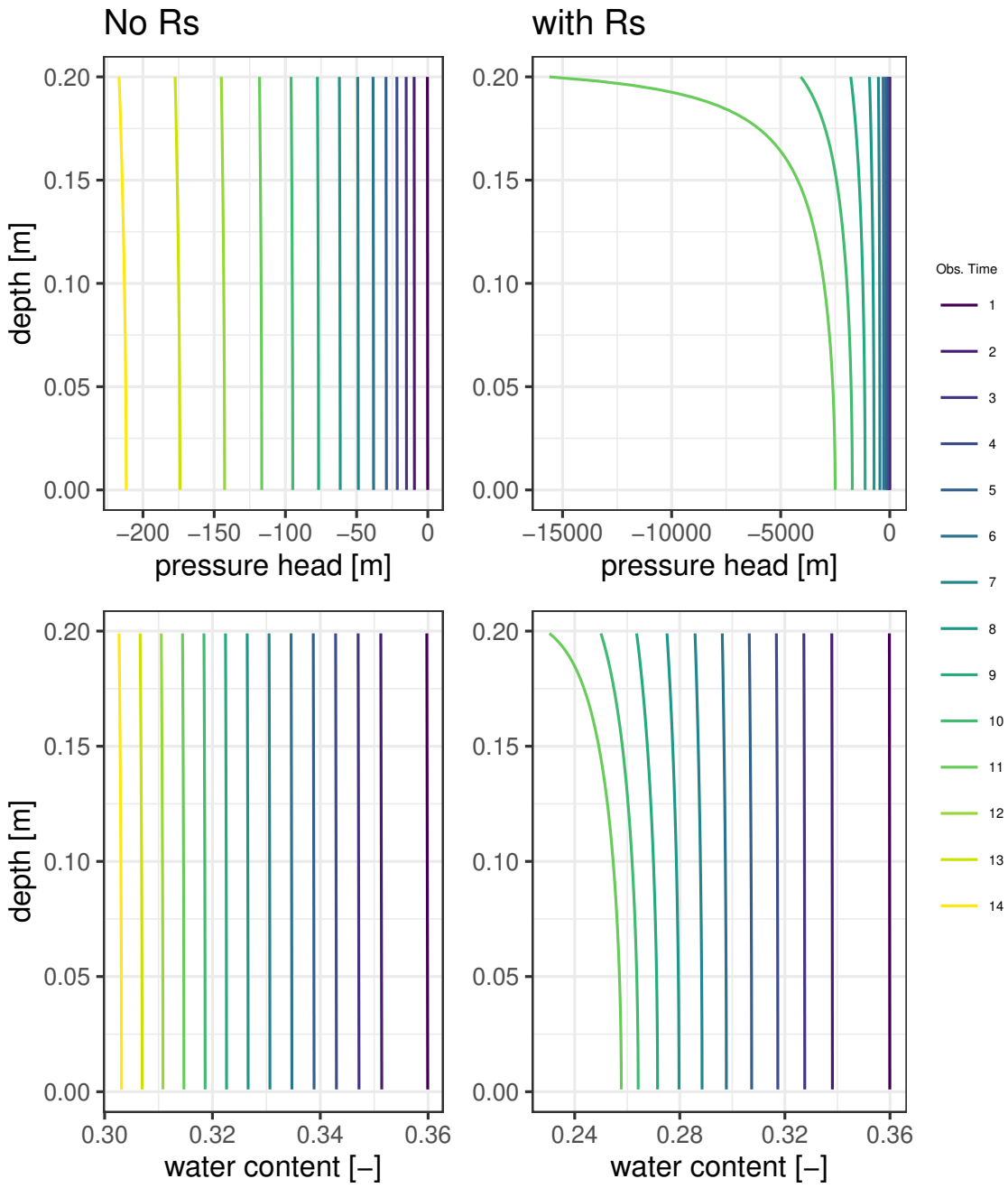

Figure 6.3: Results of numerical simulation of Pressure head (upper) and water content (bottom) with shortwave radiation (right) and without shortwave radiation (left) for the simulation time in the domain.

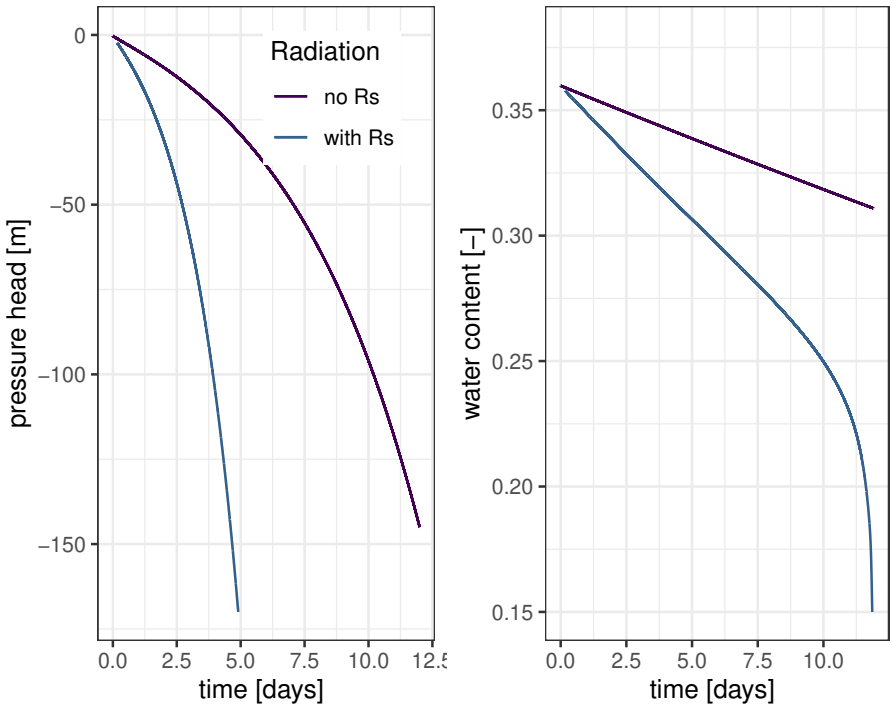

Figure 6.4: Results of numerical simulation of vertical distribution of pressure head (upper) and water content (bottom) at different simulation times without shortwave radiation (left) and with shortwave radiation (right).

changes in the water content lead to significant changes in the pressure head, and the simulation is no longer stable. Once the large gradient was developed at the boundary, the simulation did not proceed and stop around day 11.

For the dark scenario, the evaporation rate was small enough not to dry the surface significantly during the simulation time (see Figure 6.4 right). Hence, the soil could maintain the flux at the boundary without developing large gradients in pressure. By setting the shortwave radiation as 8 MJ m^{-2} d^{-1} certainly, the evaporation rate increased, and there was not soil heat flux to balance the energy at the surface and then decreased the evaporation flux. In inclusion, the results are in agreement with the assumption of the Penman-Monteith equation and its limitation.

By integrating the evaporation rate is possible to quantify the total losses of water due to evaporation. In the specific case where the evaporation rate is constant, the cumulative evaporation flux is linear. The cumulative evaporation flux is a crucial function to analyses specifically in industrial applications of water sources and their storage to minimize the losses by evaporation.

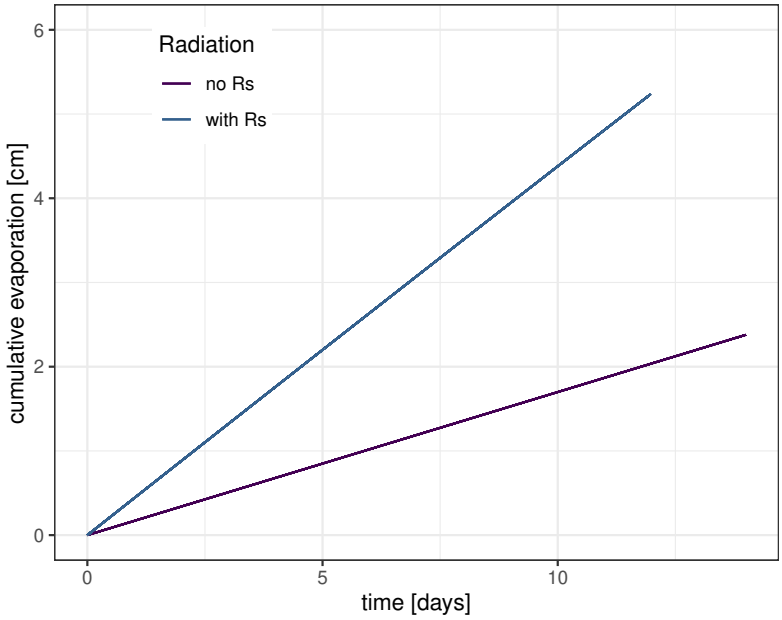

Figure 6.5: Results of numerical simulation of cumulative evaporation flux without shortwave radiation and with shortwave radiation.

6.4 Sub-surface evaporation

Surface evaporation was evaluated using the model presented in the second part of the Chapter 3. The 20 cm long soil profile was divided into 100 elements, with observation points located at depths 0, 5, 10, 15, 18, 2 cm. Two conditions must be supplied at each boundary as initial conditions since two coupled partial differential equations were solved in this model. The bottom boundary of the domain was set as Neumann no flux boundary type ($z = 0$) for water (Equation 6.4) and heat flow (Equation 6.5), these can be mathematically expressed as

$$\frac{\partial h(\mathbf{x}, t)}{\partial \mathbf{n}} + n_3(\mathbf{x}) = 0 \quad (z = 0, t) \in \Gamma_{bottom} \times [0, T) \tag{6.4}$$

$$\frac{\partial T(\mathbf{x}, t)}{\partial \mathbf{n}} + n_3(\mathbf{x}) = 0 \quad (z = 0, t) \in \Gamma_{bottom} \times [0, T) \tag{6.5}$$

The boundary condition at the soil interface was set as the Neumann atmospheric boundary ($z = 0.2$) for the water equation determined by the evaporation rate, and Robin boundary equals the soil heat flux determined by the surface energy balance for the heat equation. Both conditions are expressed mathematically as follows.

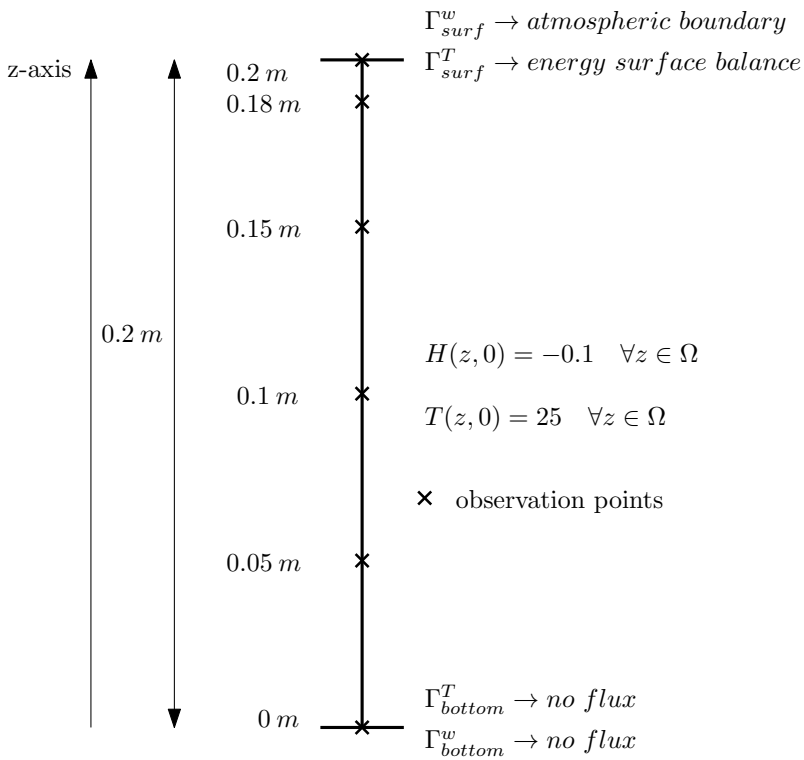

Figure 6.6: 1D domain set-up of water coupled with heat flow model.

$$\| \vec{q_v}(\mathbf{x},t) \|_{\mathbf{x}=\mathbf{n}} + \| \vec{q_l}(\mathbf{x},t) \|_{\mathbf{x}=\mathbf{n}} = E_v(t) \quad (z = 0.2, t) \in \Gamma_{surf} \times [0,T) \tag{6.6}$$

$$\vec{q_T} \cdot \mathbf{n} = -G \quad (z = 0.2, t) \in \Gamma_{surf} \times [0,T) \tag{6.7}$$

Uniform total hydraulic head of -0.1 m was given as initial condition that implies a linear distribution of pressure head again along with the vertical domain $h = 0.1 - z$ and an initial temperature of the system of 25°C the same as the air temperature. Figure 6.6 illustrates the domain used to conduct the simulation experiments.

$$H(z,0) = -0.1 \quad \forall z \in \Omega \tag{6.8}$$

$$T(z,0) = 25 \quad \forall z \in \Omega \tag{6.9}$$

Similarly to the previous model, the controlled atmospheric environment was applied, and two scenarios were studied: the dark and the constant shortwave radiation. The

atmospheric conditions are summarized in Table 6.5.

Table 6.5: Input atmospheric parameters for zero shortwave radiation and constant shortwave radiation.

Input	**units**	**Rs=0**	**Rs=const**
Air Temperature	°C	25	25
Relative humidity	%	50	50
Radiation	$\mathrm{W\,m^{-2}}$	0	100
Albedo	-	0.23	0.23

6.4.1 Results and discussion

In order to present and evaluate the simulated results, the discussion starts analyzing the hydro and thermodynamics at the boundary employing the time series of the evaporation rate for different values of air resistance that leads the discussion further to the solution of the state variables (h, θ, T) in the entire domain. Finally, some numerical aspects will be presented as the last remarks.

Water and heat dynamics at the atmospheric boundary

Figure 6.7 shows the results of evaporation rate and surface temperature for scenarios without shortwave radiation (left) and constant shortwave radiation (right) using three different aerodynamic resistances. The evaporation rate decreases rapidly at the beginning of all the scenarios. Thereafter, it stabilizes and becomes close to constant value during stage I. Further, the evaporation rate decreases again during stage II and stabilizes again when approximating to 0, which is considered as the stage III by Wilson et al., 1994. Stage I and Stage II are distinguished for both scenarios and all values of air resistances. A mean stage I evaporation rates ranged from 0.2 to 1 $\mathrm{cm\,d^{-1}}$ for dark scenarios and from 0.35 to 1.4 $\mathrm{cm\,d^{-1}}$ for constant radiation scenarios. The duration of stage I is longer for dark scenarios than for constant shortwave radiation scenarios. Hence, the higher the evaporation rate during stage I, the shorter the duration of the first stage. Scenarios with lower air resistance present higher evaporation rate, expected behavior from a direct analysis of the Equation (3.69), and validated from the results. However, the relation between the evaporation rate and air resistance is not linear since the dependency between temperature and vapor density is not linear, and consequently to the air vapor pressure.

The initial decrease of the evaporation rate is caused by the decrease of soil surface temper-

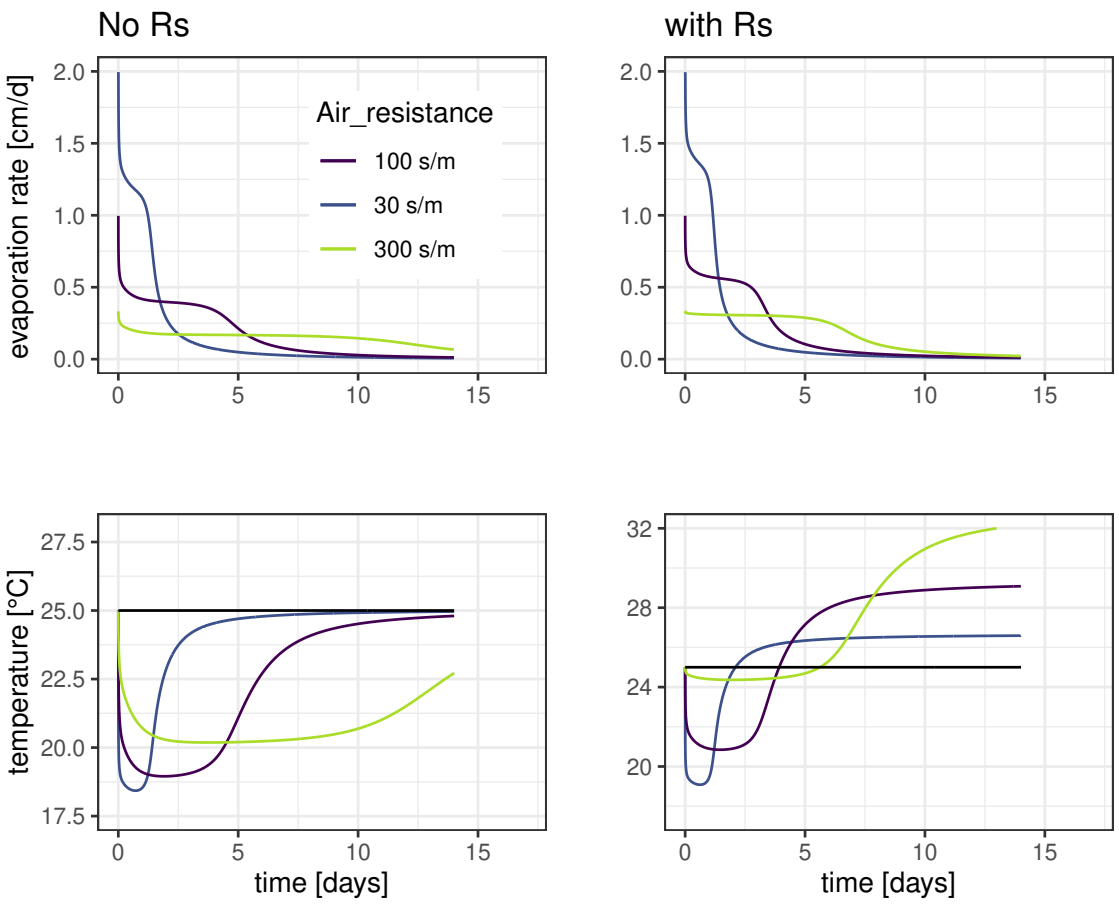

Figure 6.7: Results of numerical simulation of the evaporation rates (upper) and soil surface temperature (bottom) time series for different values of the air resistance r_a, without shortwave radiation (left) and with shortwave radiation (right).

ature (Figure 6.7 bottom). For dark scenarios, the drop in temperature ranged from 18.5 to 20.1 ℃ and for the constant radiation from 19 to 24.3 ℃. The temperature fluctuations at the surface are due to the heat loss from the latent heat of vaporization during stage I. It leads to a proportional decrease in the losses during stage II. The drop in surface temperature decreased the soil surface vapor density (see Figure 6.8 upper left and right).

According to soil relative humidity time series (see Figure 6.8 upper left and right), the end of stage I occurs when relative humidity becomes smaller than one at the surface. From the beginning of stage II, the relative humidity governs the evaporation rate even though the temperature is increasing during this period and consequently increased in the saturation vapor density and stabilization of the vapor density. A sudden but smaller drop in the evaporation rate can be noticed in stage II with an increase in the temperature. These alterations in the system occurred when the soil dried out, leading to low volumetric water content. At the begging of stage II, the pressure head rises as shown in Figure 6.9,

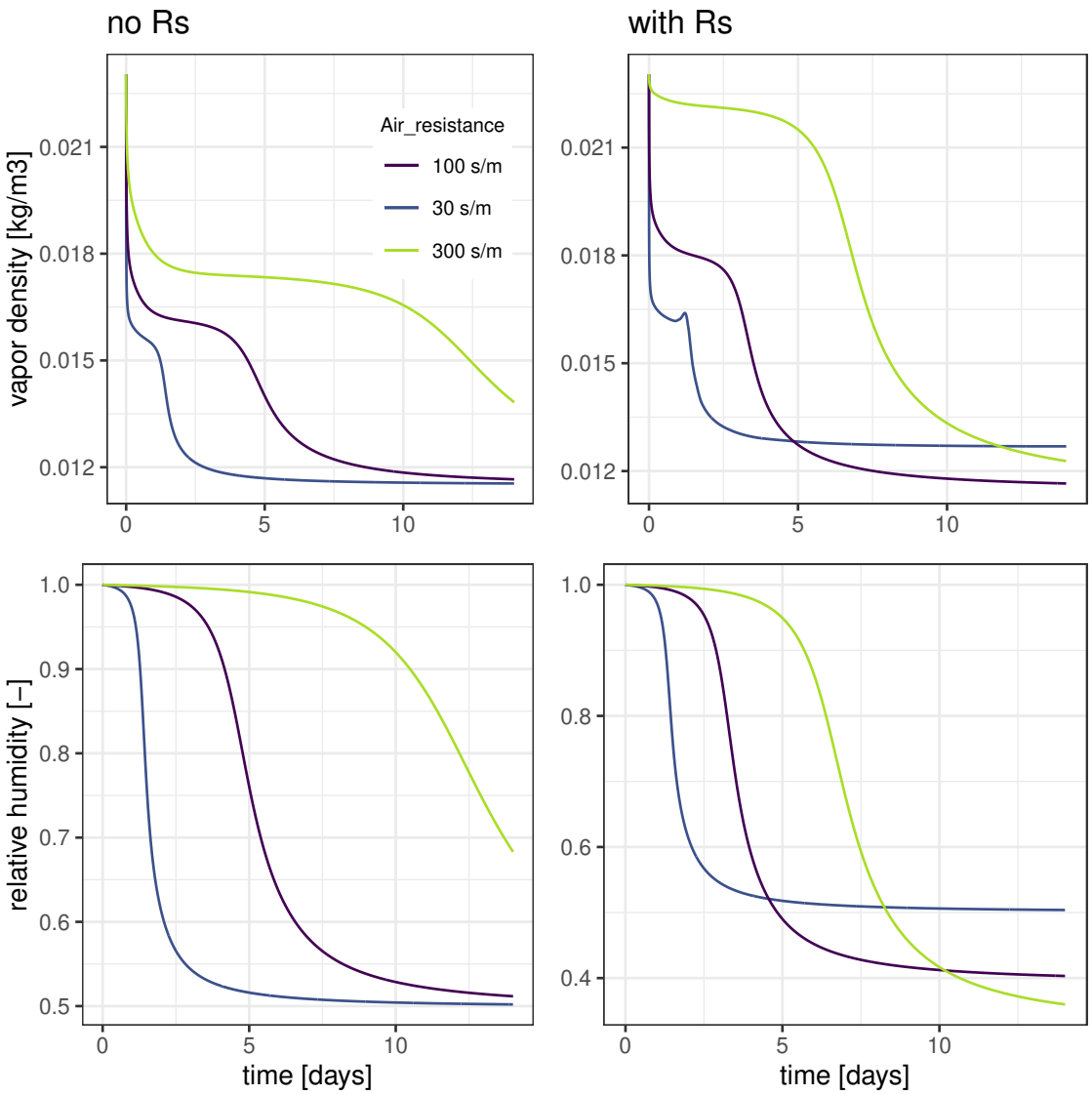

Figure 6.8: Results of numerical simulation at the soil surface of vapor density(upper) and soil relative humidity (bottom) time series for different values of the air resistance r_a, without shortwave radiation (left) and with shortwave radiation (right).

while the drying front progressed in the soil, small changes in water content leads to a significant increase in the pressure head, this increase affects the relative humidity causing a reduction that subsequently decrease the evaporation rate. The stage III is blurred and somewhat arbitrary, where is driven only by a vapor-diffusion process and it can be seen as the ending of the evaporation process as the system balance with the atmosphere and tends to the equilibrium.

The evaporation process stops when the vapor pressure in the adjacent layer of air and the vapor pressure at the surface boundary of the soil is in equilibrium. Therefore, the equilibrium is defined when these two quantities are equal. The vapor density of the

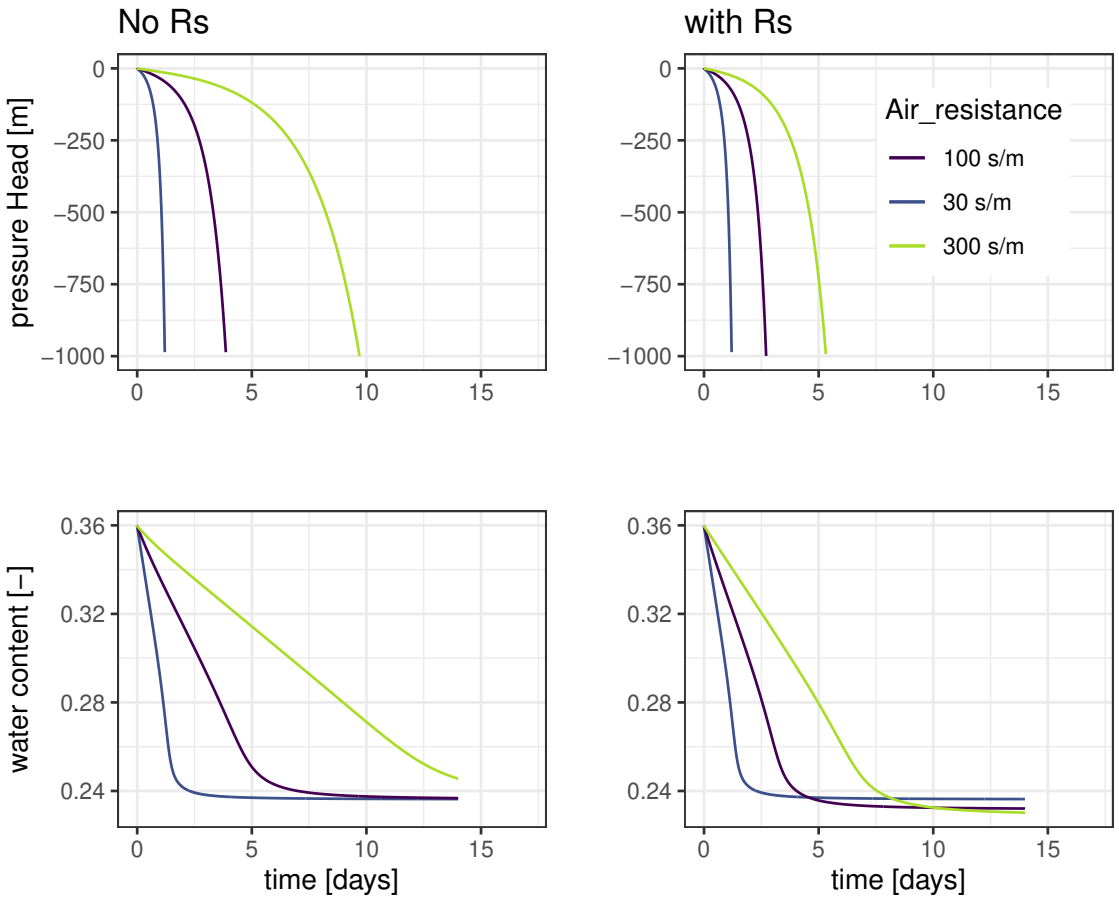

Figure 6.9: Results of numerical simulation of pressure head (upper) and liquid water content (bottom) time series for different values of the air resistance r_a, without shortwave radiation (left) and with shortwave radiation (right) at the surface boundary.

atmosphere is approximately 0.00864 kg m^{-3}, from Figure 6.8, it is possible to conclude that for the scenarios without shortwave radiation, the cases with $r_a = 30\,\mathrm{s\,m^{-1}}$ and $r_a = 100\,\mathrm{s\,m^{-1}}$ reach the equilibrium, while for the dark scenario and case of $r_a = 300\,\mathrm{s\,m^{-1}}$, the equilibrium was not accomplished yet as for all the cases with constant shortwave radiation.

At the equilibrium, it is possible to quantify the total losses of water from the soil due to the evaporation by the difference between the amount of water stored in the soil at the initial time and the water content at h= -7500 m (see Figure 6.11 upper right) multiplied by the length of the domain, for the case of $r_a = 100\ \mathrm{s\,m^{-1}}$, the cumulative evaporation rate is 2.4 cm, as shown in Figure 6.10. In conclusion, the stage I of evaporation is dominating by the hydrodynamics while stage II is dominating by the thermodynamics where the vapor flux is dominant.

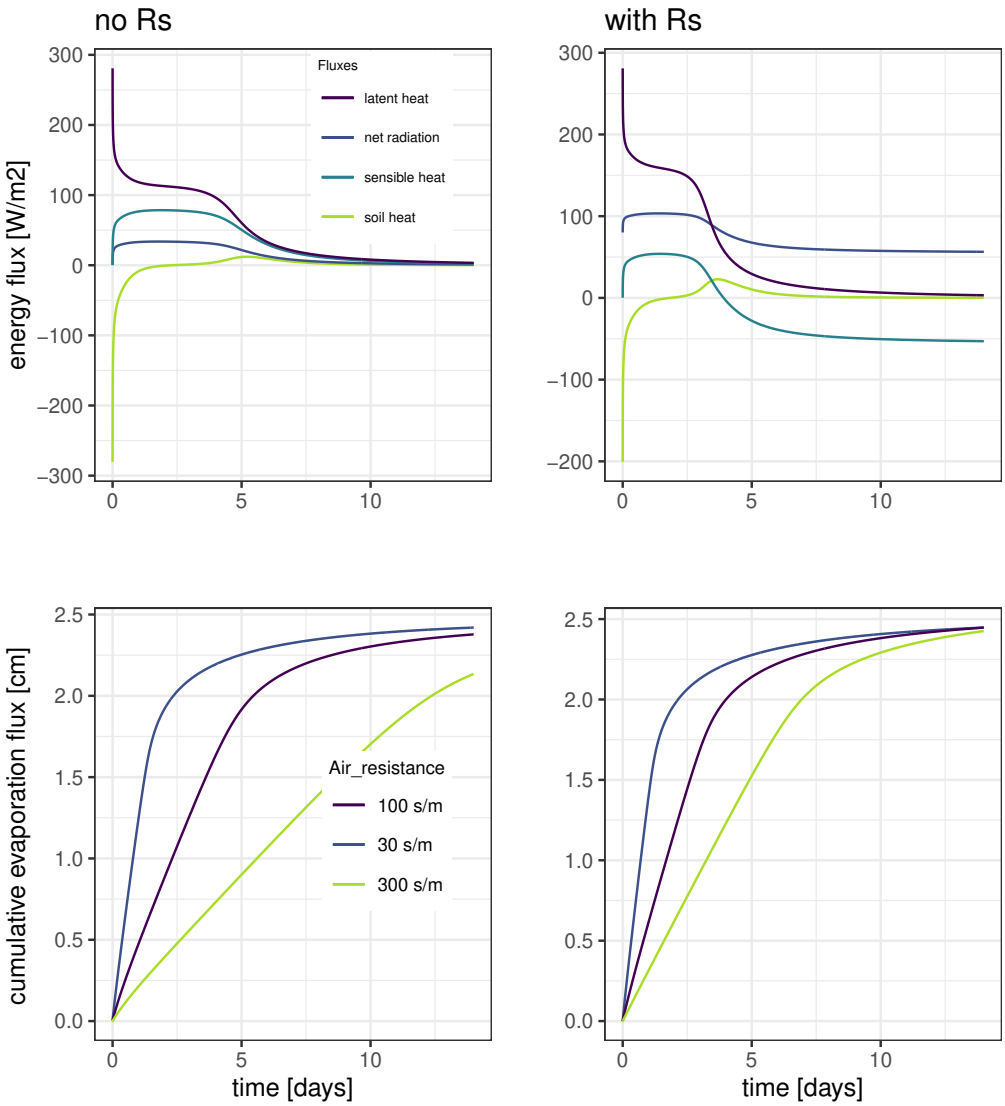

Figure 6.10: Results of numerical simulation of the components of the surface energy balance (upper) for $r_a = 100$ s m^{-1} and cumulative evaporation flux (bottom) without shortwave radiation (left) and with shortwave radiation (right) with different values of air resistance r_a.

Figure 6.10 shows the components of the surface energy balance for the case where $r_a = 100$ s m^{-1}. The soil heat flux G is negative (downward) at the beginning of stage I when the soil is warming and shows a change in the trend with a short peak approximately in day 5 (or earlier for the scenario of constant shortwave radiation) at the beginning of stage II. The peak represents the flux of latent heat towards the surface. Besides, the net radiation has a strong impact on the surface temperature and the retardation of the equilibrium state of the system. It is evident in Figure 6.10 (upper right), where fluxes have not reached the equilibrium yet. Net radiation, R_n, is leading the flow of energy towards the colder soil surface, and it is expected to tend to zero as stage II took place.

Despite the differences in the domain set-up, the presented results agree with the ones reported by Sakai; Jones, et al., 2011; Or et al., 2013; Saito et al., 2006; Wilson et al., 1994; Iden et al., 2019.

Depth profiles of state variables

Figure 6.11 shows the depth distribution of the pressure head, the water content, and the temperature for different simulation times for a value of air resistance equal to 100 $\mathrm{s\,m^{-1}}$ with shortwave radiation and without shortwave radiation. At the beginning of the simulation, the depth distribution of h, θ_l, T is linear, similar to the first model with constant shortwave radiation. With the progressing of the evaporation over time, the depth distribution of the three variables becomes not linear. The non-linear distribution is presented faster in higher evaporation rates, which can be observed with shortwave radiation.

The non-linearity of the profiles is due to the transition from stage I and II, especially impacting the pressure head. The pressure head distribution shows a robust non-linear behavior during stage II when the suction drastically increased at the top boundary. The resulting impact is the decrease in the evaporation rate and a large pressure head gradient.

The gradient of the three state variables was zero at the beginning of all the simulations, and as the time progress, the gradient became greater. It is expected that when the soil dried out until the equilibrium, the gradient should be zero, where the pressure head, water content, and temperature were the same among the depth profile. The simulation time seemed insufficient for the hydrodynamics process to reach the equilibrium, while the temperature reached gradient zero around day 11. It is clear for scenarios with shortwave radiation and aerodynamic resistance higher than 30 $\mathrm{s\,m^{-1}}$, the simulation did not last enough to evaporate the maximum amount of water available and reach the equilibrium.

Anticipating the numerical instabilities of the unsaturated hydraulic parameterization, the residual water content was lower than the value reached at the end of the simulation time for the whole domain and far from the residual value.

As can be expected, the convective flux is dominant mechanism transport that must not be neglected when modeling evaporation in soils. Equation (6.10) is depicted as a sample of the local stiffness matrix in the surface node, where the evaporation process takes place

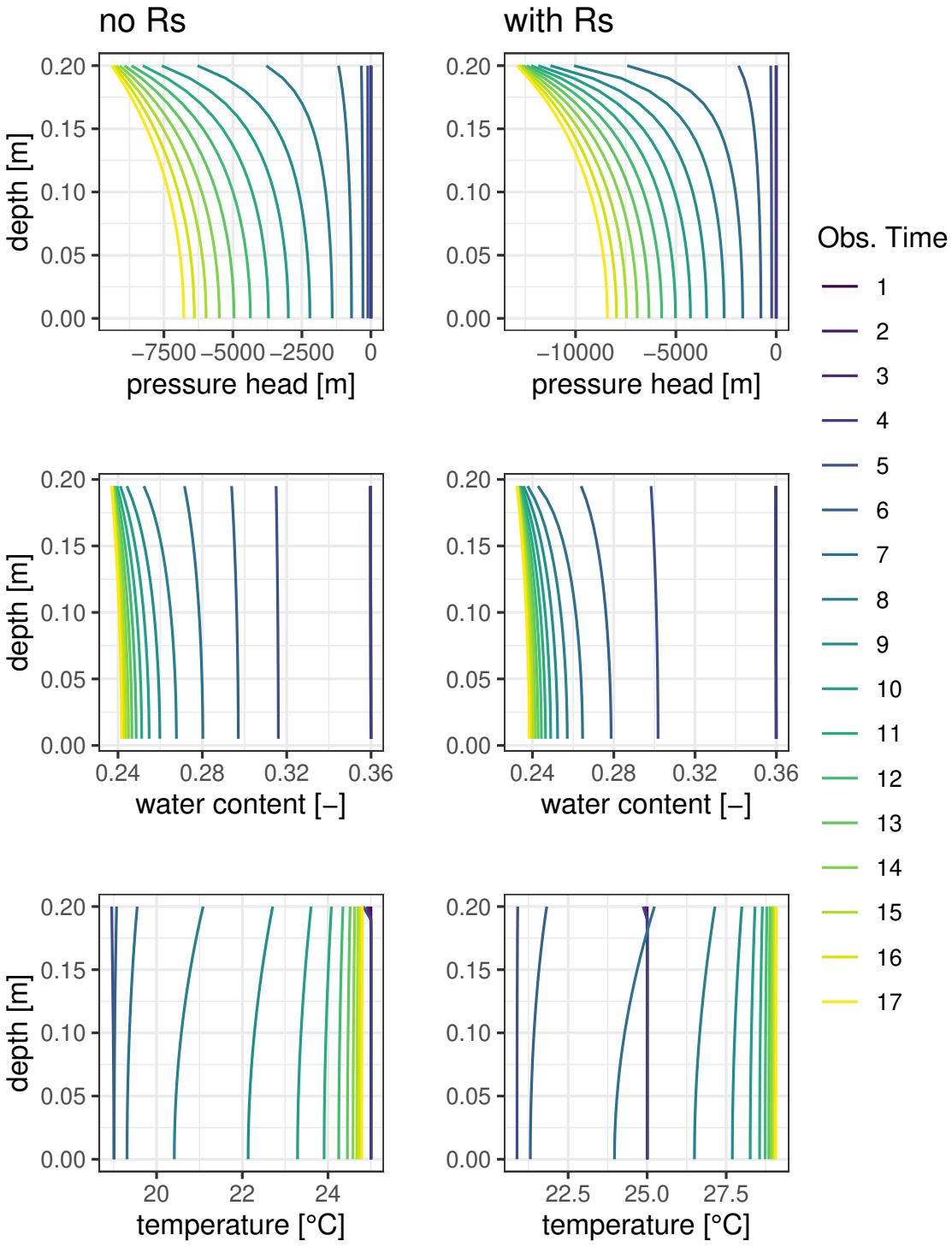

Figure 6.11: Results of the numerical simulations with an aerodynamic resistance $r_a = 100\,sm^{-1}$. Vertical distribution of pressure head (top), volumetric water content (middle), and temperature (bottom) at different simulation times without shortwave radiation (left) and with shortwave radiation (right).

mainly during the simulation time. Diffusion dominant problems are characterized by asymmetric stiffness matrix, while dominant convection problems are characterized by a non-symmetric matrix.

$$\begin{pmatrix} -1.899 \times 10^{-4} & 1.851 \times 10^{-4} & -1.215 \times 10^{-5} & 1.215 \times 10^{-5} \\ 1.845 \times 10^{-4} & -1.894 \times 10^{-4} & 1.215 \times 10^{-5} & -1.215 \times 10^{-5} \\ -7.490 \times 10^{-9} & 7.490 \times 10^{-9} & -1.6101 \times 10^{4} & 1.701 \times 10^{3} \\ 7.490 \times 10^{-9} & -7.490 \times 10^{-9} & 1.698 \times 10^{3} & -1.6098 \times 10^{4} \end{pmatrix} \tag{6.10}$$

Due to the coupling structure of the local matrix and recalling how the assembly of the local matrix is done on DRUtES, it is possible to see both hydrodynamic and thermodynamic modeling of evaporation are both convective dominant at the surface boundary.

Chapter 7

Conclusion and future work

7.1 Introduction

This chapter summarizes the conclusions and lessons learned during the execution of this thesis. The limitations of these models implemented from experience in the development of this work are also described, including the limitations stated in the literature. This chapter ends with brief descriptions of future research aims that were not contemplated in this work, but are part of the state of the art of the modeling of phase transition in porous media.

7.2 Conclusions

In this thesis, the Penman-Monteith equation was implemented as a boundary condition for the Richards' equation in the h-based form in the open-source software Dual Richard's Unsaturated Equation solver (DRUtES), the couple liquid water, water vapor, and heat model was also coded. The evaporation rate was included as a Neumann boundary condition for the water equation, and the energy surface balance was applied as a Neumann boundary condition for the heat equation. Constitutive functions and parameterization of the non-thermal and thermal-hydraulic conductivities for liquid and vapor were also presented. A test case was described to verify the behavior of the models, compare them, and identify the evaporation process stages in soils. Due to numerical instabilities associated mostly with the improper parameterization of the non-thermal liquid hydraulic conductivity when the soil reaches the drying conditions close to the residual water content and

long simulation time as a result of small-time step required for the solution of Richard's, the benchmark was not validated. Nonetheless, the preliminary results raised essential questions to lead a fruitful discussion. As part of this work, some numerical aspects of the solution and implementation were explained.

7.3 Future work

During the development of this work, some limitations were faced, and due to the scope and time constraint were not implemented, but they constitute further aims research to continue study evaporation and phase transition in soils.

Parameterization of hydraulic properties

Mualem- van Genuchten model for the liquid non-thermal hydraulic conductivity is commonly used to parameterize the unsaturated hydraulic conductivity. However, Sakai; Toride, et al., 2009 showed that it is not adequate to assume the evaporation process stops at the residual water content, an empirical parameter part of the model, which causes numerical instabilities and underestimates the unsaturated hydraulic conductivity for a dry zone in the soil. Moreover, one of the assumptions of the Mualem's model is all the capillaries are filled, and thus a systematic underestimation of hydraulic conductivity for dry soils can happen. Peters et al., 2015 studied the sensitivity of the numerical models to the parameterization of the soil hydraulic conductivities. This limitation should be considered especially for coarse soil textures that reach the residual water content at high values of pressure head (Fayer et al., 1995).

Meteorological data

During the modeling of evaporation, the interface soil-atmosphere is an important boundary condition that significantly affects the subsurface dynamics of water and heat. The uncertainty related to the measurement of all the parameters involved in the evaporation process at the boundary should be controlled by direct measurement of every component of the surface energy balance, including precipitation in short time intervals. For some applications, hourly data can be enough to catch the diurnal variations of these parameters, however for extreme events, like flash floods, where evaporation studies can

be implemented, a higher frequency of the data will be necessary (e.g., every minute.). In general, standard daily meteorological data from weather stations are available, which do not provide detailed information to carry out evaporation modeling studies. When data is not available in the frequency needed, the hourly data need to be calculated from standard daily data to get the daily maximum and minimum and their time of occurrence and use this calculated data as an input for the simulation (Saito et al., 2006). This procedure incorporates a different source of uncertainty than those frequently known for soil flow modeling, and it can have a negative impact int the results.

Resistance parameter for evaporation modeling

The surface resistance is a highly sensitive parameter for evaporation modeling. Camillo et al., 1986 studied its effect and proposed a methodology to fit this parameter based on surface temperature and soil water content. They showed the surface resistance parameter should be taken into account in the latent heat flux term in the surface energy balance. Otherwise, the evaporation would be overestimated and would lead to additional errors in long-term evaporation simulations. It is expected to have a function that relates to the surface resistance factor and water content.

Local thermal non-equilibrium modeling

In the model implemented in this thesis, assume local thermal equilibrium (LTE) between the phases, liquid water, water vapor, and porous medium, calculating then one temperature, which is assumed to be equal among the phases with a volume average thermal properties (Heinze et al., 2019). LTE is the most common approach to estimated temperature in multi-phase systems; however, in some applications, this approach seems to be insufficient to capture the real behavior of temperature in the physical domain. When the assumptions of LTE are not met, considering separate phase temperatures is another approach known as local thermal non-equilibrium (LTNE). In this approach, every phase would have a partial differential equation with a transfer term, which accounts for the heat transfer between phases, in other words, this term is either a sink or source of thermal energy in both equations (Rees et al., 2005).

References

ABBOTT, M. B.; HAVN, Karsten; LINDBERG, Sten, 1991. The fourth generation of numerical modelling in hydraulics. *Journal of Hydraulic Research*. Vol. 29, no. 5, pp. 581–600. Available from DOI: 10.1080/00221689109498978.

ABBOTT, M. B.; VOJINOVIC, Z., 2009. Applications of numerical modelling in hydroinformatics. *Journal of Hydroinformatics*. Vol. 11, no. 3-4, pp. 308–319. ISSN 1464-7141. Available from DOI: 10.2166/hydro.2009.051.

ABBOTT, M. B; TUMWESIGYE, BM; VOJINOVIC, Z, 2006. The fifth generation of modelling in Hydroinformatics. In: *The fifth generation of modelling in Hydroinformatics. Proceedings of the 7th International Conference on Hydroinformatics, Acropolis, Nice, France*, pp. 4–8.

ALLEN, Richard G; PEREIRA, Luis S; RAES, Dirk; SMITH, Martin, et al., 1998. Crop evapotranspiration-Guidelines for computing crop water requirements-FAO Irrigation and drainage paper 56. *Fao, Rome*. Vol. 300, no. 9, pp. D05109.

ALTHOFF, Daniel; RODRIGUES, Lineu Neiva; SILVA, Demetrius David da, 2020. Impacts of climate change on the evaporation and availability of water in small reservoirs in the Brazilian savannah. *Climatic Change*. ISBN 1573-1480. Available from DOI: 10.1007/s10584-020-02656-y.

ALVAREZ, V. Martínez; GONZÁLEZ-REAL, M.M.; BAILLE, A.; VALERO, J.F. Maestre; ELVIRA, B. Gallego, 2008. Regional assessment of evaporation from agricultural irrigation reservoirs in a semiarid climate. *Agricultural Water Management*. Vol. 95, no. 9, pp. 1056–1066. ISSN 0378-3774. Available from DOI: https://doi.org/10.1016/j.agwat.2008.04.003.

BARKER, R; DAWE, D; TUONG, TP; BHUIYAN, SI; GUERRA, LC, 1999. The outlook for water resources in the year 2020: challenges for research on water management in rice production. *Southeast Asia*. Vol. 1, pp. 1–5.

BLANEY, Harry F.; MORIN, Karl V., 1942. Evaporation and consumptive use of water empirical formulas. *Eos, Transactions American Geophysical Union*. Vol. 23, no. 1, pp. 76–83. Available from DOI: 10.1029/TR023i001p00076.

BRIGGS, Lyman James; SHANTZ, Homer LeRoy, 1916. *Hourly transpiration rate on clear days as determined by cyclic environmental factors*.

BUCKINGHAM, Edgar; BUCKINGHAM, E; BUCKINGHAM, R, 1907. Studies on the movement of soil moisture.

CAMILLO, P. J.; GURNEY, R. J., 1986. a Resistance Parameter for Bare-Soil Evaporation Models. *Soil Science*. Vol. 141, pp. 95–105. Available from DOI: 10.1097/00010694-198602000-00001.

CARSEL, Robert F.; PARRISH, Rudolph S., 1988. Developing joint probability distributions of soil water retention characteristics. *Water Resources Research*. Vol. 24, no. 5, pp. 755–769. Available from DOI: 10.1029/WR024i005p00755.

CHARI, M.V.K.; SALON, S.J., 2000a. 2 - OVERVIEW OF COMPUTATIONAL METHODS IN ELECTROMAGNETICS. In: CHARI, M.V.K.; SALON, S.J. (eds.). *Numerical Methods in Electromagnetism*. San Diego: Academic Press, pp. 63–104. Electromagnetism. ISBN 978-0-12-615760-4. Available from DOI: https://doi.org/10.1016/B978-012615760-4/50003-1.

CHARI, M.V.K.; SALON, S.J., 2000b. 4 - VARIATIONAL AND GALERKIN METHODS. In: – . *Numerical Methods in Electromagnetism*. San Diego: Academic Press, pp. 143–187. Electromagnetism. ISBN 978-0-12-615760-4. Available from DOI: https://doi.org/10.1016/B978-012615760-4/50005-5.

CHARI, M.V.K.; SALON, S.J., 2000c. 6 - THE FINITE ELEMENT METHOD. In: – . *Numerical Methods in Electromagnetism*. San Diego: Academic Press, pp. 283–357. Elec-

tromagnetism. ISBN 978-0-12-615760-4. Available from DOI: https://doi.org/10.1016/B978-012615760-4/50007-9.

DARCY, Henry, 1856. The public fountains of the city of Dijon. *Dalmont, Paris*. Vol. 647.

DRUtES, 2020. Available also from: http://www.drutes.org.

FAO, 2009. Global agriculture towards 2050. In: *Global agriculture towards 2050. High Level Expert Forum-How Feed World*. Vol. 2050, pp. 1–4.

FAYER, Michael J.; SIMMONS, C. Steven, 1995. Modified Soil Water Retention Functions for All Matric Suctions. *Water Resources Research*. Vol. 31, no. 5, pp. 1233–1238. Available from DOI: 10.1029/95WR00173.

GÖKBULAK, Ferhat; ÖZHAN, Süleyman, 2006. Water loss through evaporation from water surfaces of lakes and reservoirs in Turkey. *Official Publication of the European Water Association, EWA*.

HAN, Songjun; XU, Di; WANG, Shaoli, 2012. Decreasing potential evaporation trends in China from 1956 to 2005: Accelerated in regions with significant agricultural influence? *Agricultural and Forest Meteorology*. Vol. 154-155, pp. 44–56. ISSN 0168-1923. Available from DOI: https://doi.org/10.1016/j.agrformet.2011.10.009.

HEDKE, CR, 1924. Consumptive use of water by crops. *New Mexico State Engr. Office, July*.

HEINZE, Thomas; BLÖCHER, Johanna R., 2019. A model of local thermal non-equilibrium during infiltration. *Advances in Water Resources*. Vol. 132, pp. 103394. ISSN 0309-1708. Available from DOI: https://doi.org/10.1016/j.advwatres.2019.103394.

HELFER, Fernanda; LEMCKERT, Charles; ZHANG, Hong, 2012. Impacts of climate change on temperature and evaporation from a large reservoir in Australia. *Journal of Hydrology*. Vol. 475, pp. 365–378. ISSN 0022-1694. Available from DOI: https://doi.org/10.1016/j.jhydrol.2012.10.008.

HUGHES, Thomas J. R, 2000. *The finite element method : linear static and dynamic finite elment analysis*. Prentice-Hall.

IDEN, Sascha C.; BLÖCHER, Johanna R.; DIAMANTOPOULOS, Efstathios; PETERS, Andre; DURNER, Wolfgang, 2019. Numerical test of the laboratory evaporation method using coupled water, vapor and heat flow modelling. *Journal of Hydrology*. Vol. 570, pp. 574–583. ISSN 0022-1694. Available from DOI: `https://doi.org/10.1016/j.jhydrol.2018.12.045`.

JENSEN, Marvin E.; ALLEN, Richard G, 2016. *Evaporation, Evapotranspiration, and Irrigation Water Requirements*. Second Edition. American Society of Civil Engineers. Available from DOI: `10.1061/9780784414057`.

JENSEN, Marvin E; HAISE, Howard R, 1963. Estimating evapotranspiration from solar radiation. *Proceedings of the American Society of Civil Engineers, Journal of the Irrigation and Drainage Division*. Vol. 89, pp. 15–41.

JOHNSON, Fiona; SHARMA, Ashish, 2010. A Comparison of Australian Open Water Body Evaporation Trends for Current and Future Climates Estimated from Class A Evaporation Pans and General Circulation Models. *Journal of Hydrometeorology*. Vol. 11, no. 1, pp. 105–121. Available from DOI: `10.1175/2009JHM1158.1`.

JURY, iam A; HORTON, Robert, 2004. *Soil physics*. John Wiley & Sons.

KAY, A.L.; DAVIES, H.N., 2008. Calculating potential evaporation from climate model data: A source of uncertainty for hydrological climate change impacts. *Journal of Hydrology*. Vol. 358, no. 3, pp. 221–239. ISSN 0022-1694. Available from DOI: `https://doi.org/10.1016/j.jhydrol.2008.06.005`.

KURAZ, Michal, 2011. *Numerical solution of flow and transport equations in a porous medium with dual permeability conceptual approach*. VeRBuM.

KURAZ, Michal; HOLUB, Jiri, 2015. *Numerical solution of the Richards equation based catchment runoff model with dd-adaptivity algorithm and Boussinesq equation estimator*.

MAKKINK, G F, 1957. Testing the Penman formula by means of lysimeters. *Journal of the Institution of Water Engineerrs*. Vol. 11, pp. 277–288.

MATLAB, 2020. Available also from: `https://www.mathworks.com`.

MILLY, PCD, 1984. A simulation analysis of thermal effects on evaporation from soil. *Water Resources Research*. Vol. 20, no. 8, pp. 1087–1098.

MONTEITH, J. L., 1981. Evaporation and surface temperature. *Quarterly Journal of the Royal Meteorological Society*. Vol. 107, no. 451, pp. 1–27. Available from DOI: 10.1002/qj.49710745102.

MUALEM, Yechezkel, 1976. New Model for Predicting Hydraulic Conductivity of Unsaturated Porous-Media. *Water Resources Res.* Vol. 12, pp. 513–522. Available from DOI: 10.1029/WR012i003p00513.

NOBORIO, K; MCINNES, K J; HEILMAN, J L, 1996. Two-Dimensional Model for Water, Heat, and Solute Transport in Furrow-Irrigated Soil: I. Theory. *Soil Science Society of America Journal*. Vol. 60, pp. 1001–1009. Available from DOI: 10.2136/sssaj1996.03615995006000040007x.

OLIVIER, Henry, 1962. Irrigation and Climate. *Soil Science*. Vol. 93, no. 5, pp. 359.

OR, Dani; LEHMANN, Peter; SHAHRAEENI, Ebrahim; SHOKRI, Nima, 2013. Advances in soil evaporation physics—A review. *Vadose Zone Journal*. Vol. 12, no. 4.

PENMAN, H, 1963. Technical Communication No. 53, Commonwealth Bureau of Soils, Harpenden, Commonwealth Agricultural Bureaux. *Quarterly Journal of the Royal Meteorological Society*. Vol. 89, no. 382, pp. 565–566. Available from DOI: 10.1002/qj.49708938220.

PENMAN, H; KEEN, Bernard Augustus, 1948. Natural evaporation from open water, bare soil and grass. *Proceedings of the Royal Society of London. Series A. Mathematical and Physical Sciences*. Vol. 193, no. 1032, pp. 120–145. Available from DOI: 10.1098/rspa.1948.0037.

PETERS, Andre; IDEN, Sascha C.; DURNER, Wolfgang, 2015. Revisiting the simplified evaporation method: Identification of hydraulic functions considering vapor, film and corner flow. *Journal of Hydrology*. Vol. 527, pp. 531–542. ISSN 0022-1694. Available from DOI: https://doi.org/10.1016/j.jhydrol.2015.05.020.

PHILIP, J. R.; DE VRIES, D. A, 1957. Moisture movement in porous materials under temperature gradients. *Eos, Transactions American Geophysical Union*. Vol. 38, no. 2, pp. 222–232. Available from DOI: 10.1029/TR038i002p00222.

PIVEC, Jan; BRANT, Václav; MORAVEC, Dalibor, 2006. Analysis of the potential evapotranspiration demands in the Czech Republic between 1961–1990. *Biologia*. Vol. 61, no. 19, pp. S294–S299.

POTOPOVÁ, Vera; ŠTĚPÁNEK, Petr; MOŽNÝ, Martin; TÜRKOTT, Luboš; SOUKUP, Josef, 2015. Performance of the standardised precipitation evapotranspiration index at various lags for agricultural drought risk assessment in the Czech Republic. *Agricultural and Forest Meteorology*. Vol. 202, pp. 26–38. ISSN 0168-1923. Available from DOI: https://doi.org/10.1016/j.agrformet.2014.11.022.

REES, DAS; POP, I, 2005. Local thermal non-equilibrium in porous medium convection. In: *Local thermal non-equilibrium in porous medium convection. Transport phenomena in porous media III*. Elsevier, pp. 147–173.

RICHARDS, L. A., 1931. CAPILLARY CONDUCTION OF LIQUIDS THROUGH POROUS MEDIUMS. *Physics*. Vol. 1, no. 5, pp. 318–333. Available from DOI: 10.1063/1.1745010.

ROHWER, Carl, 1931. *Evaporation from free water surfaces*. US Department of Agriculture. No. 271.

SAITO, Hirotaka; SIMUNEK, Jiri; MOHANTY, Binayak P, 2006. Numerical analysis of coupled water, vapor, and heat transport in the vadose zone. *Vadose Zone Journal*. Vol. 5, no. 2, pp. 784–800.

SAKAI, Masaru; JONES, Scott B; TULLER, Markus, 2011. Numerical evaluation of subsurface soil water evaporation derived from sensible heat balance. *Water Resources Research*. Vol. 47, no. 2.

SAKAI, Masaru; TORIDE, Nobuo; SIMUNEK Jiri, Jirka, 2009. Water and Vapor Movement with Condensation and Evaporation in a Sandy Column. *Soil Science Society of America Journal - SSSAJ*. Vol. 73. Available from DOI: 10.2136/sssaj2008.0094.

SHUTTLEWORTH, W James, 2012. *Terrestrial hydrometeorology*. John Wiley & Sons.

TANNER, C. B.; PELTON, W. L., 1960. Potential evapotranspiration estimates by the approximate energy balance method of Penman. *Journal of Geophysical Research (1896-1977)*. Vol. 65, no. 10, pp. 3391–3413. Available from DOI: 10.1029/JZ065i010p03391.

THORNTHWAITE, C. W., 1948. An Approach toward a Rational Classification of Climate. *Geographical Review*. Vol. 38, no. 1, pp. 55–94. ISSN 00167428. Available also from: http://www.jstor.org/stable/210739.

TURC, L, 1961. Estimation of irrigation water requirements, potential evapotranspiration: a simple climatic formula evolved up to date. *Ann. Agron.* Vol. 12, no. 1, pp. 13–49.

VAN BAVEL, CHM; HILLEL, DI, 1976. Calculating potential and actual evaporation from a bare soil surface by simulation of concurrent flow of water and heat. *Agricultural Meteorology*. Vol. 17, no. 6, pp. 453–476.

VAN GENUCHTEN, Martinus, 1980. A Closed-form Equation for Predicting the Hydraulic Conductivity of Unsaturated Soils1. *Soil Science Society of America Journal*. Vol. 44. Available from DOI: 10.2136/sssaj1980.03615995004400050002x.

WILSON, G. Ward; FREDLUND, D.G.; BARBOUR, S.L., 1994. Coupled soil-atmosphere modelling for soil evaporation. *Canadian Geotechnical Journal*. Vol. 31, no. 2, pp. 151–161. Available from DOI: 10.1139/t94-021.

Appendix A

Additional work

A.1 Codes

A Github repository was made to get access to codes used and created in this thesis in https://github.com/julianaarbelaez/Evaporation-Modelling-2020. The following codes are available:

- DRUtES source code for the implementation of the Penman-Monteith couple to the Richards' equation and the input files in Fortran
- DRUtES source code for the implementation of the coupled model of water and heat flow and the input files in Fortran
- The post-processing scripts for plotting the results in RStudio
- The testing script for the constitutive functions in Matlab

A.2 Estimation of annual evapotranspiration using satellite spatial data

As part of understanding the trend of the evapotranspiration process and its relation with meteorological data, an online application was developed based on satellite data. The annual evaporation rate was calculated using the Penman-Monteith equation between 1970-2000 in the Czech Republic. For the calculations, the following annual data was used: average temperature, incoming solar radiation, wind speed, and water vapor pressure,

available https://www.worldclim.org. The result of this work is depicted in Figure A.1, where the evaporation rate is spatial distribute in the Czech republic. The application is available at https://rpubs.com/julianaarbelaez/evapotranspiration.

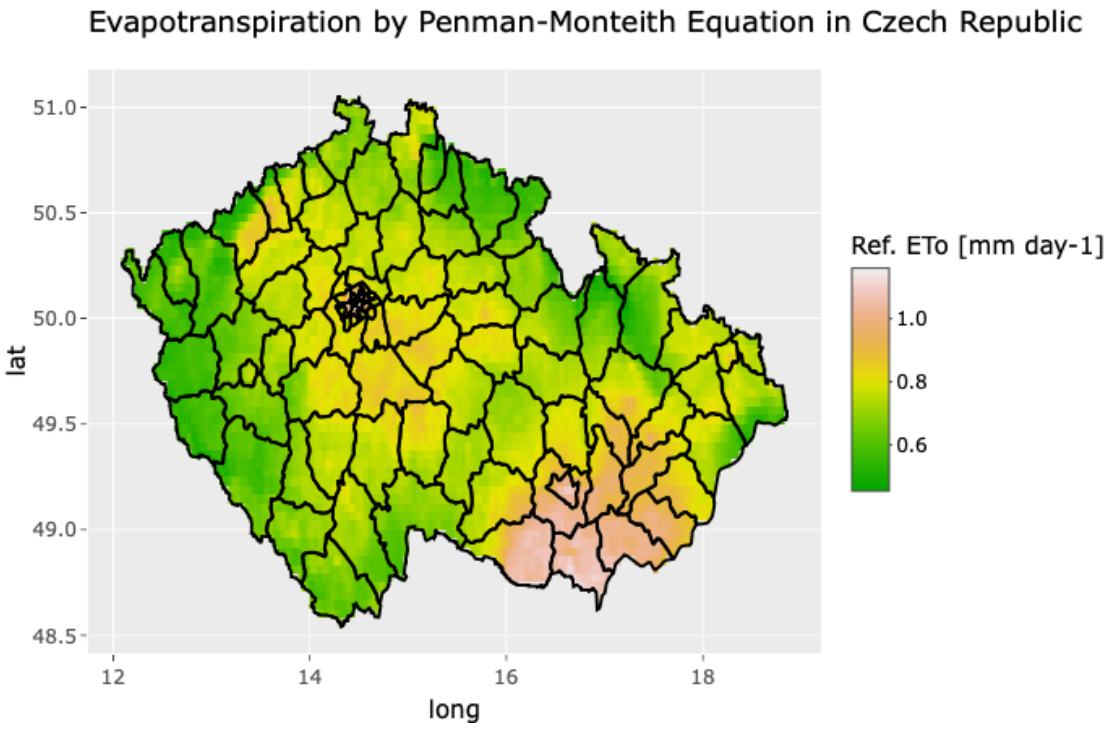

Figure A.1: Annual evapotranspiration data between 1970-2000 in Czech Republic.

A.3 Poster presentations

As a result of this thesis, three abstract and two posters were presented:

1. **Event**: International conference on mathematical modeling and computational methods in applied sciences and engineering. Olomouc, Czech Republic.September 16–20, 2019. **Title**: Mathematical model of water flow in a porous medium under phase changes due to evaporation. **Results**: One abstract and one poster.

2. **Event**: European Geosciences Union General Assembly 2020.Vienna, Austria. May 4-8, 2020. Online **Title**: Numerical solution analysis of water flow in a porous medium under phase transition due to evaporation. **Results**: Two abstracts and one poster.

Mathematical model of water flow in porous medium under phase changes due to evaporation

Michal Kuraz[1], Juliana Arbelaez Gaviria [1]

[1] Czech University of Life Sciences Prague, Prague, Czech Republic
Contact e-mail: kuraz@fzp.czu.cz

The purpose of this contribution is to present a numerical model simulating coupled water and heat flow in porous medium with phase changes due evaporation. Evaporation is a dynamic and nonlinear process that incorporates various internal transport mechanisms. The governing equations are formed out of the coupled Richards equation with heat transport equation, the boundary conditions originate from energy balance equation. The nonlinear nature of this problem, which originates both from the nonlinear Richards equation and latent heat exchange, which in turn governs the heat gradient, requires a proper temporal discretization in order to maintain numerical solution of sufficient qualities. The net evaporation rate is temperature and water content dependent, where the heat transferred downward by thermal conduction into the soil when the soil surface is warming by solar radiation or conducted back to the surface when the temperature of the top of the soil cools. Evaporation rates from terrestrial surfaces is very common to quantify in terms of flow of energy leaving the evaporating surface as latent heat of vaporization in the water vapour. In this contribution we will present numerical implementation of this coupled dynamic process and describe the computational difficulties, which arise from this nonlinear process.

Mathematical model of water flow in porous medium under phase changes due evaporation

Juliana ARBELAEZ and Michal KURAZ

Department of Water Resources and Environmental Modelling,
Czech University of Life Sciences Prague

arbelaez@fzp.czu.cz, kuraz@fzp.czu.cz

Mathematical Model

The governing equation for flow of liquid water and water vapor in a variably saturated non-deformable porous medium is given by the law of mass conservation presented in (1):

$$\frac{\partial \theta}{\partial t} = -\nabla \cdot \vec{q}_w + S \tag{1}$$

where

$$\vec{q}_w = \vec{q}_l + \vec{q}_v \tag{2}$$

The flux density of liquid water q_l is described using a modified the Darcy-Buckingham law:

$$\vec{q}_l = \vec{q}_{lh} + \vec{q}_{lT} = -\mathbb{K}_{lh}(\nabla h + \nabla z) - K_{lT}\nabla T \mathbb{I} \tag{3}$$

The flux density of water vapor $\vec{q}_l$ can also be separated into isothermal $\vec{q}_{vh}$ and thermal $\vec{q}_{vT}$ vapor flux densities as follows

$$\vec{q}_v = \vec{q}_{vh} + \vec{q}_{vT} = -K_{vh}\nabla h - K_{vT}\nabla T \tag{4}$$

Finally, the governing equation is given by combination of the law of mass conservation and the modified Darcy-Buckingham law:

$$\underbrace{C_h \frac{\partial h}{\partial t}}_{\text{Capacity}} = \underbrace{\nabla \cdot \mathbb{K}_{Th}\nabla h + \nabla \cdot K_{TT}\nabla T}_{\text{Difussion}} + \underbrace{\nabla \cdot K_{lh}\nabla z}_{\text{Convection}} - \frac{\partial \theta_v}{\partial t} \tag{5}$$

By grouping the isothermal and thermal hydraulic conductivities, it is obtained the total hydraulic conductivities as:

$$\mathbb{K}_{Th} = \mathbb{K}_{lh} + K_{vh}\mathbb{I} \tag{6}$$

$$K_{TT} = K_{lT} + K_{vT} \tag{7}$$

The volumetric water vapor content can be expressed as an equivalent water content

$$\theta_v = \theta_{air}\frac{\rho_v}{\rho_l} = (1-\theta_l)\frac{\rho_{sv} Hr}{\rho_l} \tag{8}$$

The total heat flux ,q_T, is the sum of conduction of the sensible heat, the sensible heat by convection of water and the latent heat of vapor flow

$$\vec{q}_T = -\kappa\nabla T + C_l T\vec{q}_l + C_v T\vec{q}_v + L\vec{q}_v \tag{9}$$

Local thermal equilibrium between phases is assumed.

The storage of heat in the soil is defined as the sum of the storage of sensible heat in the phases and latent heat:

$$S_T = C_T T + L\theta_v \tag{10}$$

The governing equation for the heat flow in a variably saturated non-deformable porous medium is given by the law of energy conservation:

$$\underbrace{C_T \frac{\partial T}{\partial t}}_{\text{Capacity}} = \underbrace{\nabla \cdot \mathbb{C}_{Th}\nabla h + \nabla \cdot \mathbb{C}_{TT}\nabla T}_{\text{Difussion}} + \underbrace{\nabla \cdot C_l \mathbb{K}_{lh} T\nabla z}_{\text{Convetion}} - L\frac{\partial \theta_v}{\partial t} \tag{11}$$

The terms are grouped to obtain two diffusion coefficients

$$\mathbb{C}_{TT} = \kappa\mathbb{I} + C_l T\mathbb{K}_{lT} + C_v T K_{vT}\mathbb{I} + LK_{vT}\mathbb{I} \tag{12}$$

$$\mathbb{C}_{Th} = C_l T\mathbb{K}_{lh} + C_v T K_{vh}\mathbb{I} + LK_{vh}\mathbb{I} \tag{13}$$

Constitutive Equations

The unsaturated hydraulic conductivity $\mathbb{K}_{lh}$ is obtained from the saturated hydraulic conductivity K_s and the combination of pore-size distribution model of Mualem and van Genutchen's model of the soil water retention curve:

$$\mathbb{K}_{lh} = \begin{cases} K_s \frac{(1-(-\alpha h)^{nm}(1+(-\alpha h)^n)^m)^2}{(1+(-\alpha h)^n)^{\frac{m}{2}}}, & \forall h \in (-\infty, 0) \\ K_s, & \forall h \in \langle 0, \infty) \end{cases} \tag{14}$$

The thermal hydraulic conductivity $\mathbb{K}_{lT}$ is defined as follows

$$\mathbb{K}_{lT} = \mathbb{K}_{lh}\left(hG_{wT}\frac{1}{\gamma_0}\frac{d\gamma}{dT}\right) \tag{15}$$

The thermal and isothermal vapor hydraulic conductivities are described as

$$K_{vh} = \frac{D}{\rho_l}\rho_{sv}\frac{Mg}{RT}H_r \tag{16}$$

$$K_{vT} = \frac{D}{\rho_l}\eta\frac{d\rho_{sv}}{dT}H_r \tag{17}$$

Initial and Boundary Conditions

The initial conditions for water and heat flow equations are given as:

$$h(\mathbf{x}, t_0) = h_0(\mathbf{x}) \quad \forall \mathbf{x} \in \Omega \tag{18}$$

$$T(\mathbf{x}, t_0) = T_0(\mathbf{x}) \quad \forall \mathbf{x} \in \Omega \tag{19}$$

where Ω is de computational domain bounded by $\Gamma = \partial\Omega$.

$$q_v(\mathbf{x}, t) + q_l(\mathbf{x}, t) = E_v(t) \quad \forall \mathbf{x} \in \Gamma_{surf} \times [0, T) \tag{20}$$

Evaporation rate E_v and the soil surface heat flux density G are determined from the surface energy balance.

$$-\kappa\frac{\partial T}{\partial \mathbf{n}} + [C_l T\vec{q}_l + C_v T\vec{q}_v + L\vec{q}_v]_{\mathbf{x}=\mathbf{n}} = -G \tag{21}$$

$$-G = -R_n + H_s + LE_v \tag{22}$$

where R_n is the net radiation, and H_s is the sensible heat flux density.

Implementation Challenges

- How to treat non-homogeneous domain for the convective term
- Time step selection for the temperature is also θ_v.

References

[1] Hirotaka Saito, Jiri Simunek, and Binayak P Mohanty. Numerical analysis of coupled water, vapor, and heat transport in the vadose zone. *Vadose Zone Journal*, 5(2):784–800, 2006.

[2] Masaru Sakai, Scott B Jones, and Markus Tuller. Numerical evaluation of subsurface soil water evaporation derived from sensible heat balance. *Water Resources Research*, 47(2), 2011.

Numerical solution analysis of water flow in porous medium under phase changes due to evaporation

Juliana Arbelaez Gaviria[1], Michal Kuraz[1]

[1] Czech University of Life Sciences Prague, Prague, Czech Republic
Contact e-mail: arbelaez@fzp.czu.cz

Evaporation is a dynamic and nonlinear process that incorporates various internal transport mechanisms which is important in the unsaturated zone in arid regions under low soil moisture conditions [1, 2]. The governing equations are formed out of the coupled Richards equation with the heat transport equation, where the boundary conditions originate from the surface energy balance. The purpose of this contribution is to present a numerical model simulating coupled water and heat flow in a porous medium with phase changes due to evaporation.The nonlinear nature of this problem, which originates both from the nonlinear Richards equation and latent heat exchange, which in turn governs the heat gradient, requires a proper temporal discretization in order to maintain numerical solution of sufficient qualities. The net evaporation rate is temperature and water content dependent, where the heat transferred downward by thermal conduction into the soil when the soil surface is warming by solar radiation or conducted back to the surface when the temperature of the top of the soil cools. Evaporation rates from terrestrial surfaces are very common to quantify in terms of energy flow leaving the evaporating surface as latent heat of vaporization of the water vapor. In this contribution, it is presented a numerical implementation of this coupled dynamic process and describes the computational difficulties which arise from this nonlinear process, including a numerical comparison between the common approach for evaluating evaporation in soils by using the Penman-Monteith [3] equation and the coupled water and heat flow modeling approach.

References

[1] Hirotaka Saito, Jiri Simunek, and Binayak P Mohanty. Numerical analysis of coupled water, vapor, and heat transport in the vadose zone. *Vadose Zone Journal*, 5(2):784–800, 2006.

Numerical solution analysis of water flow in porous medium under phase changes due to evaporation

Juliana Arbelaez Gaviria and Michal Kuraz

Department of Water Resources and Environmental Modelling
Czech University of Life Sciences Prague

Introduction

Evaporation (ET) is a dynamic and nonlinear process that incorporates various internal transport mechanisms, which is essential in the unsaturated zone in arid regions under low soil moisture conditions.FAO Penman-Monteith (PM) equation is the most widespread method to estimate the evaporation rate in saturated soils. This approach can be implemented as a boundary condition for the Richards' equation and related to the evaporation rate with the water content in the soil. However, the PM equation is not valid when the soil moisture is low, and the vapor flux is an essential component of the total water flux. In this case, the governing equations are formed out of the coupled Richards' equation with the heat transport, where the boundary conditions originate from the surface energy balance and the evaporation rate (Saito et al., 2006; Sakai et al., 2011).

Methodology

Two models were implemented in the Dual Richards' Unsaturated Equation Solver (DRUtES). The first model accounts for surface evaporation by coupling the Richards' equation and the Penman-Monteith equation

$$\nabla \cdot (\mathbf{K}(\theta)\nabla h) + \frac{\partial K_{zz}(\theta)}{\partial z} = C(h)\frac{\partial h}{\partial t} \tag{1}$$

The initial condition

$$h(\mathbf{x}, t_0) = h_0(\mathbf{x}) \quad \forall \mathbf{x} \in \Omega \tag{2}$$

The surface boundary condition

$$\mathbf{K}(h)\left(\frac{\partial h(\mathbf{x}, t)}{\partial \mathbf{n}} + n_3\right) = q_{\Gamma_{surf}}(t) \quad \forall (\mathbf{x}, t) \in \Gamma_{surf} \times [0, T) \tag{3}$$

Including the actual evapotranspiration

$$q_{\Gamma_{surf}}(t) = \begin{cases} r(t) - ET_o(t) & \text{if} \quad r(t) - ET_o(t) \geq 0 \\ r(t) - ET_o(t)\theta_l(h)^{2/3} & \text{if} \quad r(t) - ET_o(t) < 0 \end{cases} \tag{4}$$

And the Penman-Monteith equation for the evaporation rate

$$ET_o = \frac{0.408\Delta(R_n - G) + \gamma\frac{900}{T+273}u_2(e_s - e_a)}{\Delta + \gamma(1 + 0.34u_2)} \tag{5}$$

The second model accounts for sub-surface evaporation by coupling a modified Richards' equation and the heat equation

$$\begin{cases} C_h\dfrac{\partial h}{\partial t} = \nabla \cdot (\mathbf{K}_{Th}\nabla h) + \nabla \cdot (\mathbf{K}_{TT}\nabla T) \\ \qquad\qquad + \nabla \cdot (\mathbf{K}_{lh}\nabla z) - \dfrac{\partial \theta_v}{\partial t} \quad \forall \mathbf{x} \in \Omega \\ C_T\dfrac{\partial T}{\partial t} = \nabla \cdot (\mathbf{B}_{TT}\nabla T) + \nabla \cdot (\mathbf{B}_{Th}\nabla h) \\ -\nabla \cdot [(C_l\vec{q}_l + C_v\vec{q}_v)T]) - L\dfrac{\partial \theta_v}{\partial t} \quad \forall \mathbf{x} \in \Omega \end{cases} \tag{6}$$

Initial condition for both partial differential equations

$$h(\mathbf{x}, t_0) = h_0(\mathbf{x}) \quad \forall \mathbf{x} \in \Omega \tag{7}$$

$$T(\mathbf{x}, t_0) = T_0(\mathbf{x}) \quad \forall \mathbf{x} \in \Omega \tag{8}$$

The surface boundary condition for the water equation

$$\| \vec{q}_v(\mathbf{x}, t) \|_{\mathbf{x}=\mathbf{n}} + \| \vec{q}_l(\mathbf{x}, t) \|_{\mathbf{x}=\mathbf{n}} = E_v(t) \quad \forall \mathbf{x} \in \Gamma_{surf} \times [0, T) \tag{9}$$

Including the evaporation rate

$$E_v(t) = \frac{Hr(h, T_s)\rho_{sv}(T_s) - RH_{air}\rho_{sv}(T_a)}{\rho_l r_a} \tag{10}$$

The surface boundary condition for the heat equation

$$-\kappa\frac{\partial T}{\partial \mathbf{n}} + C_v[\| \vec{q}_v \| T]_{\mathbf{x}=\mathbf{n}} = -G - L[\| \vec{q}_v \|]_{\mathbf{x}=\mathbf{n}} \quad \forall \mathbf{x} \in \Gamma_{surf} \times [0, T) \tag{11}$$

Including the surface energy balance

$$R_n - H_s - LE_v + G = 0 \tag{12}$$

h: pressure head [m]. $\mathbf{K}(\theta)$: unsaturated hydraulic conductivity[ms^{-1}]. $C(h)$: retention water capacity [m^{-1}]. t: time [s]. $q_{\Gamma_{surf}}(t)$: boundary surface flux [ms^{-1}]. r(t): rain intensity [ms^{-1}]. θ_l: liquid water content [-]. ET_o : the reference evapotranspiration [mmday^{-1}]. R_n: the net radiation [MJm^{-2}day]. G: soil heat flux density [$\mathrm{MJm}^{-2}\mathrm{day}^{-1}$]. u_2: the wind speed measured at 2 m height [ms^{-1}].e_s:saturation vapor pressure [kPa], e_a: the actual vapor pressure [kPa]. Δ: the slope vapor pressure curve [$\mathrm{kPa°C}^{-1}$]. γ: psychometric constant [$\mathrm{kPa°C}^{-1}$]. T: temperature °C. H_s: sensible heat [$\mathrm{MJm}^{-2}\mathrm{day}^{-1}$]. L is the latent heat, $\vec{q}_v$: vapor flux [ms^{-1}]. $\vec{q}_l$: liquid flux [ms^{-1}]. θ_v: vapor water content[-]. $Hr(h, T_s)$: soil relative humidity [-]. ρ_{sv}: saturation vapor density [kgm^{-3}]. T_s: soil temperature °C. T_a: air temperature °C. RH_{air}: air relative humidity [-]. ρ_l: liquid water density [kgm^{-3}]. r_a: aerodynamic resistance to water vapor flow [sm^{-1}]. $\mathbf{n}$: normal vector to the surface.

Results

A 20 cm long soil profile was used to perform the numerical experiments in 1D. The simulated experiments had total simulation time of 14 days, where the hydraulic properties and the numeric parameters were consistent across all the simulations.Two scenarios were proposed under controlled meteorological conditions.

- The first scenario is known as a dark condition where no incoming shortwave radiation was considered, $Rs = 0$.
- The second scenario is characterized by a constant incoming shortwave radiation, $Rs = constant$.

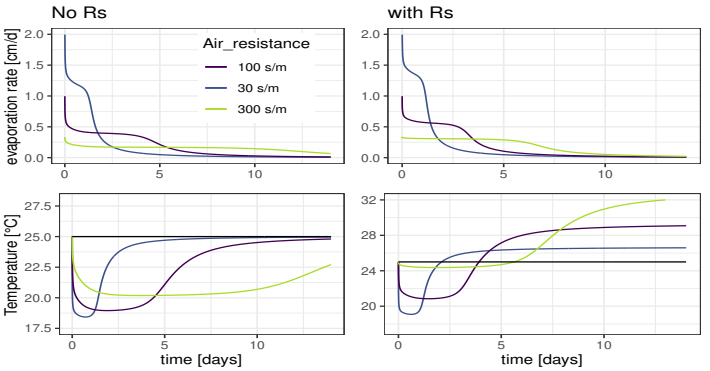

Figure 1: Results of numerical simulation of the evaporation rates (upper) and soil surface temperature (bottom) time series for different values of the air resistance r_a, without shortwave radiation (left) and with shortwave radiation (right).

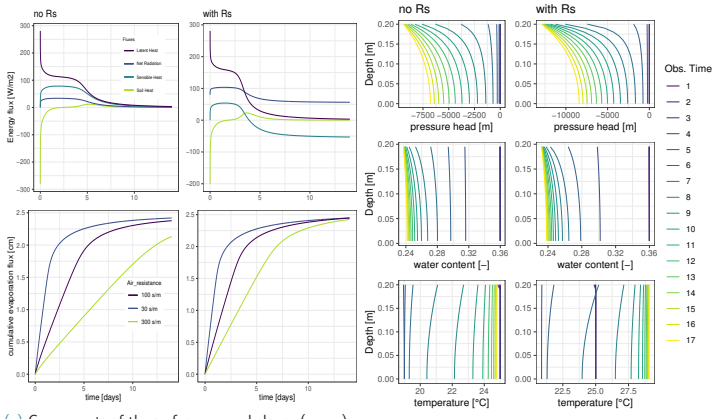

(a) Components of the surface energy balance (upper) and cumulative evaporation flux (bottom) without shortwave radiation (left) and with shortwave radiation (right) with different values of air resistance r_a.

(b) Distribution of pressure head (top), volumetric water content (middle), and temperature (bottom) at different simulation times without shortwave radiation (left) and with shortwave radiation (right).

Figure 2: Results of the numerical simulations with an aerodynamic resistance $r_a = 100\,s/m$.

Conclusions

- The numerical implementation of the Penman-Monteith method as the boundary condition of the classical Richards equation was presented.
- The application of the coupled model of heat and water flow was implemented in the free software Dual Richards Unsaturated Equation Solver (DRUtES).
- Two scenarios were designed to test the performance of both models under a controlled meteorological environment and the impact of the evaporation rate on the pressure head and water content.

References

Saito, H., Simunek, J., & Mohanty, B. P. (2006). Numerical analysis of coupled water, vapor, and heat transport in the vadose zone. *Vadose Zone Journal*, *5*(2), 784–800.

Sakai, M., Jones, S. B., & Tuller, M. (2011). Numerical evaluation of subsurface soil water evaporation derived from sensible heat balance. *Water Resources Research*, *47*(2).

arbelaez@fzp.czu.cz

Application of the Surface Energy Balance in Richards equation-based model using climatic data to calculate soil evaporation

Gustavo Cárdenas-Castillero[1] & Juliana Arbelaez Gaviria[2]

1. PhD Student. Czech University of Life Sciences. Faculty of Environmental Sciences. Department of Water and Environmental Modeling. Email: cardenas_castillero@fzp.czu.cz
2. Master Student. Czech University of Life Sciences. Faculty of Environmental Sciences. Department of Water and Environmental Modeling.

Abstract

This research aims to observe the behaviour between heat flow at the limit of the unsaturated area and the earth's surface (evaporation) through different methods based on the surface energy balance. This behavior has been determined by the DRUtES. DRUtES is a free software able to determine the evaporation in the surface using climate and hydraulic parameters determined by the Richard equation. Richards' equation describes the flow of water in an unsaturated porous medium due to the actions of gravity and capillarity neglecting the flow of the non-wetting phase, usually air.

The results obtained have been compared with the Penman-Monteith potential evapotranspiration model, this one as a referenced value. The results obtained help to understand the loss of water in the unsaturated area. This first approach using DRUtES and evaporation methods will allow a deeper investigation in the future regarding the impact of climate change on climate variables and their effects on soil moisture (unsaturated area) and natural aquifer recharge.

Key words: Evaporation, surface energy, unsaturated zone, Penman-Monteith.

Appendix B

Evaluation of constitutive relations

As presented in Section 3.3, the model for the coupled flow of liquid water, vapor water, and heat required several constitutive functions. They were analyzed separately to assure the physical and mathematical sense before proceeding with implementation to avoid incorrect code, the result of this analysis done in Matlab R2019b (*MATLAB*, 2020) is present below.

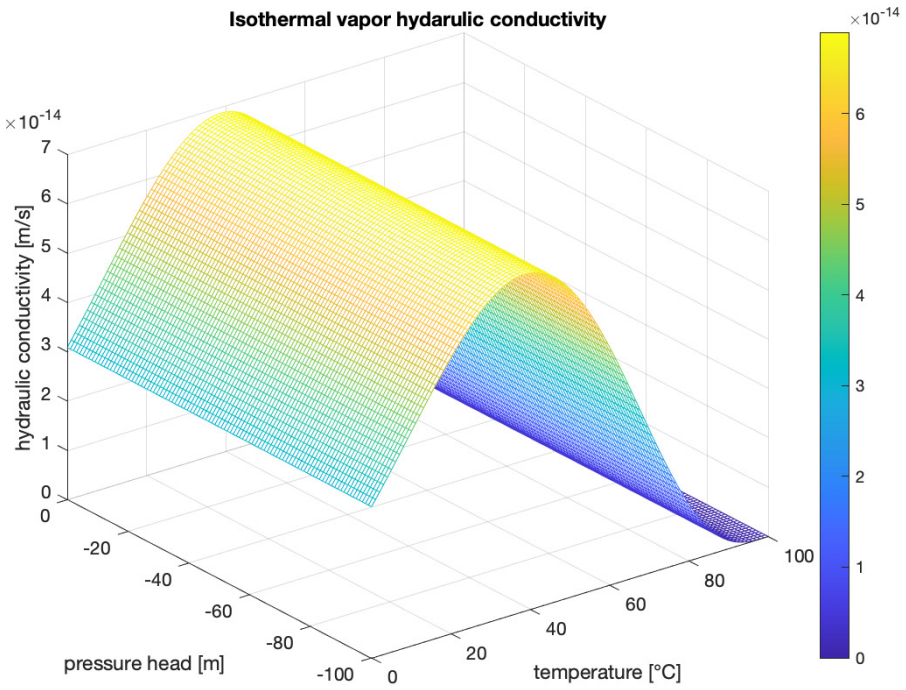

Figure B.1: Isothermal vapor hydraulic conductivity.

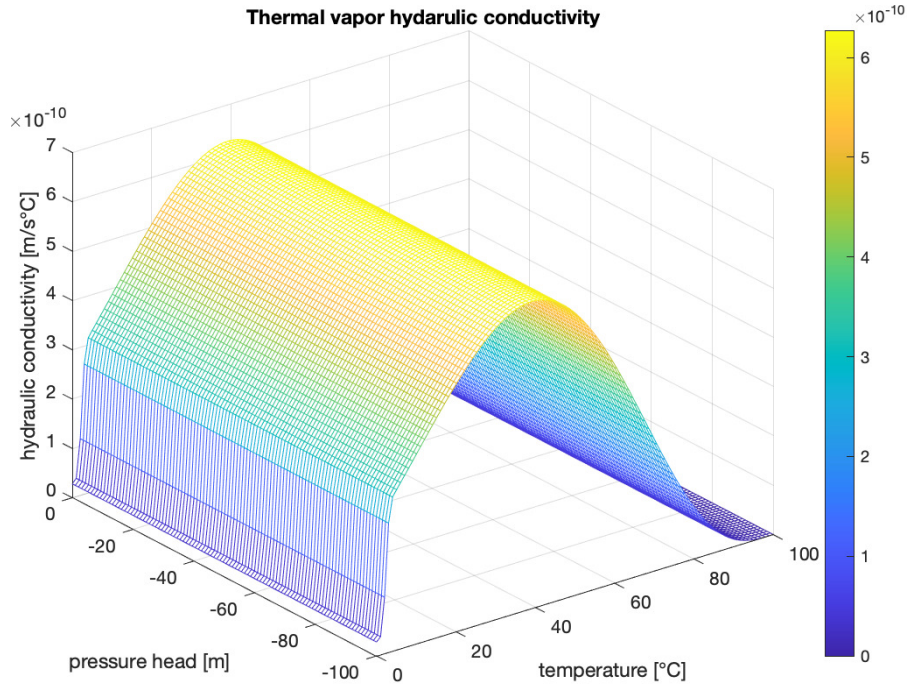

Figure B.2: Thermal vapor hydraulic conductivity.

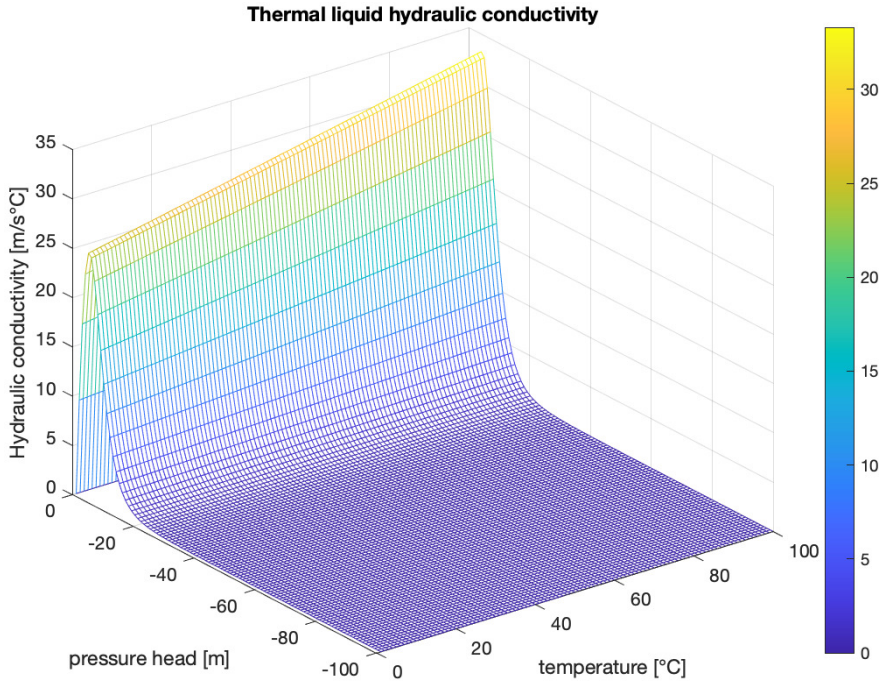

Figure B.3: Thermal liquid hydraulic conductivity.

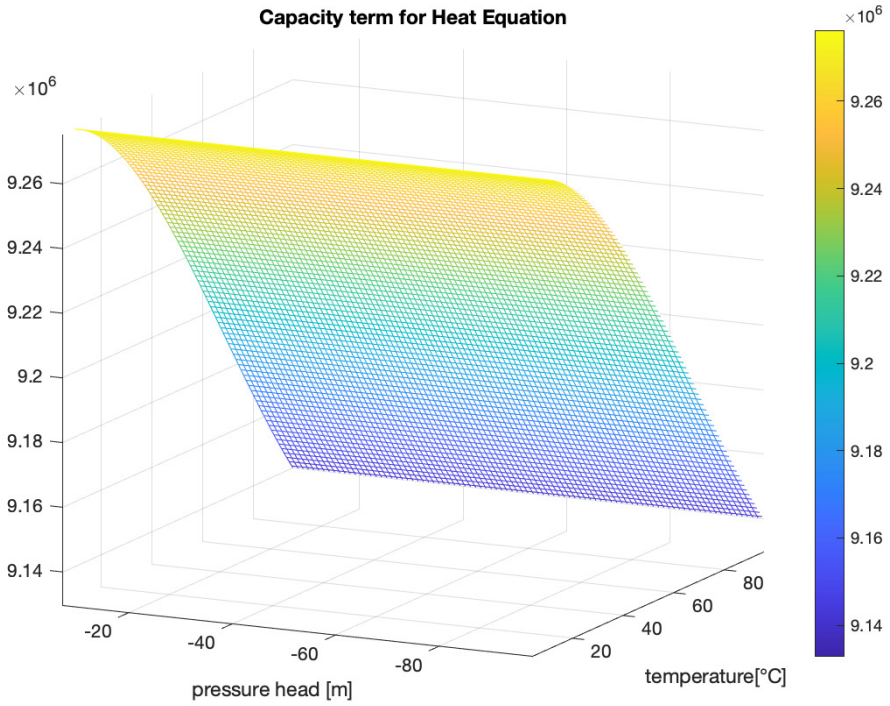

Figure B.4: Capacity term for heat equation.

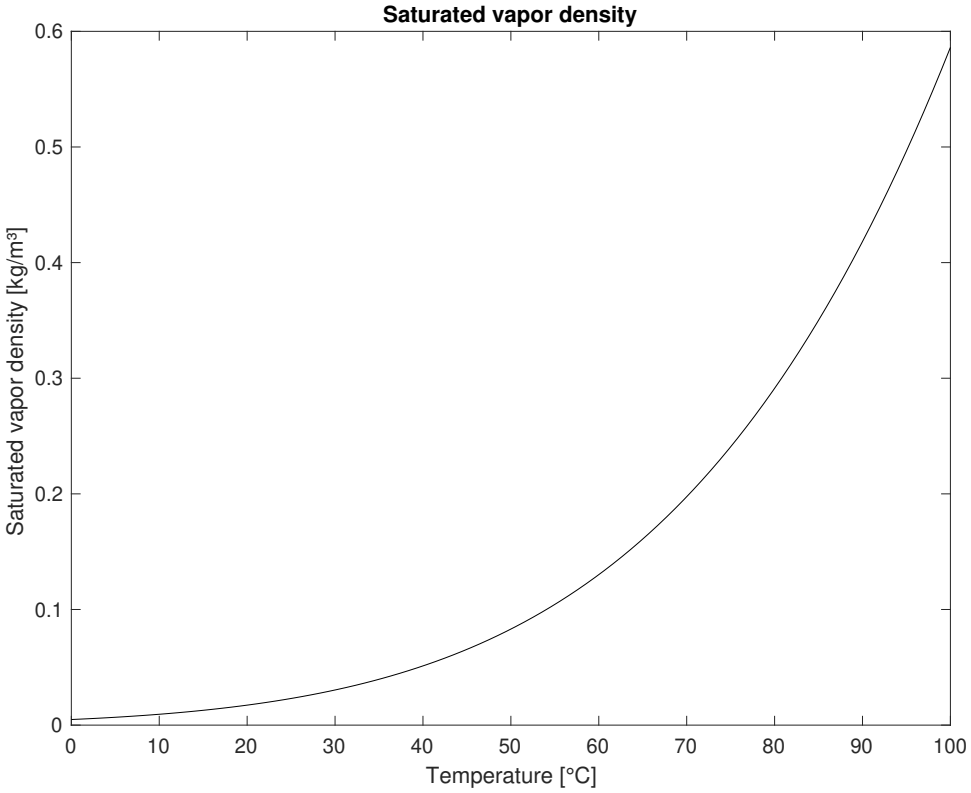

Figure B.5: Saturated water vapor density as function of temperature.

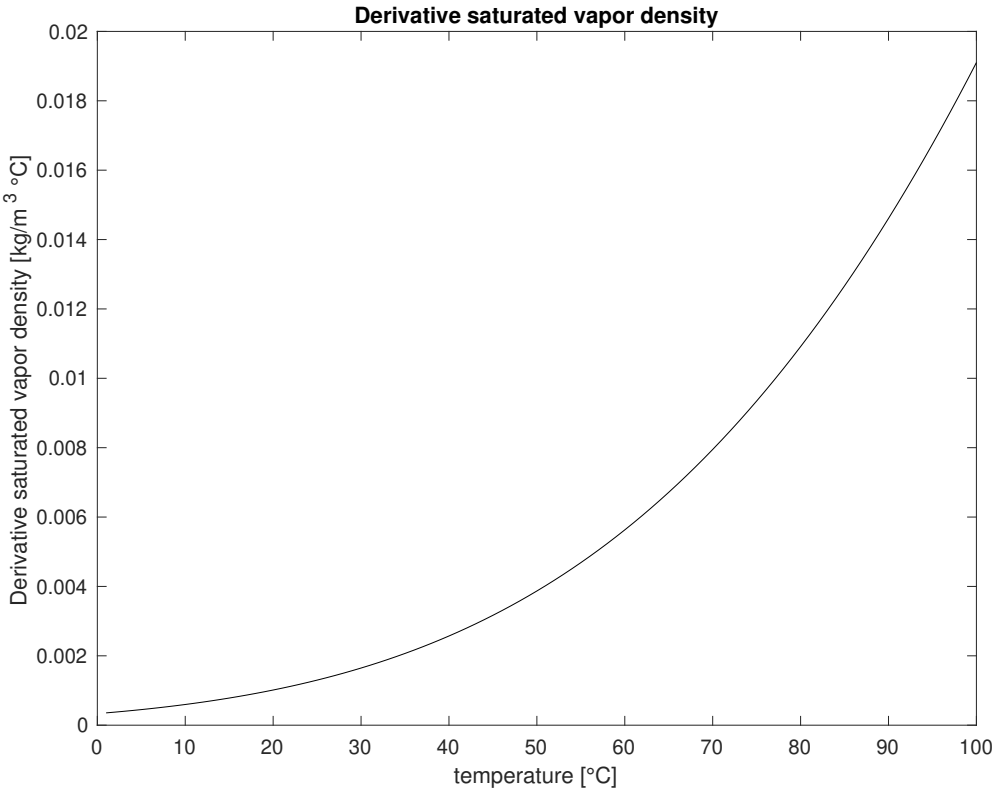

Figure B.6: Derivative of saturated water vapor density as function of temperature.

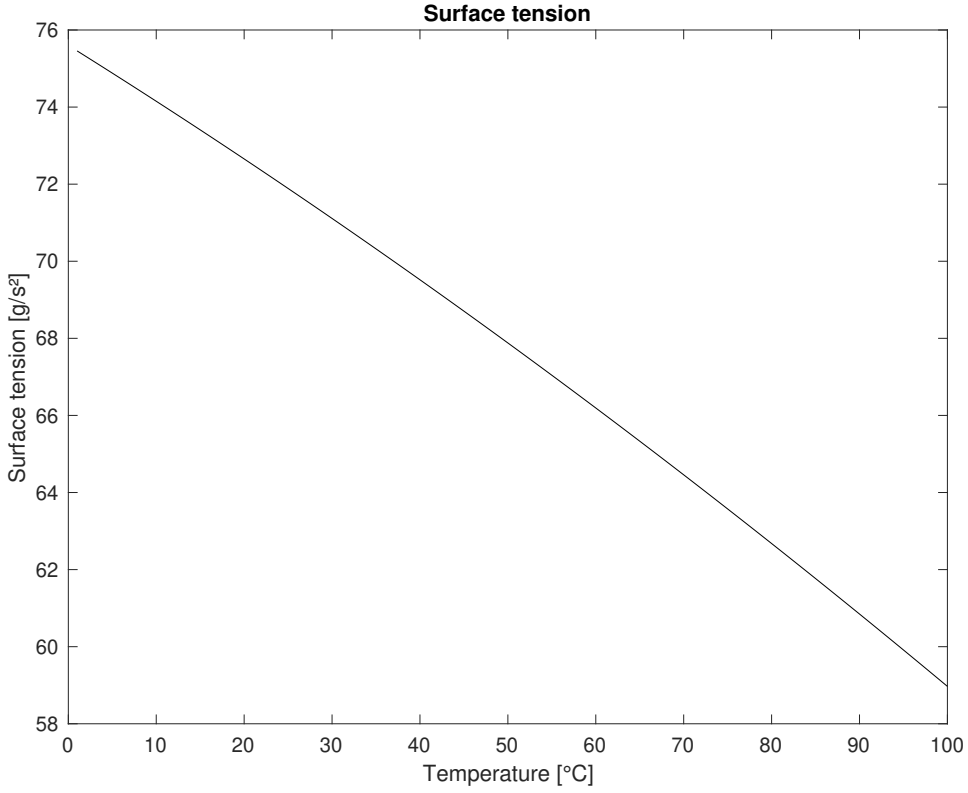

Figure B.7: Surface tension as function of temperature.

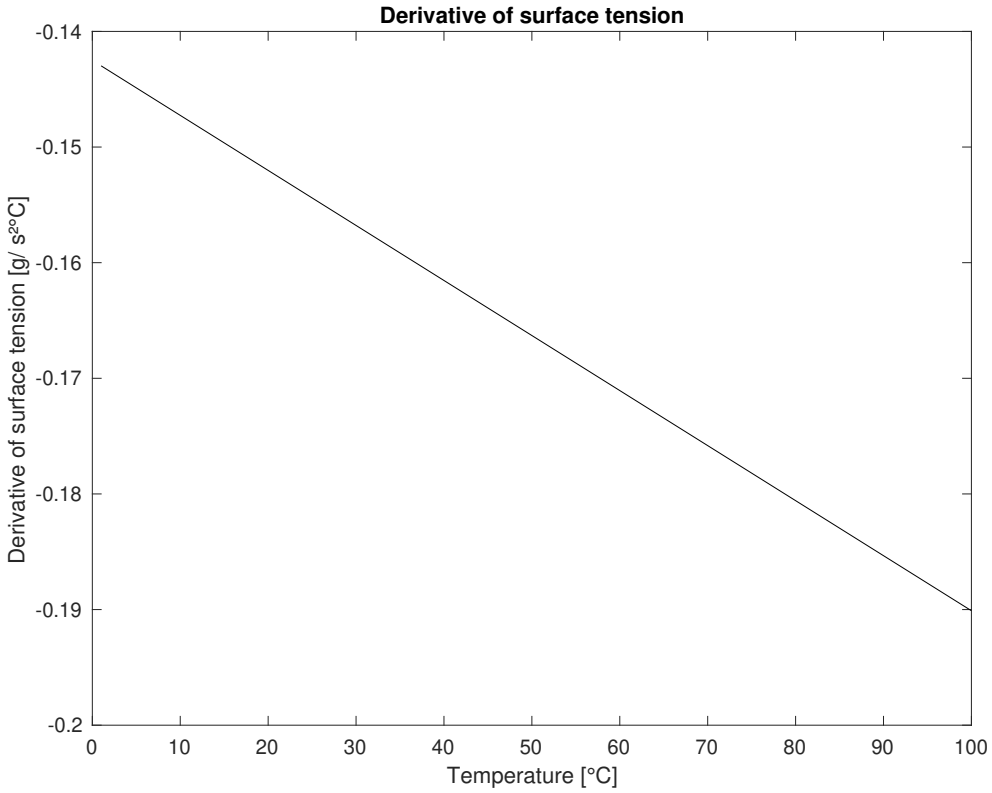

Figure B.8: Derivative of surface tension as function of temperature.

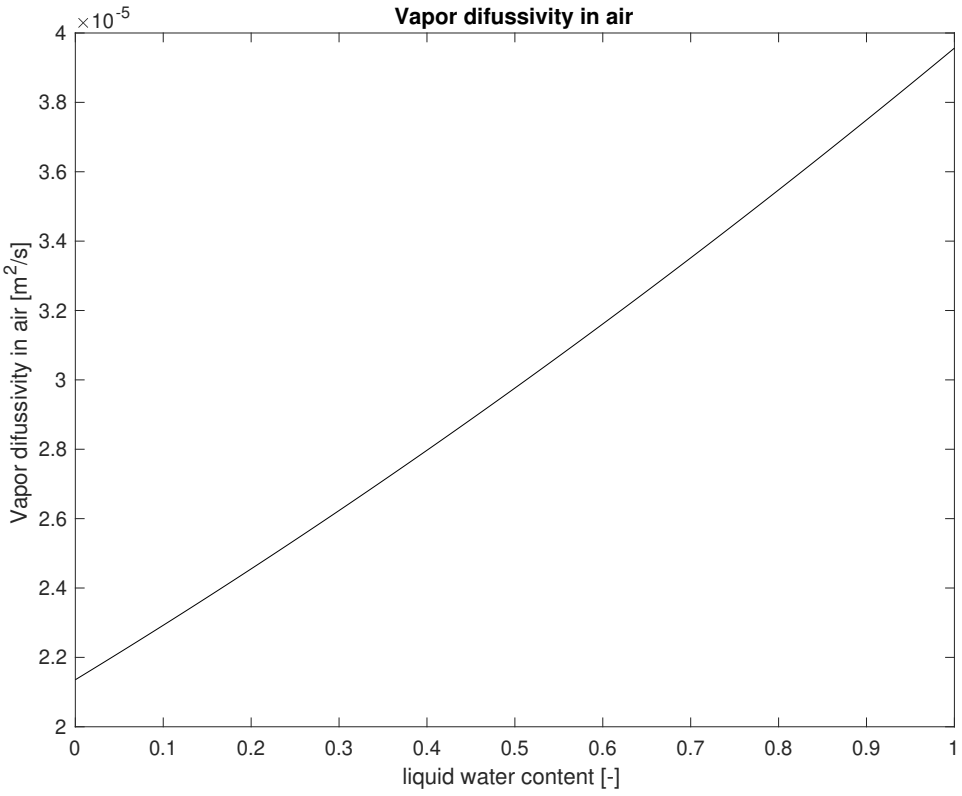

Figure B.9: Vapor diffusivity in air as of liquid water content.

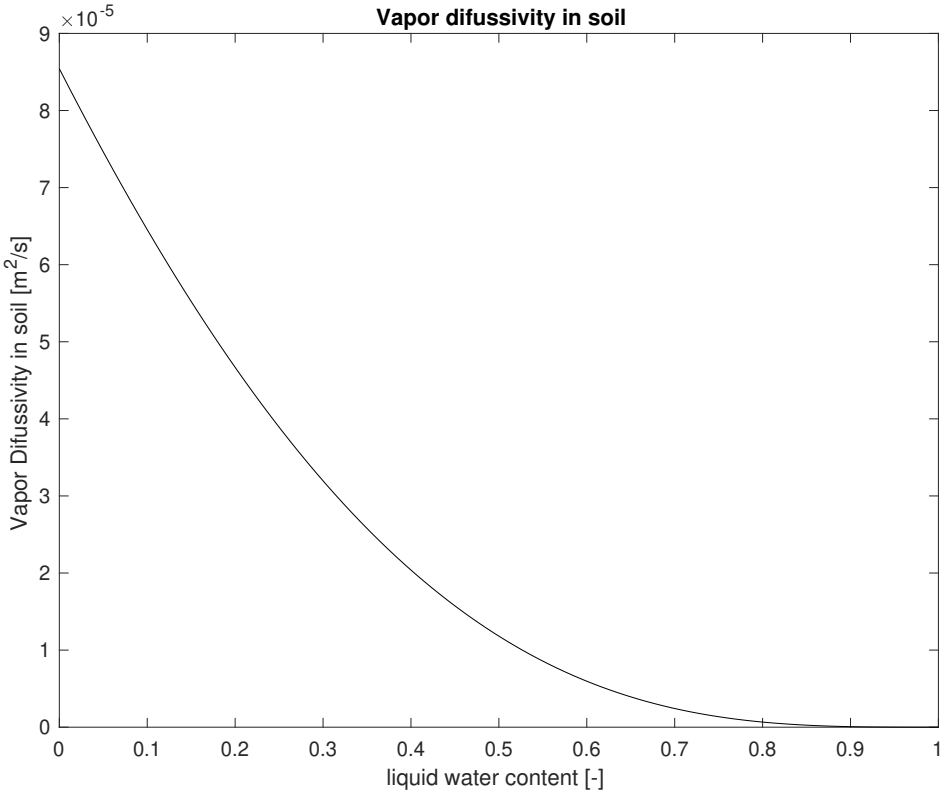

Figure B.10: Vapor diffusivity in soil as of liquid water content.

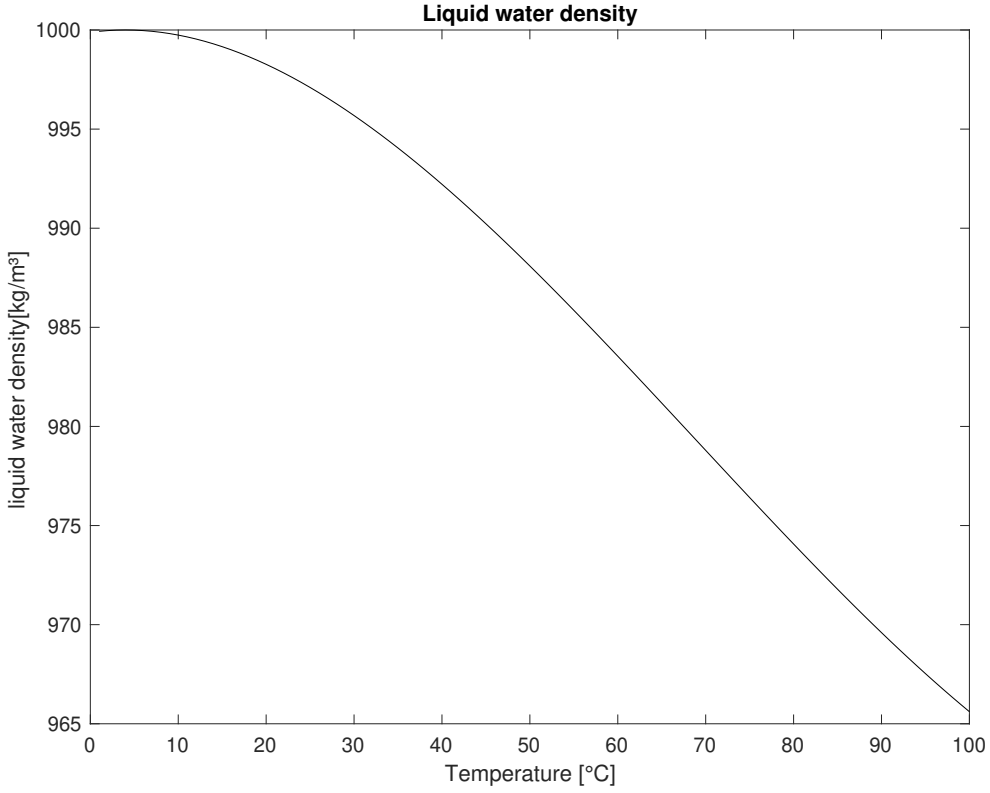

Figure B.11: Liquid water density as function of temperature.

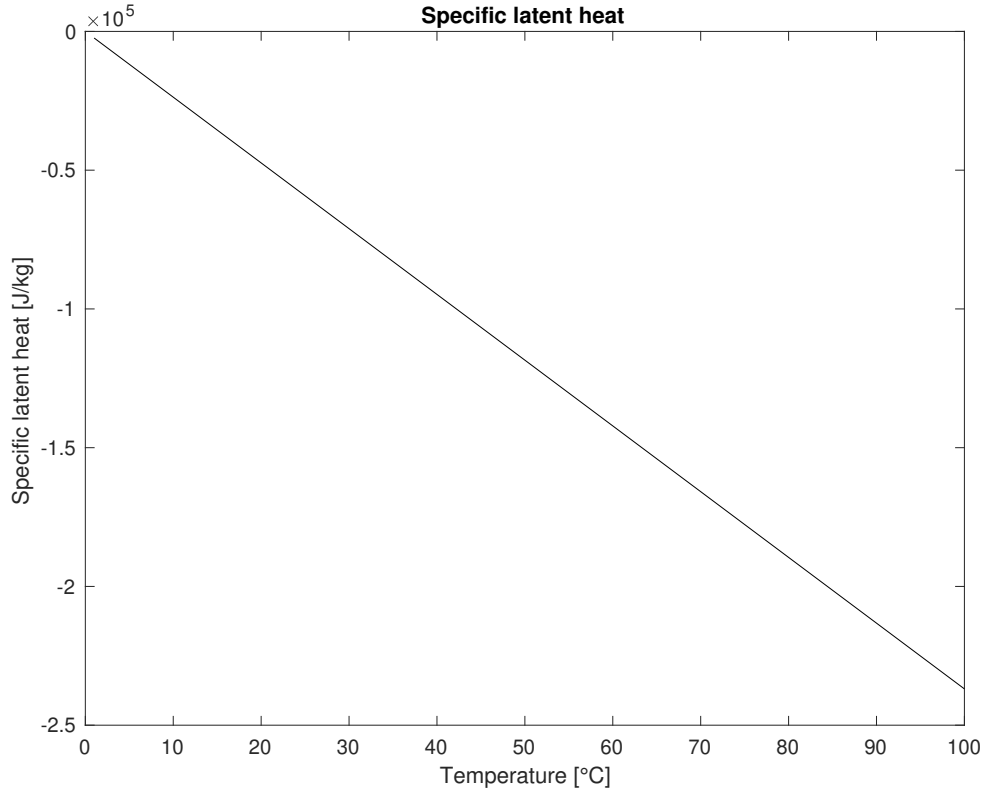

Figure B.12: Specific heat capacity as function of temperature.

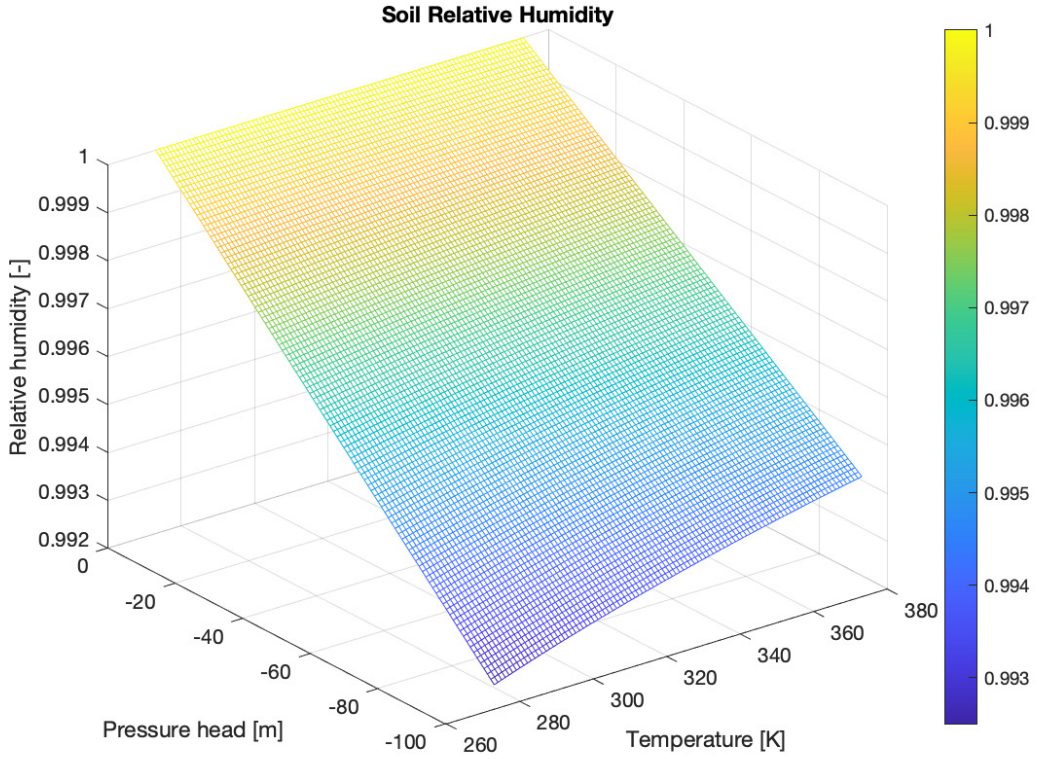

Figure B.13: Soil relative humidity as function of temperature and pressure head.

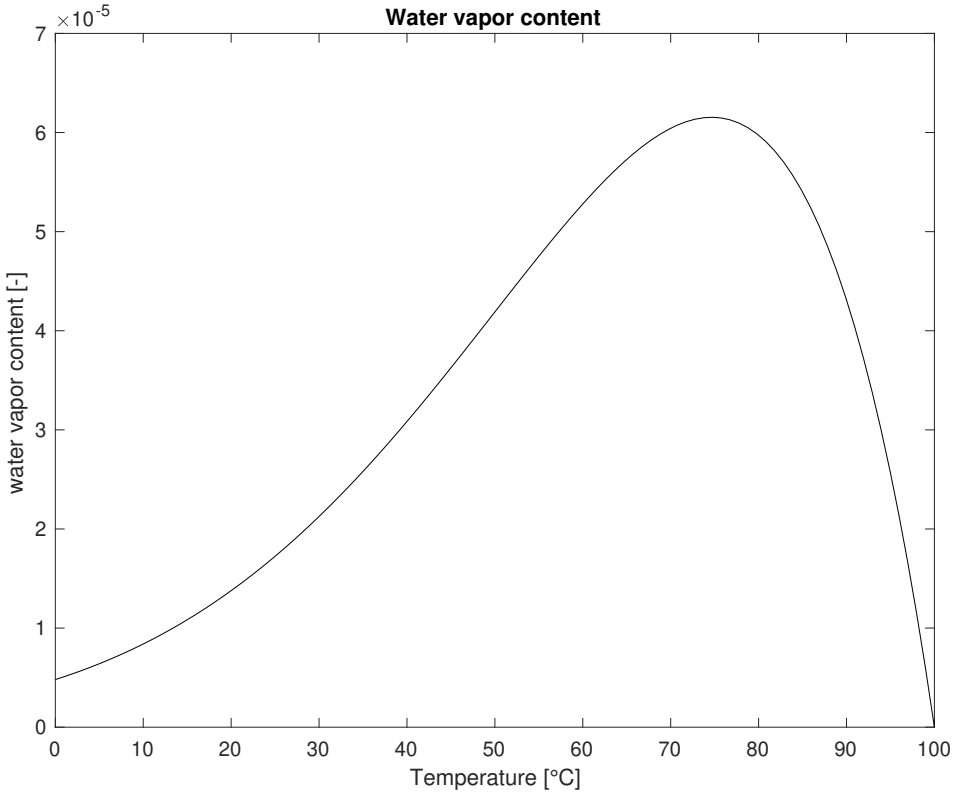

Figure B.14: Water vapor content as function of temperature.

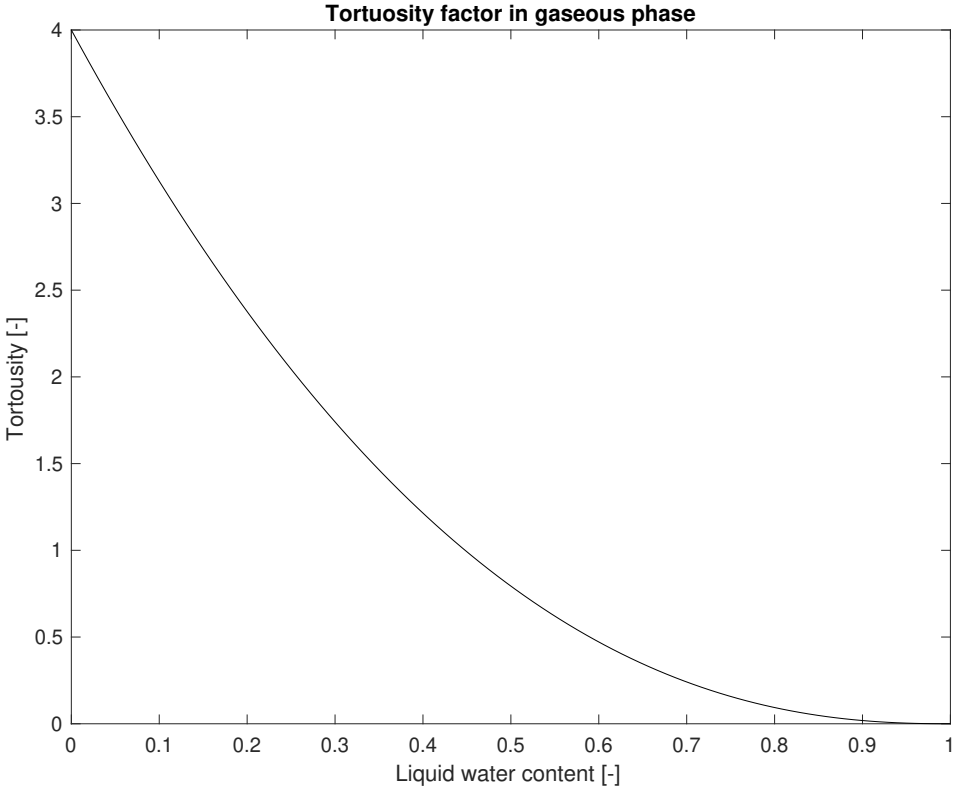

Figure B.15: Tortousity factor in gaseous phase.

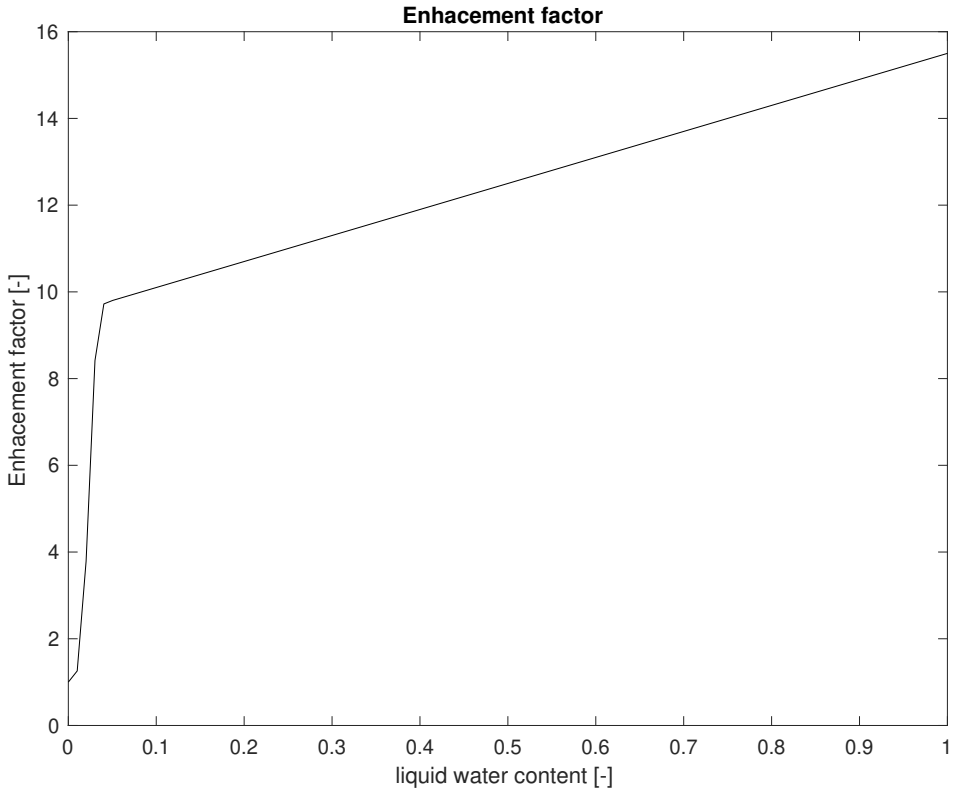

Figure B.16: Enhancement factor function.